BIFURCATIONS, CHAOS, ORGANIZED STRUCTURES, AND SOME ECOLOGICAL PRINCIPLES IN DISCRETE-TIME PREDATOR-PREY MODELS

Ph.D. Thesis

By

RAJNI

DEPARTMENT OF MATHEMATICS
INDIAN INSTITUTE OF TECHNOLOGY INDORE

APRIL 2025

BIFURCATIONS, CHAOS, ORGANIZED STRUCTURES, AND SOME ECOLOGICAL PRINCIPLES IN DISCRETE-TIME PREDATOR-PREY MODELS

A THESIS

Submitted in partial fulfillment of the
requirements for the award of the degree

of

DOCTOR OF PHILOSOPHY

by

RAJNI

DEPARTMENT OF MATHEMATICS
INDIAN INSTITUTE OF TECHNOLOGY INDORE

APRIL 2025

INDIAN INSTITUTE OF TECHNOLOGY INDORE

I hereby certify that the work which is being presented in the thesis entitled **BIFURCATIONS, CHAOS, ORGANIZED STRUCTURES, AND SOME ECOLOGICAL PRINCIPLES IN DISCRETE-TIME PREDATOR-PREY MODELS** in the partial fulfillment of the requirements for the award of the degree of **DOCTOR OF PHILOSOPHY** and submitted in the **DEPARTMENT OF MATHEMATICS, Indian Institute of Technology Indore,** is an authentic record of my own work carried out during the time period from January 2020 to April 2025 under the supervision of Dr. Bapan Ghosh, Associate Professor, Department of Mathematics, Indian Institute of Technology Indore.

The matter presented in this thesis has not been submitted by me for the award of any other degree of this or any other institute.

05/07/2025

Signature of the student with date

(Rajni)

This is to certify that the above statement made by the candidate is correct to the best of my knowledge.

July 05, 2025

Signature of Thesis Supervisor with date

(Dr. Bapan Ghosh)

Rajni has successfully given his Ph.D. Oral Examination held on **July 04, 2025**.

July 05, 2025

Signature of Thesis Supervisor with date

(Dr. Bapan Ghosh)

ACKNOWLEDGEMENTS

First and foremost, I deeply appreciate my parents and my brother. Their love and support were the foundation that made this journey possible. I am grateful to the almighty GOD who helped me through this journey.

I would like to express my gratitude to my supervisors Dr Bapan Ghosh for his support, guidance and helping nature. He provided me with a good environment for research and made a lot of discussions fruitful, moreover, he constantly encouraged me to do quality work.

I also thank Professor Suhas S. Joshi, Director of IIT Indore for the facilities provided to carry out the research work at this institute. I am grateful to my PSPC members, Dr. Sk. Safique Ahmad and Dr. Vijay Kumar Sohani, for reviewing my research progress and for their valuable suggestions. I would also like to thank the Head of the Discipline of Mathematics and the DPGC (Mathematics) for their support. Additionally, I extend my sincere thanks to all the faculty members of the Discipline of Mathematics, IIT Indore, especially Prof Swadesh Kumar Sahoo, Dr Debopriya Mukherjee and Dr Bibekanada Maji for their support and guidance. "I sincerely acknowledge the University Grants Commission, India, for providing financial support that enabled me to pursue my research work at IIT Indore

I extend my sincere gratitude to Mrs. Vijay Gupta, my high school mathematics teacher, for her steadfast support and encouragement in guiding me towards a career in mathematics. During times of adversity in this journey, I was fortunate to have met Mr. Shubham Mandsaurkar, who served not only as a counselor but also as a friend. He offered guidance and support, assisting me in navigating through my difficulties and never wavering in his commitment to stand by me.

I'm also deeply grateful to my new family—my mother-in-law Manju Dayal, father-in-law Ravi Dayal, and brother-in-law Ritesh Dayal—for their support, patience, and understanding. Your kindness and acceptance gave me a sense of belonging and strength as I balanced personal life with academic goals. And to my husband, Yadanshu Dayal—you have been my anchor, my cheerleader, and my biggest source of peace. You've made my life feel whole, and your unwavering support for my ambitions has helped me believe in myself even more.

During my time at IIT Indore, I am extremely grateful to find cherished friends in Debdeep Roy, Aniruddha Deshmukh, and Ritik Mishra. Debdeep, though my junior, became one of my closest companions—always there to help with my work, listen without judgment, and stand by me through every high and low. Aniruddha, with his steady wisdom and tea-time long talks, became a true friend and guide. Ritik brought warmth and laughter when I needed it most. And to Sajin Vincent—thank you for stepping into my life so organically; your humor and innocence brightened even the heaviest days.

Nishchal, you were a safe haven—my strength when things got overwhelming. Through you came Yagya, who brought me immense joy and became like my first baby. The memories we've made together will always hold a special place in my heart. Ayushi, my partner-in-crime, thank you for standing by me through the roughest times. From difficult days to spontaneous adventures and our little explorations, your presence made everything feel lighter, warmer, and full of life.

I'm grateful to Shubham, Sneha, Sheetal, Ashish and Shivani for the simple yet powerful gift of caring. Your kindness and quiet presence meant more than you know. My B.Tech students—Nikita, Karthik, Garima, Sahil, Pushkar, and Kisan—made teaching an unexpectedly emotional experience. Thank you all appreciating me as a teacher but caring for me like younger siblings with loyalty and warmth.

I owe thanks to my PhD seniors and colleagues —Vineeta Ma'am, Ashwini Sir, Pranav Sir, Faheem, Abhishek, Suvamit Sir, and Sumantha Sir—for their steady moral support and for being sources of encouragement and clarity throughout this journey. To my first friends here—Annu, Ashraf, and Adnan—thank you for turning this journey into one of shared laughter, support, and unforgettable memories.

Shiwani joined my PhD journey a little later, but we connected instantly. Thank you for the Karwachauth meal you made when we had just met—your kindness that day made me realize I'd found a friend for life. And finally, a special mention for my oldest friends from post-graduation, Shrinkhla and Kusum. We've walked through life side by side for over a decade, growing together from classrooms to careers, from graduation days to weddings.

Over the course of this journey, I made so many friends—some of whom became much more than that. They became my chosen family, offering love, laughter, and unwavering companionship. I will carry these bonds with me, always.

DEDICATION

To my mother Sushila Devi, father Mohinder Singh, and brother Hitesh Kumar.

SYNOPSIS

Study on population dynamics has long been a subject of interest. Within the realm of population ecology, significant focus is gathered by the dynamics exhibited by interactions of predator and prey species. Understanding the complex behaviors that arise in these systems is crucial for predicting and managing ecosystems. Continuous and discrete-time models are indeed two commonly used mathematical frameworks in population dynamics. While both types of models have their own applications and are used in describing appropriate ecosystem dynamics. There has been an increasing recognition that discrete-time models can provide a more appropriate and realistic representation of certain ecological systems. Discrete-time models are particularly well-suited for populations with non-overlapping generations. Examples of such populations include annual plants or insect species with one generation per year. One key feature of discrete-time models is that they can capture complex and rich dynamics even in lower-dimensional systems.

The study of population dynamics dates back to the year 1202 with Leonardo Fibonacci, who introduced a recursive sequence to model rabbit population growth. Euler's *Introduction in Analysin Infinitorum* (1748) explored sequences and exponential functions, implicitly introducing the idea of geometric growth. Later, in 1760, he applied mathematical reasoning to demography in *Recherches générales sur la mortalité et la multiplication du genre humain*, introducing the concept of geometric population growth and offering early insights into single-species dynamics. Later, in 1798, Thomas Malthus gave biological and socio-economic meaning to Euler's mathematical ideas by proposing that populations grow exponentially [1]. To incorporate environmental limitations, Pierre-François Verhulst introduced the logistic model in the 1838. Between 1910 to 1926, Alfred Lotka and Vito Volterra developed a model called the Lotka- Volterra model describing interactions between prey and predator species, helped establish mathematical ecology as an active area of research [2, 3].

Another important continuous-time model is the Rosenzweig-MacArthur (RM) model (1963) [4] given by,

$$\begin{aligned}\frac{\mathrm{d}x}{\mathrm{d}t} &= rx\left(1-\frac{x}{K}\right)-\frac{axy}{1+aTx},\\ \frac{\mathrm{d}y}{\mathrm{d}t} &= y\left(\frac{bax}{1+aTx}-d\right),\end{aligned}$$

where x and y represents the prey and predator population at time t, respectively, r is the intrinsic growth rate of the prey, and K is the environmental carrying capacity of the prey. The parameters a and T represent the predator's attack rate and handling time, respectively, while b is the efficiency with which predators convert consumed prey into biomass, and d is the specific mortality rate. All parameters mentioned above and other parameters appearing throughout the thesis are positive.

We define $\alpha = 1/T$, $h = 1/aT$, and $\beta = b\alpha$, which converts the above model into:

$$\frac{\mathrm{d}x}{\mathrm{d}t} = rx\left(1 - \frac{x}{K}\right) - \frac{\alpha xy}{h + x},$$
$$\frac{\mathrm{d}y}{\mathrm{d}t} = y\left(\frac{\beta x}{h + x} - d\right).$$

This transformed system will serve as the foundational model for our analysis throughout chapters 2 and 3.

The continuous-time Rosenzweig–MacArthur (RM) model can exhibit either stable coexistence or oscillatory behavior (limit cycles). To develop discrete-time counterparts of such continuous-time population models, researchers have employed various discretization techniques, with the forward Euler scheme being among the most commonly used. Hadeler and Gerstmann [5] showed that although the discrete-time version of the RM model retains the same number of equilibrium points as the continuous-time system, it can display significantly more complex dynamics, including period-doubling and chaos. Using the integral step size (δ) as a bifurcation parameter, several studies have reported dynamical changes in their models as δ is varied [6]. In contrast, Liu and Cai [7] fixed the step size at unity and instead investigated the effects of varying other parameters, revealing rich dynamical phenomena such as period-doubling cascades, period bubbling, quasiperiodicity, chaotic attractors, and multistability. Zhang and Wang [8] analyzed a discrete-time predator–prey model—also derived via the forward Euler method—featuring a weak Allee effect in the predator. They studied codimension-one bifurcations, Marotto's chaos, and the qualitative nature of fixed points under non-hyperbolic and degenerate conditions.

The key guiding questions for this thesis are:

(i) What types of dynamical behaviors can arise in discrete-time unstructured predator–prey systems?

(ii) How the stock pattern changes under the influence of species enrichment and harvesting?

(iii) How does varying dispersal affect stability and lead to the emergence of complex dynamics in spatially structured predator-prey systems?

To address these questions rigorously, in Chapter 1, we provide a detailed overview of the mathematical framework, theory, and tools that will be employed throughout the thesis. We begin by describing the discretization processes in detail. We then determine the fixed (or equilibrium) points of the system and present their associated stability theorems. Following this, we discuss bifurcations, Lyapunov exponents, quasiperiodicity, and chaotic dynamics in discrete-time models.

Chapter 2 presents a comprehensive analysis of dynamical behaviors of a discrete-time system obtained by discretizing the revised continuous-time RM model using the Forward Euler's scheme. The model is given by:

$$x_{n+1} = x_n + rx_n\left(1 - \frac{x_n}{K}\right) - \frac{\alpha x_n y_n}{h + x_n} - q_1 e_1 x_n,$$
$$y_{n+1} = y_n + \frac{\beta x_n y_n}{h + x_n} - m y_n - q_2 e_2 y_n,$$

with initial condition $x_0 = x(0) > 0$ and $y_0 = y(0) > 0$. Here, x_n and y_n are population size of prey and predator species at any time $n(n \in \mathbb{N})$, respectively. Further, e_1 (q_1) and e_2 (q_2) are harvesting efforts (catchability coefficients) of the prey and predator population, respectively. The key findings of this chapter are as follows:

(i) The system exhibits a Neimark–Sacker bifurcation, which leads to complex dynamical behaviors such as quasiperiodicity, period-bubbling phenomena, periodic windows, and chaotic dynamics.

(ii) Increasing the carrying capacity of the prey species, often referred to as species enrichment, paradoxically destabilizes the system. This increase in carrying capacity also leads to a decrease in the predator mean population, resulting in the paradox of enrichment (Figure 0.0.1a).

(iii) Two distinct forms of bistability are identified: (a) coexistence of two different periodic attractors and (b) co-stability of a periodic and a chaotic attractor.

(iv) Harvesting either species sufficiently suppresses chaotic dynamics and restores equilibrium stability.

(v) Increasing the mortality rate of predators under certain conditions could lead to an increment in the mean population size of the predator, demonstrating a hydra effect (Figure 0.0.1b).

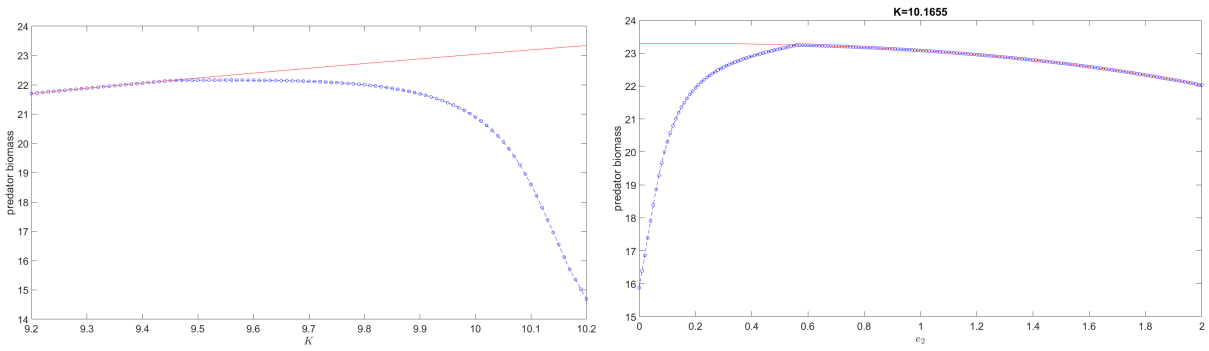

(a) **(b)**

Figure 0.0.1: *(a) Paradox of enrichment: mean predator population vs carrying capacity. (b) Hydra effect: mean predator population predator harvesting rate. Equilibrium biomass in red color and mean predator population in blue color*

In Chapter 3, we discretize the continuous-time RM model using the method of piecewise constant argument [9]. The model is given by:

$$x_{n+1} = x_n \exp\left(r\left(1-\frac{x_n}{K}\right) - \frac{\alpha y_n}{h+x_n} - q_1 e_1\right),$$
$$y_{n+1} = y_n \exp\left(\frac{\beta x_n}{h+x_n} - m - q_2 e_2\right),$$

where the parameters have same meaning as aforementioned. This discretization scheme preserves the non-negativity of the solutions. We examine the dynamics through bifurcation diagram, phase portraits, Lyapunov exponent diagram, and isoperiodic diagram to show the intricate behavior of the models. Unlike the previous model discussed in Chapter 2, the current model exhibits a sequence of bifurcations in which the carrying capacity first stabilizes and then destabilizes the coexisting equilibrium through a flip bifurcation followed by a Neimark–Sacker bifurcation. The model can exhibit two, three, and even four stable coexisting attractors, depending on the initial conditions exhibiting multistability (Figure 0.0.2).

We also study the influence of harvesting on the dynamics in two-parameter space. The effort e_1e_2- plane is divided into three main regions: the region of instability of coexisting equilibrium, the region where stability the coexisting equilibrium occurs, and

the predator extinction region. Neimark-Sacker is generated by the separatrix of the region of instability and the stability of the coexisting equilibrium. The predator extinction curve separates the domain of a stable coexisting equilibrium from the region where predators go extinct. Notably, organized periodic structures appear when varying both

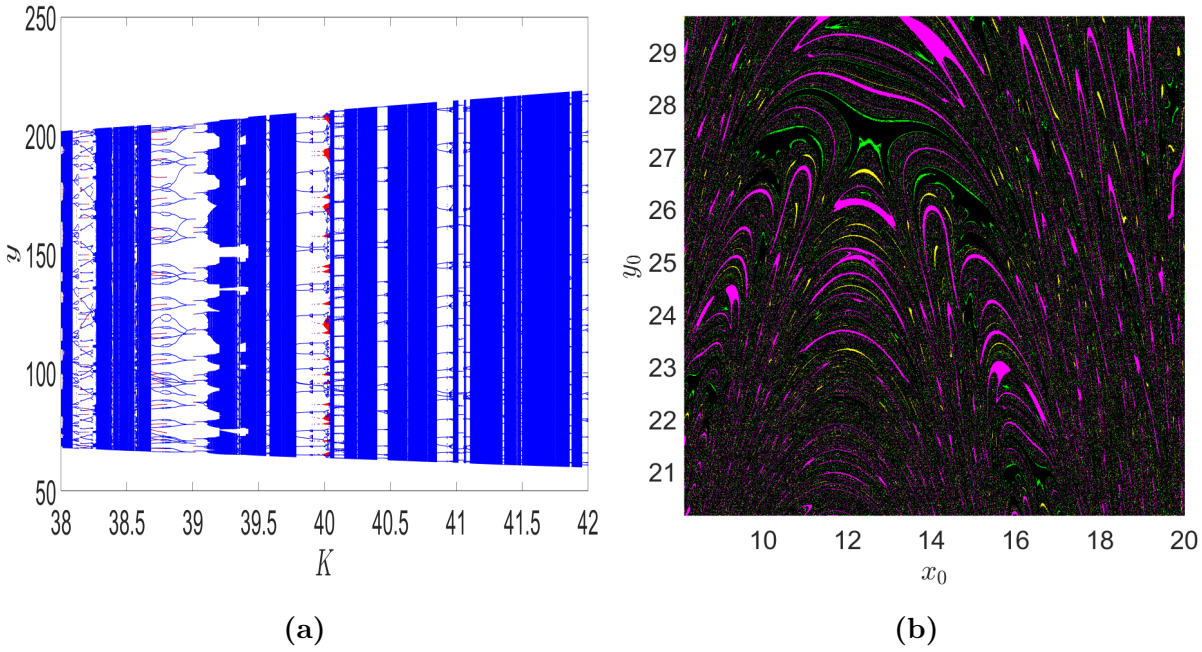

Figure 0.0.2: *(a) Bifurcation diagram featuring multistability: two bifurcation curves with different colors (red and blue). (b) Basin of attraction with quadruple attractors (see black, magenta, yellow and green colored regions).*

harvesting rates simultaneously. The analysis reveals an infinite array of periodic Arnold tongues (Figure 0.0.3a) with period-adding sequences in non-periodic regions. Another notable organized periodic structure observed in the chaotic regime is the shrimp structure (popularized by J.A.C. Gallas [10]), characterized by a head and four tails (Figure 0.0.3b). These structures exhibit self-similarity and display a period-doubling phenomenon, which is part of a period-doubling cascade that ultimately leads to chaos.

In chapter 4, we examine the role of dispersal in two-patch predator-prey systems and its impact on stability and species coexistence. Dispersal, a fundamental ecological process, encompasses the movement of individuals, or organisms from one location to another within an ecosystem or landscape. Incorporating spatial dynamics into population models, particularly through the concept of dispersal, has become increasingly crucial in the face of habitat fragmentation and climate-induced shifts in species distributions.

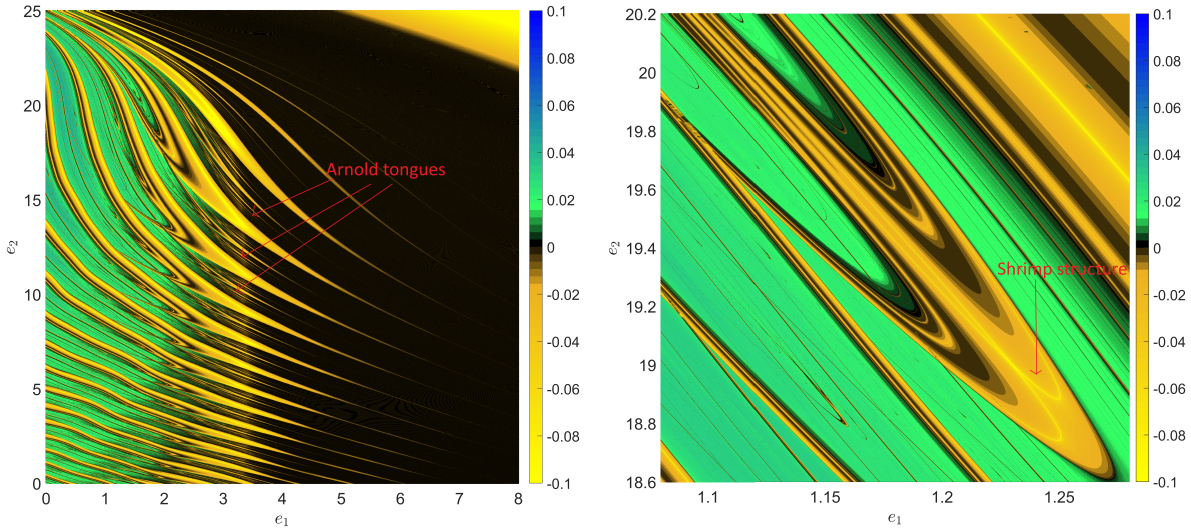

(a) **(b)**

Figure 0.0.3: *Maximum Lyapunov exponent diagram featuring (a) Arnold tongues and (b) a shrimp structure.*

Understanding these dispersal patterns is critical for predicting species' responses to global climatic change. In complex ecosystems, dispersal affects species coexistence, predator-prey interactions, and the formation of spatial patterns. This influence has profound implications for biodiversity conservation and ecosystem management.

Many studies have been dedicated to the exploration of logistic coupled maps in terms of nonlinear dynamics. However, over time, these maps are used to understand the population dynamics of the species living in different sites. A typical continuous-time predator-prey model with two homogeneous patches can be proposed as:

$$\begin{aligned}
\dot{x} &= rx\left(1-\frac{x}{K}\right)-\frac{\alpha xu}{h+x}+d_1(y-x),\\
\dot{u} &= su\left(1-\frac{u}{L}\right)+\frac{\beta xu}{h+x}+d_2(v-u),\\
\dot{y} &= ry\left(1-\frac{y}{K}\right)-\frac{\alpha yv}{h+y}+d_1(x-y),\\
\dot{v} &= sv\left(1-\frac{v}{L}\right)+\frac{\beta yv}{h+y}+d_2(u-v),
\end{aligned}$$

with initial population $x(0) > 0$, $u(0) > 0$, $y(0) > 0$ and $v(0) > 0$. The prey (and predator) species, denoted by x (and u) and y (and v) represent population sizes in patch 1 and 2, respectively. We assume that the prey and predator in each patch evolve following

a logistic growth rate. Therefore, the predator is generalist in nature. The carrying capacity of the prey and predator species are denoted by r and s, respectively. The dispersal rates of the prey and predator species between patches are denoted by d_1 and d_2, respectively.

We discretize this continuous-time model using forward Euler's scheme, hence, the model in consideration is:

$$\begin{aligned}
x_{n+1} &= x_n + rx_n\left(1-\frac{x_n}{K}\right) - \frac{\alpha x_n u_n}{h+x_n} + d_1(y_n - x_n),\\
u_{n+1} &= u_n + su_n\left(1-\frac{u_n}{L}\right) + \frac{\beta x_n u_n}{h+x_n} + d_2(v_n - u_n),\\
y_{n+1} &= y_n + ry_n\left(1-\frac{y_n}{K}\right) - \frac{\alpha y_n v_n}{h+y_n} + d_1(x_n - y_n),\\
v_{n+1} &= v_n + sv_n\left(1-\frac{v_n}{L}\right) + \frac{\beta y_n v_n}{h+y_n} + d_2(u_n - v_n),
\end{aligned}$$

with initial population $x_0 = x(0),\ u_0 = u(0),\ y_0 = y(0)$ and $v_0 = v(0)$. Some main results of this chapter are:

(i) The stability zone with bifurcation curves is established by simultaneously varying both prey and predator dispersal rates.

(ii) This work identifies scenarios where dispersal leads to catastrophic bifurcations, causing sudden and irreversible shifts in population dynamics (Figure 0.0.4).

(iii) In our model, ten invariant closed curves emerge from the period-10 orbit with dispersal. Such findings have profound implications for conservation biology, where species dispersal is often manipulated through habitat corridors and controlled relocation.

(iv) For the first time, we discover the bistability between the coexisting equilibrium and a period-2 orbit in such a coupled population model.

(v) In the unstable zone, we find Arnold tongues and shrimp structures. This chapter provides an in-depth exploration of the effect of dispersal on a discrete-time predator-prey model.

Overall, the investigations in the thesis delve into intricate dynamical behaviors of discrete-time predator-prey systems, focusing on the interplay between multistability, chaos, bifurcations, and dispersal-induced phenomena. By employing mathematical modeling, bifurcation analysis, and numerical simulations, the evolution of predator-prey dynamics under varying environmental and interaction constraints is thoroughly examined.

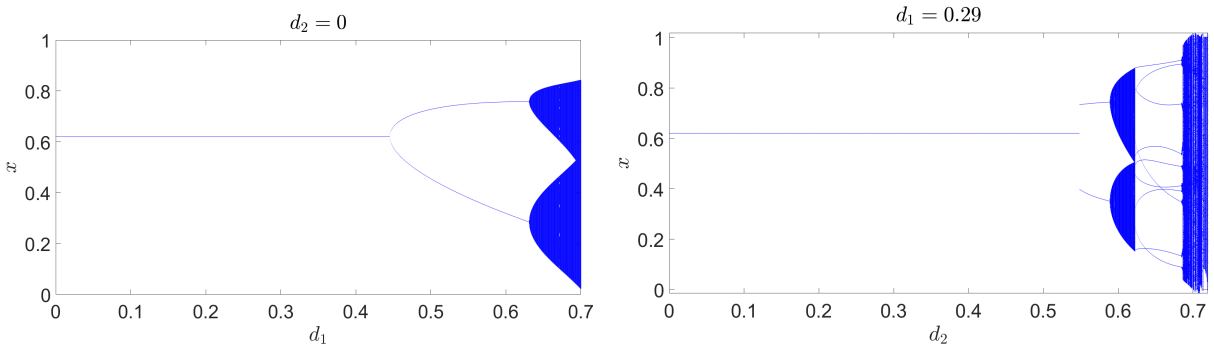

(a) **(b)**

Figure 0.0.4: *(a) Bifurcation diagram featuring a smooth flip bifurcation, where a period-2 orbit transitions to two invariant closed curves. (b) Bifurcation diagram featuring a non-smooth flip bifurcation. Here, the period-10 orbit gives birth to two invariant closed curves.*

The work also presents several ecological principles, including complex stock patterns, species enrichment, and the hydra effect.

LIST OF PUBLICATIONS

List of Published Research Papers from the Thesis

1. Rajni, Bapan Ghosh, Multistability, chaos and mean population density in a discrete-time predator-prey system, *Chaos, Solitons & Fractals* (2022), 162: 112497.
   Doi: https://doi.org/10.1016/j.chaos.2022.112497.
2. Rajni, Bapan Ghosh, Arnold tongues, shrimp structures, multistability, and ecological paradoxes in a discrete-time predator–prey system, *Chaos* (2024), 34(12): 123103.
   Doi: https://doi.org/10.1063/5.0230994.
3. Rajni, Bapan Ghosh, Dispersal induced catastrophic bifurcations, Arnold tongues, shrimp structures, and stock patterns in an ecological system, *Chaos* (2024), 34(12): 123139.
   Doi: https://doi.org/10.1063/5.0240974.

List of Published Research Papers Other Than the Thesis

4. Rajni, Shuchi Sahu, Suruchi Sarda, Bapan Ghosh, Stock patterns in a class of delayed discrete-time population models, *Discrete and Continuous Dynamical Systems-S* (2024), 18(5):1285–1303.
   Doi: https://doi.org/10.3934/dcdss.2024078.

TABLE OF CONTENTS

LIST OF FIGURES

LIST OF TABLES

NOTATIONS

x, y, u, v	denote species population
r, s	denote prey and predator growth rate respectively
m	denotes the specific mortality rate
K, L	denote the carrying capacity of prey and predator respectively
α	denotes predation coefficient
$\beta = \alpha c$	where c is the conversion coefficient of prey biomass to predator biomass
h	half-saturation coefficient
q_1, q_2	catachibility coefficients of prey and predator respectively
e_1, e_2	prey and predator harvesting rate respectively
d_1, d_2	prey and predator dispersal rate from one patch to another

CHAPTER 1

Introduction

Mathematical modeling is a powerful tool for analyzing real-life phenomena without disturbing natural systems. Differential and difference equations are used for modeling diverse processes across various disciplines, including physics, chemistry, biology, and engineering. Combining the mathematical analysis with real-world data provides more realistic results and insights without damaging the environment's integrity. In the context of biological and ecological phenomena, population models play an essential role as they have many applications, as they help understand, predict, and manage population dynamics in biological, ecological, and social systems. Here are some key areas where population modeling is applied:

1. *Ecology conversation*: The population models help to predict the critical threshold for species survival. These models help understand the interaction between the prey and predator species and their effects on ecological stability. The prediction of the species' behavior in case of habitat or climate changes can be made by analyzing the theoretical models. It helps with the precautions to take to avoid extinction or ecological instability.
2. *Epidemiology*: Mathematical models in epidemiology are helpful for understanding, forecasting, and predicting outbreaks and applying control measures. The pioneering work in the field of infectious disease modeling is provided by R.M. Anderson [17].
3. *Fisheries management*: Fish harvesting leads to over-exploitation of fish stocks. The researchers developed fisheries management strategies that consider the intricate dynamics of marine ecosystems. The term "Maximum Sustainable Yield (MSY)" was introduced in fisheries science to represent the largest yield that can be sustainably harvested from a fish population, based on its growth in isolation and modeled using logistic growth dynamics [18]. Several fisheries have adopted this method to preserve the fishing stocks. The Gordon-Schaefer model is a widely used bio-economic model in fisheries management that combines ecological and economic principles to determine the optimal use of fishery resources. It is named after H. Scott Gordon (1954) and Milton Schaefer (1957), who independently developed the theoretical framework.
4. *Marine protected areas*: Population modeling helps design and Marine Protected Areas evaluate MPAs to conserve marine biodiversity, protect endangered species,

and ensure the sustainable use of marine resources. MPAs are designated regions of oceans, seas, or coastal waters. These areas limit or regulate human activities, such as fishing, tourism, and industrial exploitation, to prevent habitat degradation and over-exploitation.

1.1 History of Population Models

In the early history of population modeling, Leonardo of Pisa, later nicknamed Fibonacci in the 13th century, introduced a famous modeling problem in his arithmetic text *Liber Abaci* (1202). The exercise involves a hypothetical rabbit population with a simplified reproduction pattern. It begins with a single pair of immature rabbits (male and female) at the start of a breeding season. After one season, this pair matures and, from then on, produces one new pair of immature rabbits every season while remaining fertile indefinitely. Each new pair follows the same cycle, maturing after one season and reproducing each subsequent season.

Let P_n represent the number of rabbit pairs at the n-th reproductive stage, and normalize the reproductive period to a time step of 1, the dynamics can be expressed as:

$$P_{n+1} = P_n + P_{t-1}, \quad n = 2, 3, \ldots,$$

with initial conditions $P_0 = 1$ and $P_1 = 1$. This recursive formula generates the sequence: $1, 1, 2, 3, 5, 8, 13, \ldots$, known today as the Fibonacci sequence, where each term is the sum of the two preceding ones. This can be considered as the first population model. Another notable figure in the history of population dynamics is **Leonhard Euler**, a prolific mathematician and physicist. In 1748, he published the seminal treatise *Introductio in Analysin Infinitorum* (*Introduction to the Analysis of the Infinite*), which laid the foundation for modern mathematical analysis. Later, in 1760, Euler applied mathematical reasoning to demography in his paper *Recherches générales sur la mortalité et la multiplication du genre humain*, where he introduced the concept of geometric population growth, offering early insights into single-species population dynamics.

1.2 Single species continuous-time model

Population models have long provided a framework to understand how species grow and interact within ecosystems. Euler's treatment of geometric growth involved the formulation of mathematical expressions to describe how populations increase in size when

resources are unlimited and reproduction occurs continuously. Euler's work was revolutionary as it demonstrated the mathematical principles underlying population growth, influencing later scholars such as Thomas Malthus and Pierre-François Verhulst, who incorporated these ideas into more complex models. His contributions laid the groundwork for quantitative approaches in demography, ecology, and resource management, highlighting the significance of mathematical modeling in understanding biological systems. Early research, in the late 18th century, focused on single-species dynamics, beginning with Thomas Malthus's *An Essay on the Principle of Population* published in 1798 [1], take on exponential growth that assumes populations grow without limits when resources are abundant. Later, researchers interpreted the Malthusian model as described by the differential equation:

$$\frac{\mathrm{d}N}{\mathrm{d}t} = rN,$$

where N is the population size at time t and r is the per capita growth rate, assumed to be constant. This model predicts unbounded exponential growth, leading to the solution $N(t) = N_0 e^{rt}$, where N_0 is the initial population size. However, Malthus also noted that real populations rarely grow without limits, as resources are finite and environmental factors impose constraints.

Recognizing these limitations, Pierre-François Verhulst [19] introduced the logistic growth model in 1838, which incorporates the concept of carrying capacity, or the maximum population size that the environment can sustain. The logistic model is given by:

$$\frac{\mathrm{d}N}{\mathrm{d}t} = rN\left(1 - \frac{N}{K}\right),$$

where K is the carrying capacity. This model captures the idea that as N approaches K, the growth rate slows and eventually stabilizes, resulting in an S-shaped (sigmoidal) growth curve. The logistic growth model became a cornerstone in population ecology, as it reflects the self-limiting nature of population growth due to resource competition and environmental constraints, providing a more realistic framework than the exponential model for understanding population dynamics in isolated systems. In 1920, Raymond Pearl and Lowell Reed rediscovered the logistic equation and initiated a vigorous campaign to establish it as a fundamental "law of nature" in population dynamics.

The Gompertz model, introduced by Benjamin Gompertz in 1825 [20], is a widely recognized empirical model that analyses the mortality tables for describing the human

age distribution. The Gompertz function operates on the assumption that the mortality rate increases exponentially with age. As a result, the function represents the number of individuals surviving to a given age as a function of age. It has found many applications, particularly in modeling tumor growth.

1.3 Continuous-time predator-prey models

Following the foundational work on single-species models, researchers turned their attention to the interactions between multiple species, leading to the development of predator-prey models. These models aim to capture the feedback dynamics that arise when one species (the predator) depends on another species (the prey) for survival. Early mathematical formulations of prey-predator interactions were introduced in the early 20th century by Alfred Lotka (an American biophysicist) and Vito Volterra (an Italian mathematician and physicist), resulting in the well-known Lotka-Volterra model.

1.3.1 Lotka-Volterra model

The Lotka-Volterra (LV) model is a foundational framework to study population ecology, describing the interactions between predator and prey species through a system of differential equations. This model was independently developed by Alfred Lotka in 1925 and Vito Volterra in 1926. Lotka's work on the model emerged from his research on chemical reactions, where he noticed that predator-prey interactions could be described analogously to reactant interactions. In his book *Elements of Physical Biology* (1925) [2], Lotka applied these ideas to biological systems, presenting the model as a way to understand population oscillations in predator-prey dynamics.

Volterra [3], meanwhile, came upon the equations after studying the biomass pattern of fish populations in the Adriatic Sea. Volterra formulated a mathematical model to capture how predators and prey interact, showing that, under certain conditions, populations of both species oscillate in regular cycles. The model is given by the system:

$$\frac{\mathrm{d}x}{\mathrm{d}t} = \alpha x - \beta xy, \quad \frac{\mathrm{d}y}{\mathrm{d}t} = \delta xy - \gamma y,$$

where x and y represent the prey and predator population, α and γ are the per capita growth and death rates of prey and predators, respectively, and β and δ represent the rates at which predators encounter prey and convert them into predator biomass.

The Lotka-Volterra model provided a mathematical basis for understanding predator-prey interactions and demonstrated how two populations could cyclically fluctuate without external influences. Although the model makes simplifying assumptions—such as constant rates and no resource limits—it has been pivotal in advancing ecological theory and has inspired numerous extensions to study more complex and realistic ecological dynamics.

1.3.2 Logistic Lotka-Volterra model

The logistic Lotka-Volterra model is an adaptation of the traditional LV predator-prey system that incorporates density-dependent limitations on prey growth. The model is given by

$$\begin{aligned}\frac{\mathrm{d}x}{\mathrm{d}t} &= rx\left(1-\frac{x}{K}\right)-axy,\\ \frac{\mathrm{d}y}{\mathrm{d}t} &= baxy-dy,\end{aligned}$$

where $x(t)$ and $y(t)$ denote the prey and predator populations at time t, respectively. The prey population grows logistically with intrinsic growth rate r and carrying capacity K, while a is the predation rate coefficient, b is the conversion efficiency of prey into predator offspring, and d is the specific death rate of predators.

In contrast to the classical Lotka-Volterra model, which assumes exponential growth of prey in the absence of predators, the logistic version accounts for limited resources by introducing a carrying capacity. The classical LV model shows oscillatory behavior, specifically closed orbits around a non-trivial interior equilibrium, while the logistic model can exhibit damped oscillatory, or even non-oscillatory dynamics depending on parameters.

1.3.3 Rosenzweig-MacArthur model

The Rosenzweig-MacArthur (RM) model [4] is an extension of the classic Lotka-Volterra predator-prey model, introduced by Michael L. Rosenzweig and Roy H. MacArthur in the 1960s to address some limitations of the original model. The Lotka-Volterra model assumes a linear functional response, meaning that predator consumption increases indefinitely with prey density. However, in natural systems, predators often exhibit a saturating or "Type II" functional response, where consumption rate plateaus as prey density increases due to factors like handling time. The Rosenzweig-MacArthur model is presented by the following system of equations:

$$\frac{\mathrm{d}x}{\mathrm{d}t} = rx\left(1 - \frac{x}{K}\right) - \frac{axy}{1 + aTx},$$
$$\frac{\mathrm{d}y}{\mathrm{d}t} = y\left(\frac{bax}{1 + aTx} - d\right),$$

where x represents the prey population, y represents the predator population, r is the intrinsic growth rate of the prey, and K is the carrying capacity of the environment for the prey. The parameters a and T represent the predator's attack rate and handling time, respectively, while b is the efficiency with which predators convert consumed prey into offspring, and d is the predator's mortality rate. Taking $\alpha = \frac{1}{T}$, $h = \frac{1}{aT}$, and $\beta = b\alpha$, the model can be written as:

$$\frac{\mathrm{d}x}{\mathrm{d}t} = rx\left(1 - \frac{x}{K}\right) - \frac{\alpha xy}{h + x},$$
$$\frac{\mathrm{d}y}{\mathrm{d}t} = y\left(\frac{\beta x}{h + x} - d\right).$$

We will use this form of RM model throughout this thesis.

The Rosenzweig-MacArthur model introduced new ecological insights by predicting conditions under which predator-prey systems could exhibit stable equilibrium, sustained oscillations. This model has been influential in theoretical ecology, as it demonstrates the complexity of predator-prey interactions and highlights the importance of incorporating realistic functional responses into ecological models.

There are many other predator-prey models like the Leslie-Gower model (1960) [21] and Beddington–DeAngelis model (1975) [22]. We can obtain other predator-prey models by incorporating different functional responses, fear effect, Allee effect, hunting corporation and so on.

1.4 Single species discrete-time models

Discrete-time models are particularly well-suited for species with non-overlapping generations, where individuals from one generation do not coexist with those from the next. Examples include many insects, such as certain species of moths and cicadas, as well as annual plants that complete their life cycles within a single season. In these cases, population changes occur in discrete steps, typically reflecting seasonal breeding.

Early work in the 1950s and 1960s recognized that continuous-time models, while insightful, did not capture the step-wise changes often observed in species like insects,

annual plants, and certain fish. The pioneering contributions of ecologists such as Robert May in the 1970s popularized discrete-time approaches by highlighting their ability to generate complex dynamics, including oscillations and chaos, in response to simple rules in continuous-time model. May's work,entitled *Stability and Complexity in Model Ecosystems* (1973) [23], highlighted the power of discrete models in understanding population dynamics. He [24] discussed the discrete-time logistic growth model:

$$x_{n+1} = rx_n(1 - x_n), \tag{1.4.1}$$

where x_n is the population size at time step n. This foundational work spurred extensive research on discrete ecological models, particularly for species with distinct generational structures. In 1954, Bill Ricker [25], proposed another key model for populations with non-overlapping generations, often used in fish and insect studies. The **Ricker model** (1954, 1958) is given by:

$$x_{n+1} = x_n e^{r\left(1-\frac{x_n}{K}\right)},$$

where the exponential term allows for more variability, producing oscillations, and even chaos at high growth rates. Together, these discrete-time models are essential for studying the complex population dynamics.

The Beverton-Holt model is a fundamental discrete-time population model used in ecology to describe the dynamics of a population with density-dependent regulation [26]. Originally introduced by Beverton and Holt (1957) in the context of fisheries, this model provides insights into population regulation under limited resources. The model is given by the recurrence relation

$$x_{n+1} = \frac{R_0 x_n}{1 + x_n/M},$$

where x_n represents the population size at time step n, R_0 is the per-generation proliferation rate, and M is a parameter related to resource availability. The model exhibits a carrying capacity $K = (R_0 - 1)M$, which represents the maximum sustainable population size in the environment. Unlike chaotic or oscillatory discrete-time models, the Beverton-Holt model always converges to a stable equilibrium, making it particularly useful for studying populations where overcompensation effects are minimal. Its application extends beyond fisheries to various ecological and conservation studies where resource constraints shape population growth.

1.5 Discretization process

The discretization process in population modeling involves converting continuous-time models into discrete-time formulations to solve the continuous differential equations using difference equations. Discretization is commonly achieved by replacing the continuous-time derivatives with finite difference approximations or by applying suitable discrete analogs that preserve most of the behavior of the continuous model. Some discretization methods are:

(i) **Forward Euler's scheme**:

The Forward Euler's scheme is one of the simplest and most widely used methods for discretizing differential equations. Mathematically, the Forward Euler's method for a autonomous differential equation $\frac{\mathrm{d}x}{\mathrm{d}t} = f(x)$ is expressed as:

$$x_{n+1} = x_n + \Delta t \cdot f(x_n),$$

where x_n is the state x at time $t = t_n$ and Δt is the step size. This method is computationally simple and easy to implement but can lead to numerical instability if the time step Δt is too large or if the system exhibits stiff behavior. Despite its limitations, the Forward Euler's scheme is widely used for its simplicity and as a starting point for more advanced discretization techniques in solving differential equations.

(ii) **Method of Piecewise Constant Argument**:

One way to discretize a continuous-time population model is by using the piecewise constant argument method as introduced by Shah (1983). Consider the continuous-time system given by the following equations:

$$\frac{\mathrm{d}x}{\mathrm{d}t} = xf(x(t)),$$

The system can be rewritten as:

$$\frac{1}{x(t)}\frac{\mathrm{d}x(t)}{\mathrm{d}t} = f(x[t]),$$

where $[t]$ denotes the integer part of t, meaning $t \in [n, n+1)$ corresponds to $[t] = n$ for $n = 0, 1, 2, \ldots$. Therefore, $x(t)$ can be written as $x(n)$ for $t \in [n, n+1)$.

Under this formulation, the system is updated with constant rate functions over

each time interval $t \in [n, n+1)$. Thus, the system becomes:

$$\frac{1}{x(t)}\frac{\mathrm{d}x(t)}{\mathrm{d}t} = f(x(n)),$$

where $f(x(n)$ is constant over the interval $t \in [n, n+1)$.

We now integrate the system over the interval $t \in [n, n+1)$. This results in:

$$\ln(x(t))\Big|_n^t = f(x(n))(t-n),$$

which simplifies to: $x(t) = x(n)\exp\left(f(x(n))(t-n)\right),$

By taking $t \to n+1$, we obtain the discretized model:

$$x(n+1) = x(n)\exp\left(f(x(n))\right),$$

which is the desired discretized model.

(iii) **Non-Standard Finite Difference (NSFD) scheme**:

The Non-Standard Finite Difference (NSFD) scheme is a method for discretizing differential equations [27], to solve in a cost effective manner. Unlike standard methods, which use simple linear approximations, NSFD introduces modifications to account for the system's nonlinearity and stability properties, ensuring more accurate and feasible numerical solutions. These adjustments prevent issues like negative populations and nonphysical oscillations, making NSFD especially useful in modeling real-world systems. We begin with a continuous differential equation describing the dynamics of the system, where the rate of change of the dependent variable $x(t)$ is given by a function $f(x(t))$,

$$\frac{\mathrm{d}x}{\mathrm{d}t} = f(x(t)).$$

Here, we discretize the continuous equation using a standard finite difference method, where the time derivative is approximated by the difference between the function values at consecutive time steps.

$$\frac{\mathrm{d}x(t)}{\mathrm{d}t} \approx \frac{x(t+h)-x(t)}{\phi(h)} \quad \Rightarrow \quad x(t+h) = x(t) + \phi(h)f(x(t))$$

with $0 < \phi(h) < 1$ and $\phi(h) \to 0$ as $h \to 0$. We modify the function $f(x(t))$ in a non-local representation to ensure more accurate and stable results in the numerical solution. This avoids issues like negative values for variables that should always be positive. We will show this process of NSFD through an example soon.

1.6 Discrete-time models using discretization

1.6.1 Single species models

The well-known single species models discussed in section 1.4 can be obtained by discretizing the continuous-time logistic growth model, viz,

$$\frac{\mathrm{d}N}{\mathrm{d}t} = rN\left(1 - \frac{N}{K}\right),$$

using different discretization schemes. Let $f(N) = rN\left(1 - \frac{N}{K}\right)$.

(i) *Derivation of the Logistic Map*: Euler's method for numerical integration is given by:

$$N_{n+1} = N_n + h\frac{\mathrm{d}f}{\mathrm{d}t}.$$

Substituting the logistic equation:

$$N_{n+1} = N_n + h \cdot rN_n\left(1 - \frac{N_n}{K}\right).$$

Define the normalized population: $x_n = N_n/K$. Thus, we rewrite N_n in terms of x_n: $N_n = Kx_n$. Substituting this into the discrete equation:

$$Kx_{n+1} = Kx_n + hrKx_n(1 - x_n).$$

$$\begin{aligned} \text{i.e.,} \quad x_{n+1} &= x_n + hrx_n(1 - x_n) \\ &= x_n(1 + hr) - hrx_n^2 \\ \Rightarrow \quad \frac{hr}{1+hr}x_{n+1} &= \frac{hr(1+hr)}{1+hr}x_n\left(1 - \frac{hr}{1+hr}x_n\right) \end{aligned}$$

Take $\dfrac{rh}{1+rh}x_n = X_n$, then we have,

$$X_{n+1} = (1 + rh)X_n(1 - X_n),$$

which is the standard logistic map: $X_{n+1} = aX_n(1 - X_n)$, with $a = 1 + rh$.

(ii) *Derivation of the Ricker model*: Following the approach of the *method of piecewise constant argument*, the logistic growth equation is rewritten as:

$$\frac{1}{N(t)}\frac{\mathrm{d}N(t)}{\mathrm{d}t} = r\left(1 - \frac{N([t])}{K}\right),$$

where $[t]$ is the integer part of t, and $t \in (0, \infty)$. Then, $[t] = n$ for $t \in [n, n+1)$. Hence, $N([t]) = x(n)$. The equation can be rewritten as:

$$\frac{1}{N(t)} \frac{\mathrm{d}N(t)}{\mathrm{d}t} = r\left(1 - \frac{N(n)}{K}\right).$$

Integrating the system on the intervals $t \in [n, n+1)$ with $n = 0, 1, 2, ...$, we obtain

$$\ln(N(t))|_n^t = r\left(1 - \frac{N(n)}{K}\right)(t - n).$$

Note that, $N(t) > 0$, for positive initial population in continuous logistic map.

$$N(t) = N(n)e^{r(1-N(n)/K)}(t - n).$$

By taking $t \to n + 1$, we derive the discretized model,

$$N_{n+1} = N_n e^{r(1-N_n/K)}.$$

We redefine as: $x_n = N_n/K$.

Substituting this into the recurrence relation, we get the well-known Ricker model:

$$x_{n+1} = x_n e^{r(1-x_n)}.$$

(iii) *Derivation of the Beverton-Holt Model*: Applying the standard forward difference approximation to logistic growth model, with $h = 1$ and non-local representation of N^2 as $N_{n+1}N_n$, we obtain,

$$N_{n+1} - N_n = rN_n - r\frac{N_{n+1}N_n}{K}.$$

$$N_{n+1} = \frac{(r+1)N_n}{1 + r\dfrac{N_n}{K}}$$

Before changing the notation, we introduce x_n as a normalized form of N_n to simplify the mathematical expressions and align with standard discrete-time population models. Defining $R_0 = (r + 1)$ and $M = \dfrac{K}{r}$, we obtain:

$$x_{n+1} = \frac{R_0 x_n}{1 + x_n/M},$$

which is the Beverton-Holt model.

1.6.2 Multi-species models

As we show in the last section, the independent single-species discrete-time models can be derived from the continuous-time logistic growth model. One example of an independent discrete-time multi-species model is the Nicholson-Bailey model, which serves as a standard model for host-parasitoid interactions. The Nicholson-Bailey model [28] is a classic discrete-time predator-prey model developed by A. J. Nicholson and V. A. Bailey in the 1930s to describe host-parasitoid interactions. Unlike typical predator-prey models, which focus on predators that consume multiple prey, the Nicholson-Bailey model specifically addresses parasitoids, which lay eggs in or on host organisms, resulting in the death of the host. The model describes population changes over generations, assuming that each parasitoid targets one host and that host populations do not overlap across generations. The model is defined by the equations:

$$H_{t+1} = rH_t e^{-aP_t},$$
$$P_{t+1} = H_t \left(1 - e^{-aP_t}\right),$$

where H_t and P_t represent the host and parasitoid populations at time t, r is the reproductive rate of the host, and a is the searching efficiency of the parasitoid. The Nicholson-Bailey model was groundbreaking in demonstrating how specific interactions, such as host-parasitoid relationships, could lead to population oscillations. Hupfaker [29] examined the interactions between the six-spotted mite *Eotetranychus sexmaculatus* and the predatory mite *Typhlodromus occidentalis*, offering empirical support for the Nicholson-Bailey model.

We can obtain the multi-species discrete-time models by discretizing the continuous models using the methods discussed in previous section 1.5. In particular, our thesis, we will derive discrete-time models from Rosenzweig-MacArthur system using Euler's and method of piecewise constant argument in chapters 2 and 3, respectively.

1.7 Preliminary stability results

For any m-dimensional discrete-time model,

$$X_{n+1} = F(X_n),\ X \in \mathbb{R}^m,$$

the fixed (or equilibrium) points are given by

$$X_{n+1} = X_n \Longrightarrow F(X_n) = X_n.$$

The stability of the equilibrium points (X^*) is determined by the eigenvalues of the Jacobian matrix

$$J(X^*) = \frac{\partial F}{\partial X}(X^*)$$

derived from the model. The following lemmas characterize the nature of stability of the equilibria.

Lemma 1.1. *[30] Consider a fixed point (x^*, y^*) of a discrete-time system. Let λ_1 and λ_2 be the eigenvalues of the Jacobian matrix evaluated at this point. Then:*

(I) The point (x^*, y^*) is locally asymptotically stable (a sink) if $|\lambda_1| < 1$ and $|\lambda_2| < 1$;

(II) It is unstable (a source) if $|\lambda_1| > 1$ and $|\lambda_2| > 1$;

(III) It is a saddle point (partially stable) if one eigenvalue lies inside the unit circle and the other outside, i.e., either $|\lambda_1| > 1$ and $|\lambda_2| < 1$, or $|\lambda_1| < 1$ and $|\lambda_2| > 1$;

(IV) The point is non-hyperbolic if at least one eigenvalue has modulus exactly equal to one, that is, $|\lambda_1| = 1$ or $|\lambda_2| = 1$.

Lemma 1.2. *[30] Let the Jacobian matrix at the equilibrium point (x^*, y^*) have characteristic polynomial given by $C(\lambda) = \lambda^2 - a\lambda + b$, and let λ_1 and λ_2 be its eigenvalues (i.e., the roots of $C(\lambda) = 0$). Then:*

(I) Both eigenvalues lie inside the unit circle, i.e., $|\lambda_1| < 1$ and $|\lambda_2| < 1$, if and only if $C(1) > 0$, $C(-1) < 0$, and $b < 1$;

(II) Both eigenvalues lie outside the unit circle, i.e., $|\lambda_1| > 1$ and $|\lambda_2| > 1$, if and only if $C(1) > 0$ and $b > 1$;

(III) The equilibrium is a saddle point (i.e., exactly one eigenvalue has modulus greater than one) if and only if $C(1) > 0$ and $C(-1) < 0$;

(IV) Exactly one eigenvalue lies on the unit circle (with modulus one) while the other does not if and only if $C(1) > 0$, $C(-1) = 0$, and $a \neq 0, 2$;

(V) The eigenvalues are complex conjugates with modulus one if and only if $C(1) > 0$, $a^2 - 4b < 0$, and $b = 1$.

1.8 Bifurcations in discrete-time models

Discrete-time models can exhibit complex dynamical phenomena through bifurcations, where small changes in parameters lead to qualitative shifts in system behavior. Two prominent types of bifurcations in these models are the flip bifurcation and the Neimark-Sacker bifurcation. In a flip (or period-doubling) bifurcation, as a parameter crosses a critical value, a stable fixed point becomes unstable, giving rise to a stable period-2 cycle. The Neimark-Sacker bifurcation, on the other hand, occurs when a fixed point loses stability and gives birth to an invariant closed curve, inducing quasiperiodic behavior. These bifurcations are essential for understanding the onset of oscillatory and chaotic dynamics in discrete-time models, providing insight into phenomena like predator-prey cycles and the transition to complex ecological behaviors.

Lemma 1.3. *[31] Consider a discrete-time system*

$$X_{n+1} = F(X_n),\ X \in \mathbb{R}^m,$$

with a fixed point X^*. The system undergoes different types of bifurcations based on the eigenvalues of the Jacobian matrix $J(X^*)$ evaluated at X^*:

(i) ***Flip (Period-Doubling) Bifurcation:*** *A flip bifurcation occurs when one eigenvalue of $J(X^*)$ satisfies $\lambda = -1$. This results in the birth of a period-2 orbit from the coexisting equilibrium.*

(ii) ***Neimark-Sacker (Torus) Bifurcation:*** *A Neimark-Sacker bifurcation occurs when a complex conjugate pair of eigenvalues satisfies $|\lambda_{1,2}| = 1, \quad \lambda_{1,2} = e^{\pm i\theta}, \quad \theta \neq 0, \pi$. This leads to the emergence of an invariant closed curve around the fixed point.*

(iii) ***Saddle-Node (Fold) Bifurcation:*** *A saddle-node bifurcation occurs when one eigenvalue satisfies $\lambda = 1$. This results in the creation or annihilation of two fixed points.*

In the bifurcation diagram of the logistic map (1.4.1), a period-doubling bifurcation marks the onset of increasingly complex dynamics as r is raised. For values of $r < 3$, the system has a stable fixed point, but as r increases beyond the critical threshold $r = 3$, this fixed point loses stability, giving rise to a stable period-2 cycle. As r continues to increase, a series of period-doubling bifurcations occurs, with each successive bifurcation introducing cycles of progressively higher periods (period-4, period-8, etc.). This cascade

continues until the system reaches a chaotic regime (Figure 1.8.1). As we have seen earlier, logistic map is used to characterize single species dynamics. This route to chaos via period-doubling is a universal phenomenon observed not only in population models but also in many other nonlinear systems, illustrating how simple deterministic equations can produce rich and intricate patterns of behavior.

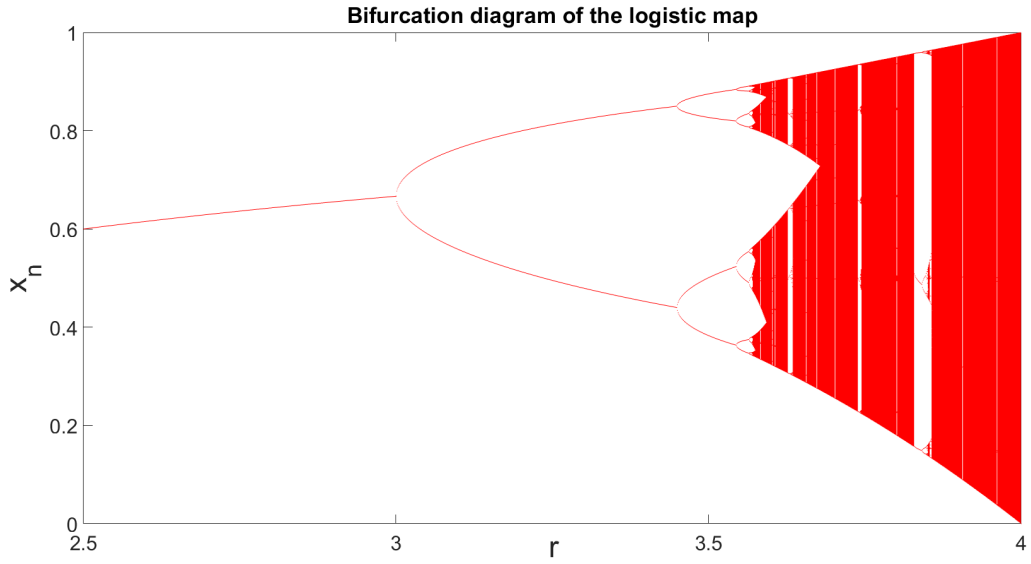

Figure 1.8.1: Flip Bifurcation in logistic map $x_{n+1} = rx_n(1 - x_n)$ for $2.5 < r < 4$.

To demonstrate a Neimark–Sacker bifurcation, a two-dimensional map is required. In this thesis, we will discuss this bifurcation in detail across different chapters.

1.9 Chaos and its quantification

Strogatz [32] defines chaos as *"Chaos is aperiodic long-term behavior in a deterministic system that exhibits sensitive dependence on initial conditions."* "Aperiodic long-term behavior" refers to trajectories that do not converge to fixed points, periodic cycles, or invariant closed curves as time progresses toward infinity. The term "deterministic" implies that the system evolves without any random inputs or noise affecting the dynamics."Sensitive dependence on initial conditions" means that nearby trajectories diverge at an exponential rate, making long-term prediction practically impossible despite the deterministic nature of the system. One classic example is the logistic map (1.4.1), where chaos appears as the growth rate r increases beyond a critical threshold. The study of

chaos in population models provides valuable insights into population stability, extinction risks, and the resilience of ecosystems under varying environmental conditions.

The Lyapunov exponent is a key measure for identifying chaos in dynamical systems, capturing the rate at which nearby trajectories diverge over time. In a one-dimensional system, such as the logistic map, the Lyapunov exponent Λ quantifies the average exponential rate of separation between two initially close points. If $\Lambda > 0$, trajectories diverge, indicating chaotic behavior, while $\Lambda < 0$ suggests that trajectories converge, leading to stable, predictable dynamics. In case of $\Lambda = 0$, the sytem shows quasiperiodic behavior which is defined as follows:

Definition 1.4. [32]: Quasiperiodic motion is characterized by the presence of two or more incommensurate frequencies. The motion never repeats but it is not chaotic—the trajectory lies on a torus and is bounded.

In higher-dimensional systems, multiple Lyapunov exponents exist, corresponding to each dimension of the phase space. The largest Lyapunov exponent typically determines the system's overall stability: a positive value signifies chaos, while all negative exponents indicate convergence to a fixed point or a stable cycle. Calculating the full spectrum of Lyapunov exponents allows for a more detailed understanding of complex systems, revealing structures like strange attractors and quasiperiodic behavior. Lyapunov exponents thus provide a quantitative tool to differentiate between order and chaos, making them essential for analyzing stability and unpredictability.

Definition 1.5. [11]: Let $\mathbf{f}$ be a smooth map of the real line. The Lyapunov number $L(x_1)$ of the orbit $x_1, x_2, x_3, \ldots$ is defined as

$$L(x_1) = \lim_{n\to\infty} \left(|f'(x_1)| \cdot |f'(x_2)| \cdots |f'(x_n)|\right)^{\frac{1}{n}},$$

if this limit exists. The Lyapunov exponent $\Lambda(x_1)$ is then given by

$$\Lambda(x_1) = \lim_{n\to\infty} \frac{1}{n} \left(\ln|f'(x_1)| + \ln|f'(x_2)| + \cdots + \ln|f'(x_n)|\right),$$

if this limit exists.
Note that $\Lambda(x_1)$ exists if and only if $L(x_1)$ exists and is nonzero, with $\ln L(x_1) = \Lambda(x_1)$.

For a map on $\mathbb{R}^m$, each orbit has m Lyapunov numbers, which measure the rates of separation from the current orbit point along m orthogonal directions.

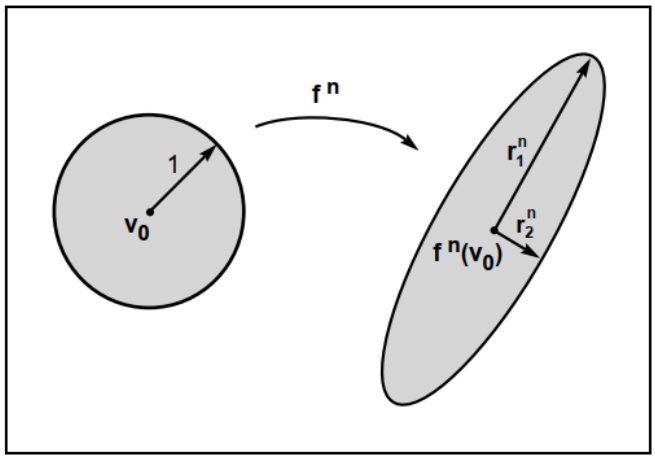

Figure 1.9.1: Evolution of initial infinitesimal disk into ellipse after n iterations in two-dimensional maps.(Source: *Figure5.1, page194 [11]*)

.

Definition 1.6. [11]: For m-dimensional maps, let $\mathbf{f}$ be a smooth map on $\mathbb{R}^m$, let $J_n = \mathbf{Df}^n(v_0)$, and for $k = 1, \ldots, m$, let r_n^k represent the length of the k-th longest orthogonal axis of the ellipsoid $J_n N$ (N is a unit circle in $\mathbb{R}^m$) along an orbit with initial point v_0. The value r_n^k thus measures the rate of expansion or contraction near the orbit of v_0 over the first n iterations. The k-th Lyapunov number of v_0 is then defined as

$$L_k = \lim_{n\to\infty} (r_n^k)^{\frac{1}{n}},$$

if this limit exists. The k-th Lyapunov exponent of v_0 is $\Lambda_k = \ln L_k$. By definition, the Lyapunov exponents are ordered such that $\Lambda_1 \geq \Lambda_2 \geq \cdots \geq \Lambda_m$, and correspondingly, $L_1 \geq L_2 \geq \cdots \geq L_m$.

The Lyapunov exponent spectrum for a four-dimensional continuous and discrete-time system is stated below.

Dynamics	**Lyapunov Exponent Spectrum**
Fixed point	$\Lambda_1 < 0, \Lambda_2 < 0, \Lambda_3 < 0, \Lambda_4 < 0$
Periodic cycle	$\Lambda_1 = 0, \Lambda_2 < 0, \Lambda_3 < 0, \Lambda_4 < 0$
Quasiperiodic	$\Lambda_1 = 0, \Lambda_2 = 0, \Lambda_3 < 0, \Lambda_4 < 0$
Chaos	$\Lambda_1 > 0, \Lambda_2 < 0, \Lambda_3 < 0, \Lambda_4 < 0$

Table 1.9.1: Lyapunov Exponent Spectrum for different dynamical behaviors of a continuous-time system [12].

Dynamics	Lyapunov Exponent Spectrum
Fixed point or periodic cycle	$\Lambda_1 < 0, \Lambda_2 < 0, \Lambda_3 < 0, \Lambda_4 < 0$
Quasiperiodic	$\Lambda_1 = 0, \Lambda_2 < 0, \Lambda_3 < 0, \Lambda_4 < 0$
Chaos	$\Lambda_1 > 0, \Lambda_2 < 0, \Lambda_3 < 0, \Lambda_4 < 0$

Table 1.9.2: Lyapunov Exponent Spectrum for different dynamical behaviors of a discrete-time system [13–16].

To find the Lyapunov exponents, the algorithm provided by Wolf *et al.* [33] is used in this thesis.

1.10 Outline of the Thesis

This thesis consists of five chapters. Chapter 1 is the introduction containing the brief history of population models and preliminaries required for the analysis done in rest of the chapters. We discuss three discrete-time predator-prey models on rest of the chapters.

In chapter 2, we study a discrete-time version of the classical RM predator–prey model, derived using the forward Euler's method with unit step size. Our goal is to understand how varying model parameters, such as prey carrying capacity and harvesting rates, influence coexisting equilibrium stability and long-term behavior. One of the main questions we ask is: Does increase in nutrient supply of the prey always help the predator, or can it make the system unstable? We find the conditions for which the system experiences a Neimark-Sacker bifurcation. As the carrying capacity increases, the system goes through a Neimark–Sacker bifurcation, leading to complex patterns such as quasiperiodic motion, periodic windows, period-bubbling, and chaos. Next, we look at how different types of long-term behaviors (like periodic or chaos) can coexist depending on the initial condition. We also study the basins of attraction for different types of multistability. Finally, we vary the harvesting rate of prey or predator independently and examine whether it makes the system stable or induces new complex dynamics. We calculate the mean density under the influence of harvesting and find the presence of hydra effects, the recently highlighted paradoxical phenomena.

Chapter 3 investigates a discrete-time predator–prey system derived from the same classical Rosenzweig–MacArthur model using the piecewise constant argument. This discretization scheme maintains the non-negativity of the solutions which was not the case in

the discrete-time model in chapter 2. Also, increase carrying capacity in chapter 2 leads to a Neimark-Sacker bifurcation, we would like to investigate that if this discretization scheme can induce flip bifurcation at the coexisting equilibrium or whether increase in carrying capacity can lead to stabilization of the coexisting equilibrium. These questions motivate us to discretize the same model using the method of piecewise constant argument. The aim is to explore how variations in prey carrying capacity and harvesting efforts influence the system's dynamics. We focus on identifying and analyzing different types of bifurcations at equilibrium, including complex behaviors such as periodicity, quasiperiodicity, and chaos. The study also examines the emergence of multistability and the structure of basins of attraction when multiple stable states coexist. Furthermore, we explore the dynamics in two-parameter spaces involving prey and predator harvesting rates, with special attention to the appearance of organized structures such as Arnold tongues and shrimp-like patterns. Finally, we consider the ecological implications of predator harvesting, including the possibility of counter-intuitive responses such as the hydra effect.

Chapter 4 focuses on a discrete-time predator–prey model in a homogeneous two-patch environment, incorporating the dispersal of both prey and predator species. The model assumes that within each isolated patch, both the species have logistic growth and the predation process is followed by the Holling type-II functional response. The main objective is to study how prey and predator dispersal, considered independently and jointly, affect the existence and stability of equilibria and the overall dynamics of the system. We analyze various bifurcations and transitions that arise as dispersal rates are varied. Particular attention is given to exploring periodic, and quasiperiodic as well as complex spatial dynamics. A two-parameter space analysis is also conducted to examine the effects of coupled dispersal rates on system behavior. Additionally, we investigate the population stock patterns of both species, aiming to gain insights into the ecological implications of movement in spatially structured environments.

In Chapter 5, we summarize all findings from all this thesis. Therein, we also outlines potential avenues for future research, highlighting areas of interest from both mathematical and ecological dynamics perspectives.

CHAPTER 2

A discretized Rosenzweig-MacArthur model with harvesting using forward Euler's scheme

2.1 Introduction

In this chapter *, we analyze a discretized model of the continuous-time Rosenzweig-MacArthur predator-prey system with harvesting. One of the ways to discretize the continuous system is using the forward Euler's scheme with integral time step, say δ, $\delta > 0$. Several researchers such as Hadeler and Gerstmann [5], Salman *et al.* [34], Cheng and Cao [35], Hu and Cao [36], Liu and Xiao [37], Rana and Kulsum [38], Ajaz *et al.* [6], and reference therein have used this scheme for discretization and varied δ as a bifurcation parameter. Hu and Cao [36] stated that changing the integral step size, δ, makes difference in global and local stability of the corresponding discrete-time system. As a special case, Liu and Cai [7] used a fixed integral step size ($\delta = 1$) in their discrete model, which exhibited complex dynamics such as invariant circles, superstable phenomena, period-doubling cascades, and chaotic sets. An alternative discretization method, employing the technique of piecewise constant arguments for differential equations, is presented by Din [39], Ishaque *et al.* [40], Khan [41], and the references therein. In these discretized systems, they demonstrated the non-negativity and uniform boundedness of solutions, as well as the existence and uniqueness of positive steady states, which are challenging to prove using Euler's discretization method. Rech [42] compared two discrete-time predator-prey models obtained from a same continuous-time system using the above two discretization schemes. He observed that the stability region in two-parameter plane were somewhat similar over a wide range of parameter space, showing chaos, quasiperiodicity, and periodicity. However, the system obtained using Euler's discretization offers a large domain of unbounded orbits which "escape" to infinity.

The increment of carrying capacity of prey species may lead to predator extinction. This phenomenon is called as the paradox of enrichment [43–47]. Weide *et al.* [46] reported that in a Nicholson-Bailey framework based discrete-time predator-prey model, increase in carrying capacity destabilizes the system. Recently, Pattanayak *et al.* [47] observed that increasing carrying capacity of the resource level species results in extinction of species at

* This chapter based on the following article: **Rajni, Bapan Ghosh**, Multistability, chaos and mean population density in a discrete-time predator–prey system, *Chaos, Solitons & Fractals,* 162 (2022), 112497.

higher trophic level (bottom-up effect). They showed that varying the carrying capacity induced bistability into the system.

The effect of harvesting on the population dynamics models has been a matter of great importance. It is necessary to find an ecologically stable method for harvesting the maximum yield with minimum effort. The systems, including the harvesting factor, show different kinds of bifurcations and complex behavior depending on the harvest rate and strategies. In chaotic systems, increase in harvesting rate leads to the stability of the stable equilibrium state (Liz and Ruiz-Herrera [48], and Weide *et al.* [46]). In a population model incorporating age-specific harvesting, Neverova *et al.* [49] demonstrated that the system exhibits different multistable states when adult individuals are harvested.

The chapter is divided into different sections as follows: In section 2.2, we discretize the continuous-time model. The existence and stability of the fixed points of the system is discussed in section 2.3. Section 2.4 deals with normal form analysis of bifurcations at the coexisting equilibrium point of the model. The dynamics of the unharvested (varying carrying capacity), prey harvested, and predator harvested system for fixed values of other parameters are examined in section 2.5. In the last section 2.6, conclusion of the whole analysis is presented.

2.2 Model Formulation

The continuous-time Rosenzweig-MacArthur (RM) model under harvesting is,

$$\begin{aligned} \frac{\mathrm{d}x}{\mathrm{d}t} &= rx\left(1-\frac{x}{K}\right)-\frac{\alpha xy}{h+x}-q_1e_1x, \\ \frac{\mathrm{d}y}{\mathrm{d}t} &= \frac{\beta xy}{h+x}-my-q_2e_2y. \end{aligned} \tag{2.2.1}$$

Here, x and y are population densities of prey and predator species at any time t, with initial population $x(0) > 0$ and $y(0) > 0$, respectively. The parameters have the same meaning as mentioned in subsection 1.3.3. Further, e_1 and e_2 serve as harvesting efforts with q_1 and q_2 as catchability coefficients of the prey and predator population, respectively. This particular harvesting strategy is referred as constant-effort harvesting [50]. Interested readers could learn how a constant-yield harvesting may destroy populations as revealed by Huang *et al.* [50].

The first way that we use to discretize (2.2.1) by using forward Euler's scheme with integral step size as unity. May [24] and Alligood *et al.* [11] have explored the dynamics

of the logistic map. However, one can construct a similar logistic map by discretizing the logistic differential equation with Euler's scheme. This motivates us to discrete the model (2.2.1) by using the forward Euler scheme with an integral step size of one. If x_n and y_n represent the population size of prey and predator species at time n then the discretized model is given by

$$\begin{aligned} x_{n+1} &= x_n + rx_n\left(1-\frac{x_n}{K}\right) - \frac{\alpha x_n y_n}{h+x_n} - q_1 e_1 x_n, \\ y_{n+1} &= y_n + \frac{\beta x_n y_n}{h+x_n} - m y_n - q_2 e_2 y_n, \end{aligned} \tag{2.2.2}$$

with initial condition $x_0 = x(0)$ and $y_0 = y(0)$. The system of difference equations (2.2.2) can be written in mapping form as follows:

$$\begin{pmatrix} x \\ y \end{pmatrix} \longmapsto \begin{pmatrix} x + rx\left(1-\frac{x}{K}\right) - \frac{\alpha xy}{h+x} - q_1 e_1 x \\ y + \frac{\beta xy}{h+x} - my - q_2 e_2 y \end{pmatrix}. \tag{2.2.3}$$

We will be analyzing the different dynamics exhibited by the map (2.2.3) due varying carrying capacity of prey population, and harvesting effort on both the species separately.

2.3 Fixed points and stability analysis

In this section, we find the fixed points of the map (2.2.3) and determine their stable behavior. The fixed points of the map (2.2.3) are computed from

$$\begin{aligned} x + rx\left(1-\frac{x}{K}\right) - \frac{\alpha xy}{h+x} - q_1 e_1 x &= x, \\ y + \frac{\beta xy}{h+x} - my - q_2 e_2 y &= y. \end{aligned}$$

Clearly, $E^0 = (0,0)$ is the trivial fixed point and $E^b = \left(K(1-\frac{q_1 e_1}{r}), 0\right)$ is the boundary fixed point of system (2.2.2). The coexisting fixed point can be obtained by solving

$$\begin{aligned} r\left(1-\frac{x}{K}\right) - \frac{\alpha y}{h+x} - q_1 e_1 &= 0, \\ \frac{\beta x}{h+x} - m - q_2 e_2 &= 0. \end{aligned}$$

The coexisting fixed point is $E^*(x^*, y^*) = \left(\frac{h(m+q_2e_2)}{\beta-m-q_2e_2}, \frac{\beta h(K(\beta-m-q_2e_2)(r-q_1e_1)-rh(m+q_2e_2))}{K\alpha(\beta-m-q_2e_2)^2}\right)$.
In the unharvested system, the coexisting equilibrium $E_u^*(x_u^*, y_u^*) = \left(\frac{mh}{\beta-m}, \frac{\beta hr(K\beta-mK-mh)}{K\alpha(\beta-m)^2}\right)$ exists iff $\beta > m$ and $K > \frac{mh}{(\beta-m)}$.
When only prey is harvested (i.e., $e_2 = 0$), $E_{e_1}^*(x_{e_1}^*, y_{e_1}^*) = \left(\frac{hm}{\beta-m}, \frac{\beta h(K(\beta-m)(r-q_1e_1)-rhm)}{K\alpha(\beta-m)^2}\right)$

exists iff $0 < e_1 < \frac{r(K(\beta-m)-mh)}{K(\beta-m)q_1}$.

When only predator is harvested (i.e., $e_1 = 0$),

$$E^*_{e_2}(x^*_{e_2}, y^*_{e_2}) = \left(\frac{h(m+q_2e_2)}{\beta - m - q_2e_2}, \frac{\beta h(Kr(\beta - m - q_2e_2) - rh(m+q_2e_2))}{K\alpha(\beta - m - q_2e_2)^2} \right)$$

exists iff $e_2 < \dfrac{K(\beta - m) - mh}{q_2(K+h)}$.

The local stability of system (2.2.2) can be determined by eigenvalues of Jacobian matrix J at the fixed points, where

$$J(x^*, y^*) = \begin{pmatrix} 1 + r\left(1 - \dfrac{2x^*}{K}\right) - \dfrac{\alpha h y^*}{(h+x^*)^2} - q_1e_1 & -\dfrac{\alpha x^*}{h+x^*} \\ \dfrac{\beta h y^*}{(h+x^*)^2} & 1 + \dfrac{\beta x^*}{h+x^*} - m - q_2e_2 \end{pmatrix}. \tag{2.3.1}$$

The characteristic polynomial of $J(x^*, y^*)$ at the equilibrium is given by

$$C(\lambda) = \lambda^2 - p(x^*, y^*)\lambda + q(x^*, y^*), \tag{2.3.2}$$

where

$$p(x^*, y^*) = 2 + r\left(1 - \frac{2x^*}{K}\right) - \frac{\alpha h y^*}{(h+x^*)^2} + \frac{\beta x^*}{h+x^*} - m - q_1e_1 - q_2e_2,$$

and

$$q(x^*, y^*) = \left(1 + r\left(1 - \frac{2x^*}{K}\right) - \frac{\alpha h y^*}{(h+x^*)^2} - q_1e_1\right)\left(1 + \frac{\beta x^*}{h+x^*} - m - q_2e_2\right) + \frac{\alpha\beta h x^* y^*}{(h+x^*)^3}.$$

Using Lemma 1.1 and 1.2 , we explore the following results:

2.3.1 Unharvested system

Proposition 2.1. *In the unharvested system (2.2.2), i.e., when $e_1 = 0$ and $e_2 = 0$, then*

(i) According to Lemma 1.2 (II), E^0 is always unstable.

(ii) From Lemma 1.2 (I), E^b is locally asymptotically stable if $0 < r < 2$ and $K < \dfrac{mh}{\beta - m}$. The coexisting equilibrium exists only when the second condition is violated, i.e., when $K > \dfrac{mh}{\beta - m}$. Thus, non-existence of interior equilibrium leads to a stability of the boundary equilibrium.

(iii) E^* *is locally asymptotically stable (Lemma 1.2 (I)) if*

$$hmr(m^2 - 2\beta - m(2+\beta)) - K(\beta - m)(m^2 - 4\beta - mr(2+\beta)) < 0$$

and

$$m(1-m)(h+K) + \beta K(2m - \beta - 1) + h\beta(1+m) < 0.$$

2.3.2 Prey harvesting

Proposition 2.2. *When only the prey is harvested, then using Lemma 1.1 (I) and 1.2 (I),*

(i) E^0 *is locally asymptotically stable if* $0 < q_1e_1 - 2 < r < q_1e_1$ *and* $0 < m < 2$. *The first condition represents prey extinction.* E^b *exists only when* $r > q_1e_1$. *The stability of the system shifts to boundary equilibrium as employed effort is smaller than* $\dfrac{r}{q_1}$.

(ii) E^b *is locally asymptotically stable if* $\dfrac{r-2}{q_1} < e_1 < \dfrac{r}{q_1}$ *and* $e_1 > \dfrac{1}{q_1}\left(r - \dfrac{mrh}{K(\beta - m)}\right)$. *The first condition implies the instability of trivial equilibrium. The coexisting equilibrium comes into existence and disturbs the stability of* E^b *when second condition is negated.*

(iii) $E^*_{e_1}$ *is locally asymptotically stable if*

$$hmr(m^2 - 2\beta - m(2+\beta)) - K(\beta - m)(m^2 - 4\beta - mr(2+\beta))$$
$$- Kmq_1e_1(m^2 - 2m(1+\beta) + \beta(2+\beta)) < 0$$

and

$$(\beta - m)(Km(\beta - m + 1)(q_1e_1 - r) + hmr(1-m) + K\beta) < 1.$$

2.3.3 Predator harvesting

Proposition 2.3. *When only the predator is harvested,*

(i) Lemma 1.2 (II) infers that E^0 *is always unstable.*

(ii) E^b *is locally asymptotically stable if* $0 < r < 2$ *and* $e_2 > \dfrac{1}{q_2}\left(\dfrac{\beta K}{h+K} - m\right)$ *which is deduced from Lemma 1.2 (I). These conditions are for extinction of predator at the coexisting equilibrium.*

(iii) Lemma 1.2 (I) concludes that $E^*_{e_2}$ is locally asymptotically stable if

$$(m+q_2e_2-\beta)(4\beta+r(m+q_2e_2)(K\beta+(h+K)(m+q_2e_2-2)))+4h\beta r(m+q_2e_2)<0$$

and

$$K(m+q_2e_2-\beta)(K(m+q_2e_2-1)-h(m+q_2e_2+1)+\beta)+2h(m+q_2e_2)<0.$$

One of the bifurcations at the equilibrium point $(K,0)$ in the unharvested system is the transcritical bifurcation when stability exchange happens between the boundary and the coexisting fixed point at the bifurcation point $K^*=\frac{mh}{\beta-m}$. Similarly, a couple of transcritical bifurcations could occur successively when prey species is harvested. However, only one transcritical bifurcation is possible when the predator is exploited. Since, the steady-state where both prey and predator coexist is more important from biological point of view, we will consider the bifurcations at the coexisting equilibrium point in detail in the next section.

2.4 Bifurcations analysis at coexisting equilibrium

In this section, we analyze Neimark-Sacker bifurcation of the unique positive equilibrium of system (2.2.2). We will derive the normal form of the bifurcation and determine the first Lyapunov coefficient [31]. We discuss the bifurcation occurring when prey harvesting ($e_2=0$) is introduced to the system. Taking e_1 as bifurcation parameter, we state the following conditions for existence of the Neimark-Sacker bifurcation at the positive equilibrium of the system. The characteristic polynomial at coexisting equilibrium subjected to prey harvesting is

$$C(\lambda)=\lambda^2-p(x^*,y^*)\lambda+q(x^*,y^*),$$

where $x^*=\dfrac{hm}{\beta-m}$ and $y^*=\dfrac{\beta h(K(\beta-m)(r-q_1e_1)-rhm)}{K\alpha(\beta-m)^2}$.
We can rewrite $p(x^*,y^*)$ and $q(x^*,y^*)$ as,

$$p(x^*,y^*)=1+\Theta+\theta-q_1e_1,$$

and

$$q(x^*,y^*)=(\Theta-q_1e_1)(1+\theta)+\vartheta,$$

where $\Theta=1+r\left(1-\dfrac{2x^*}{K}\right)-\dfrac{\alpha hy^*}{(h+x^*)^2}$, $\theta=\dfrac{\beta x^*}{h+x^*}-m$ and $\vartheta=\dfrac{\alpha\beta hx^*y^*}{(h+x^*)^3}$.

Now, the characteristic equation $C(\lambda) = 0$ has complex conjugate roots with modulus one if the following conditions are satisfied (Lemma 1.2 (v)):

$$e_1 = \frac{1}{q_1}\left(\Theta - \frac{1-\vartheta}{1+\theta}\right),$$

and

$$|1 + \Theta + \theta - q_1 e_1| < 2.$$

Define

$$\Omega_{NS}^{e_1} = \left\{(r, K, \alpha, \beta, m, q_1, e_1) : e_1 = \frac{1}{q_1}\left(\Theta - \frac{1-\vartheta}{1+\theta}\right), |1 + \Theta + \theta - q_1 e_1| < 2\right\}.$$

The unique coexistence equilibrium of the system (2.2.2) with prey harvesting undergoes a Neimark-Sacker bifurcation when the bifurcation parameter e_1 varies in a small neighborhood of the set $\Omega_{NS}^{e_1}$. Choose parameters $(r, K, \alpha, \beta, m, q_1, e_1)$ arbitrarily from the set $\Omega_{NS}^{e_1}$. Taking $\widetilde{e_1}$ as the bifurcation parameter, perturbing system (2.2.2) as follows:

$$\begin{pmatrix} X \\ Y \end{pmatrix} \longmapsto \begin{pmatrix} X + rX\left(1 - \frac{X}{K}\right) - \frac{\alpha XY}{h+X} - q_1(e_1 + \widetilde{e_1})X \\ Y + \frac{\beta XY}{h+X} - mY \end{pmatrix}, \tag{2.4.1}$$

where $|\widetilde{e_1}| \ll 1$ is a small perturbation in the bifurcation parameter.
Then Θ and ϑ become a function of $\widetilde{e_1}$, since after perturbation

$$x^*(\widetilde{e_1}) = \frac{hm}{\beta - m} \text{ and } y^*(\widetilde{e_1}) = \frac{\beta h(K(\beta - m)(r - q_1(e_1 + \widetilde{e_1})) - rhm)}{K\alpha(\beta - m)^2}.$$

Consider the transformation $x = X - x^*(\widetilde{e_1})$, $y = Y - y^*(\widetilde{e_1})$, where (x^*, y^*) is the unique positive equilibrium of the system (2.2.2) with $e_2 = 0$, then the map (2.4.1) can be expressed in the form:

$$\begin{pmatrix} x \\ y \end{pmatrix} \longmapsto \begin{pmatrix} a_{11} & a_{12} \\ a_{21} & a_{22} \end{pmatrix} \begin{pmatrix} x \\ y \end{pmatrix} + \begin{pmatrix} f_1(x, y) \\ g_1(x, y) \end{pmatrix}, \tag{2.4.2}$$

where

$$f_1(x, y) = a_1x^2 + a_2xy + a_3y^2 + a_4x^3 + a_5x^2y + a_6xy^2 + a_7y^3 + O((|x| + |y|)^4),$$
$$g_1(x, y) = b_1x^2 + b_2xy + b_3y^2 + b_4x^3 + b_5x^2y + b_6xy^2 + b_7y^3 + O((|x| + |y|)^4),$$

and

$$a_{11} = 1 + r - \frac{2rx^*}{K} - \frac{\alpha h y^*}{h + x^*} - q_1(e_1 + \widetilde{e_1}),$$
$$a_{12} = -\frac{\alpha x^*}{h + x^*}, \quad a_{21} = \frac{\beta h y^*}{(h + x^*)}, \quad a_{22} = 1 + \frac{\beta x^*}{h + x^*} - m,$$
$$a_1 = -2\left(\frac{r}{K} - \frac{\alpha h y^*}{(h + x^*)^3}\right), a_2 = -\frac{\alpha h}{(h + x^*)^2}, \quad a_4 = -\frac{6\alpha h y^*}{(h + x^*)^4}, \quad a_5 = \frac{2\alpha h}{(h + x^*)^3},$$
$$b_1 = -\frac{2\beta h y^*}{(h + x^*)^3}, \quad b_2 = \frac{\beta h}{(h + x^*)^2}, \quad b_4 = \frac{6\beta h y^*}{(h + x^*)^4}, \quad b_5 = -\frac{2\beta h}{(h + x^*)^3} \text{ and}$$
$$a_3 = a_6 = a_7 = b_3 = b_6 = b_7 = 0.$$

The characteristic equation of the equilibrium $(0, 0)$ of the linearized system is

$$\lambda^2 - p(\widetilde{e_1})\lambda + q(\widetilde{e_1}) = 0, \tag{2.4.3}$$

where

$$p(\widetilde{e_1}) = 1 + \Theta(\widetilde{e_1}) + \theta - q_1(e_1 + \widetilde{e_1})$$

and

$$q(\widetilde{e_1}) = (\Theta(\widetilde{e_1}) - q_1(e_1 + \widetilde{e_1}))(1 + \theta) + \vartheta(\widetilde{e_1}).$$

Since $(r, K, \alpha, \beta, m, q_1, e_1) \in \Omega_{NS}^{e_1}$, the roots of equation (2.4.3) are complex conjugate with modulus one if $\widetilde{e_1} = 0$. The roots λ_1 and λ_2 of equation (2.4.3) can be written as

$$\lambda_1, \lambda_2 = \frac{p(\widetilde{e_1})}{2} \pm \frac{i}{2}\sqrt{4q(C) - p^2(\widetilde{e_1})}.$$

Then

$$|\lambda_1| = |\lambda_2| = \sqrt{q(\widetilde{e_1})}.$$

$$\left(\frac{d|\lambda_1|}{d\widetilde{e_1}}\right)_{\widetilde{e_1}=0} = \left(\frac{d|\lambda_2|}{d\widetilde{e_1}}\right)_{\widetilde{e_1}=0} = \left(\frac{d\sqrt{q(\widetilde{e_1})}}{d\widetilde{e_1}}\right)_{\widetilde{e_1}=0}$$
$$= \frac{1}{2\sqrt{q(0)}}\left[\left(\frac{d\Theta}{d\widetilde{e_1}} - q_1\right)(1 + \theta) + \frac{d\vartheta}{d\widetilde{e_1}}\right]_{\widetilde{e_1}=0}$$
$$= \frac{1}{2\sqrt{q(0)}}\left[\left(\frac{-\alpha h}{(h + x^*)^2}\frac{dy^*(\widetilde{e_1})}{d\widetilde{e_1}} - q_1\right)(1 + \theta) + \frac{\alpha\beta h x^*}{(h + x^*)^3}\frac{dy^*(\widetilde{e_1})}{d\widetilde{e_1}}\right]_{\widetilde{e_1}=0}$$
$$= \frac{-mq_1(\beta - m + 1)}{2\beta\sqrt{1 + m\left(-q_1e_1 + r + \frac{(m-1)(Kq_1e_1 - (h+K)r))}{K\beta} - \frac{2hr}{K(\beta - m)}\right)}}.$$

Here, as we introduced perturbation parameter in the system (2.2.2), the coexisting fixed point of the perturbed system is also function of $\widetilde{e_1}$. On the other hand, Khan [51], and

Yao and Li [52] have followed different approach by considering coexisting equilibrium independent of the perturbation parameter. In our method, due to the complicated form of the derivative of the modulus of the eigenvalues, it is difficult to determine its sign analytically. We will check it in the examples provided soon enough.

Assuming that $p(0) = 1 + \Theta(0) + \theta - q_1 e_1 \neq 0, -1$, and since $(r, K, \alpha, \beta, m, q_1, e_1) \in \Omega_{NS}^{e_1}$, we have $-2 < p(0) < 2$. Then $p(0) \neq \pm 2, -1, 0$ implies $\lambda_1^m, \lambda_2^m \neq 1, \forall m = 1, 2, 3, 4$ at $\widetilde{e_1} = 0$. Hence when $\widetilde{e_1} = 0$ and if the following conditions are satisfied:

$$1 + \Theta(0) + \theta \neq q_1 e_1 \text{ and } 1 + \Theta(0) + \theta \neq q_1 e_1 - 1, \tag{2.4.4}$$

then roots of equation (2.4.3) do not lie on the real or imaginary axes of the unit circle (i.e., they are not equal to ± 1 or $\pm i$).

To obtain the normal form of equation (2.4.2) at $\widetilde{e_1} = 0$, we take $\kappa = \dfrac{p(0)}{2}$ and $\eta = \dfrac{1}{2}\sqrt{4q(0) - p^2(0)}$. Consider the following transformation:

$$\begin{pmatrix} x \\ y \end{pmatrix} = \begin{pmatrix} 0 & a_{12} \\ \eta & \kappa - a_{11} \end{pmatrix} \begin{pmatrix} u \\ v \end{pmatrix}. \tag{2.4.5}$$

The normal form of equation (2.4.2) using transformation (2.4.5) can be written as:

$$\begin{pmatrix} u \\ v \end{pmatrix} \longmapsto \begin{pmatrix} \kappa & -\eta \\ \eta & \kappa \end{pmatrix} \begin{pmatrix} u \\ v \end{pmatrix} + \begin{pmatrix} f_2(u, v) + O((|u| + |v|)^4) \\ g_2(u, v) + O((|u| + |v|)^4) \end{pmatrix}, \tag{2.4.6}$$

where

$$f_2(u, v) = \frac{a_{11} - \kappa}{a_{12}\eta} f_1(a_{12}v, \eta u + (\kappa - a_{11})v) + \frac{1}{\eta} g_1(a_{12}v, \eta u + (\kappa - a_{11})v)$$

$$g_2(u, v) = \frac{1}{a_{12}} f_1(a_{12}v, \eta u + (\kappa - a_{11})v).$$

Now, define the Lyapunov coefficient [31] as follows:

$$L = \left(\left[-Re\left(\frac{(1 - 2\lambda_1)\lambda_2^2}{1 - \lambda_1} \tau_{20}\tau_{11} \right) - \frac{1}{2}|\tau_{11}|^2 - |\tau_{02}|^2 + Re(\lambda_2 \tau_{21}) \right] \right)_{\widetilde{e_1}=0},$$

where

$$\tau_{20} = \frac{1}{2}[f_{2uu} - f_{2vv} + 2g_{2uv} + i(g_{2uu} - g_{2vv} - 2f_{2uv})],$$
$$\tau_{11} = \frac{1}{4}[f_{2uu} + f_{2vv} + i(g_{2uu} + g_{2vv})],$$
$$\tau_{02} = \frac{1}{8}[f_{2uu} - f_{2vv} - 2g_{2uv} + i(g_{2uu} - g_{2vv} + 2f_{2uv})],$$
$$\tau_{21} = \frac{1}{16}[f_{2uuu} + f_{2uvv} + g_{2uuv} + g_{2vvv} + i(g_{2uuu} + g_{2uvv} - f_{2uuv} - f_{2vvv})].$$

The following theorem is a result of the above analysis.

Theorem 2.4. *[31] If $L \neq 0$ then system (2.2.2) undergoes a Neimark-Sacker bifurcation about the unique positive equilibrium point (x^*, y^*) when the parameter e_1 varies in the neighborhood of $\Omega_{NS}^{e_1}$. An attracting (respectively repelling) invariant closed curve bifurcates from (x^*, y^*) if $L < 0$ (resp. $L > 0$).*

Remark 2.5. By similar analysis, we can show that the unique positive equilibrium of system (2.2.2) undergoes Neimark-Sacker bifurcation as parameter K is varied in the unharvested system ($e_1 = 0$ and $e_2 = 0$), and e_2 is varied in the predator harvested system ($e_1 = 0$).

We provide numerical examples to illustrate the occurrence of a Neimark-Sacker bifurcation at the interior fixed point when K, e_1, or e_2 are used as bifurcation parameters in the unharvested system, prey harvested system, and predator harvested system, respectively. The Lyapunov coefficient (L) as described in Theorem 2.4, is calculated using Mathematica.

Example 2.6. Taking $r = \frac{5}{2}, \alpha = \frac{4}{5}, \beta = \frac{1}{2}, h = 1$ and $m = \frac{1}{10}$, the Neimark-Sacker bifurcation occurs at $K^* = \frac{8}{7}$ in the unharvested system around the fixed point $(x^*, y^*) = \left(\frac{1}{4}, \frac{3125}{1024}\right)$. The eigenvalues of the Jacobian matrix at the interior fixed point (x^*, y^*) are

$$\lambda_1 = \frac{59 - i\sqrt{615}}{64}, \ \lambda_2 = \frac{59 + i\sqrt{615}}{64}.$$

The modulus of λ_1 and λ_2 at the bifurcation point K^* is exactly one. The transversality condition is calculated as,

$$\left(\frac{d|\lambda_{1,2}|}{d\widetilde{K}}\right)_{\widetilde{K}=0} = \frac{hmr(\beta + m(1-m+\beta))}{2(K^*)^2\beta(\beta-m)\sqrt{1+\frac{mr\left(1-m+\beta+\frac{h(\beta+m(1-m+\beta))}{K^*(m-\beta)}\right)}{\beta}}}$$
$$= \frac{49}{60} = 0.81667.$$

We have calculated the derivative of the $|\lambda_{1,2}|$ using the same analysis as done with respect to e_1 earlier. The positive value of the derivative of modulus of eigenvalues implies the instability of the system after going through Neimark-Sacker bifurcation. For $K < K^*$, the eigenvalues will lie in the interior of the unit circle. As $K > K^*$, the eigenvalues will escape from the unit circle. For instance if we take $K = \frac{10}{7} > K^*$ then eigenvalues are

$$\lambda_{1,2} = \frac{79 \pm i\sqrt{1055}}{80}$$

with $|\lambda_{1,2}| = 1.06771$.
The Lyapunov coefficient

$$L = -\frac{1784999421559}{82000000000} \approx -21.768286 < 0$$

which means that an attracting invariant curve bifurcates at the interior fixed point (Figure 2.4.1a).

Example 2.7. For the same parameter set as mentioned in Example 2.6 and taking $K = \frac{23}{14}$, the system exhibits nonequilibrium dynamics. When prey harvesting is introduced, increasing the harvesting effort leads the system to stabilize at an equilibrium state via a Neimark-Sacker bifurcation. We set catchability coefficient, $q_1 = 1$, then a Neimark-Sacker bifurcation occurs at $e_1^* = \frac{35}{46}$. The eigenvalues of the Jacobian matrix at the positive fixed point $(\frac{1}{4}, \frac{3125}{1472})$ are

$$\lambda_1 = \frac{87 - i\sqrt{895}}{92} \text{ and } \lambda_2 = \frac{87 + i\sqrt{895}}{92},$$

with $|\lambda_1| = |\lambda_2| = 1$. The system stabilizes for $e_1 > e_1^*$ because the transversality condition,

$$\left(\frac{d|\lambda_{1,2}|}{d\widetilde{e_1}}\right)_{\widetilde{e_1}=0} = \frac{-mq_1(\beta - m + 1)}{2\beta\sqrt{1 + m\left(-q_1e_1^* + r + \frac{(m-1)(Kq_1e_1^* - (h+K)r))}{K\beta} - \frac{2hr}{K(\beta-m)}\right)}}$$
$$= -\frac{7}{50} = -0.14,$$

is negative implying that the eigenvalues lie inside the unit circle after the bifurcation. The invariant closed curve (Figure 2.4.1b) is attracting since the Lyapunov coefficient is

$$L = -\frac{151308570108254}{4253697265625} \approx -35.571072 < 0.$$

In Example 2.6 , the modulus of the eigenvalues expanded for increasing K more than the critical value whereas under prey harvesting, the same are contracting leading to stability of the fixed point.

Example 2.8. In the predator harvested system, taking the same values of the parameters as in Example 2.7 and $q_2 = \frac{1}{10}$, a quasiperiodic orbit (Figure 2.4.1c) arises due to Neimark-Sacker bifurcation for the critical harvest effort $e_2^* = \frac{2(149-5\sqrt{743})}{37} \approx 0.6870199$ at the positive fixed point

$$(x^*, y^*) = \left(\frac{67 - 2\sqrt{743}}{2(-15 + \sqrt{743})}, \frac{34225(22 - \sqrt{743})}{732(-484 + 15\sqrt{743})}\right) \approx (0.50921523, 3.2544477).$$

It is difficult to calculate the exact eigenvalues of the Jacobian matrix at (x^*, y^*) and the Lyapunov coefficient without approximation because of the complexity of the expression to find exact value of the bifurcation point e_2^*. The eigenvalues of the Jacobian matrix at the positive fixed point are

$$\lambda_1 = 0.903582661813367 - i\,0.42841378744185,$$
$$\text{and} \quad \lambda_2 = 0.903582661813367 + i\,0.42841378744185$$

with $|\lambda_{1,2}| \approx 1$. For $e_2 > e_2^*$, the eigenvalues lie inside the unit circle as the derivative of the modulus of the eigenvalues with respect to the perturbation parameter is negative. To be precise,

$$\left(\frac{d|\lambda_{1,2}|}{d\widetilde{e_2}}\right)_{\widetilde{e_2}=0} = -0.301744.$$

The value of Lyapunov coefficient is $L = -10.753104$ which indicates that the quasiperiodic orbit is attracting in nature.

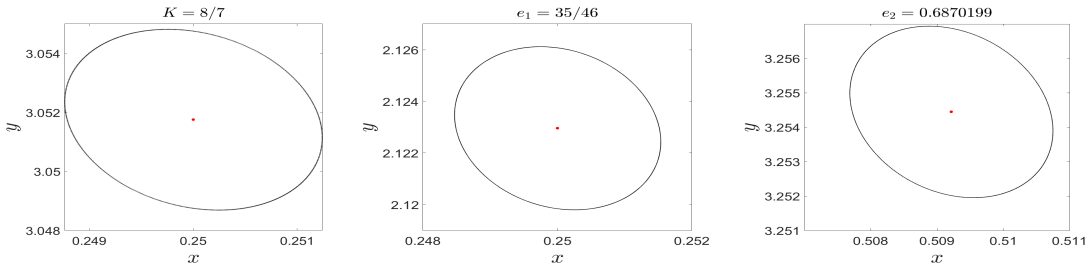

(a) **(b)** **(c)**

Figure 2.4.1: Phase portrait of the system with $r = \frac{5}{2}, \alpha = \frac{4}{5}, \beta = \frac{1}{2}, h = 1, m = \frac{1}{10}$ and (a) $K = \frac{8}{7}$ in the unharvested system, (b) $K = \frac{23}{14}, q_1 = 1$ and $e_1 = \frac{35}{46}$ in prey harvested system, and (c) $K = \frac{23}{14}, q_2 = 0.1$ and $e_2 = 0.6870199$ in predator harvested system. The red dot denotes the equilibrium point at the fixed parameter values. The invariant closed curve is presented in black color.

2.5 Dynamics and ecological interpretations

In the previous section, we discussed the occurrence of a Neimark-Sacker bifurcation when K, e_1, or e_2 were used as bifurcation parameters. In this section, we will analyze the dynamical changes and complex phenomena occurring along with Neimark-Sacker bifurcation by fixing other parameter values and varying either carrying capacity of prey, harvesting effort on prey, or exploitation rate of predator separately. We will also provide the ecological interpretations of the results obtained from the dynamic solutions.

2.5.1 Analyzing unharvested system

We discuss the changes in dynamics occurring as the carrying capacity K of the prey population is varied.

Consider the parameter set $r = 3.2, \alpha = 0.5, \beta = 0.3, h = 2,$ and $m = 0.2$. The trivial fixed point $(0, 0)$ is always unstable. The boundary fixed point $(K, 0)$ is also unstable since $r > 2$. When $K = 9.2$, the coexisting steady state $(4, 21.704)$ is stable. A bifurcation diagram is shown for increasing K in Figure 2.5.1a for a fixed initial condition $(4.87, 30.43)$. The stable fixed point loses its stability leading to an invariant closed orbit as a result of Neimark-Sacker bifurcation occurring at $K = 104/11 \approx 9.454$. The eigenvalues of the corresponding Jacobian matrix of system (2.2.2) at the positive fixed point are $\frac{1}{65}(61 \pm i6\sqrt{14})$ if $K = 9.454$. This invariant closed curve doesn't remain stable as K is increased further. The quasiperiodic orbit loses its stability to periodic orbits several times for very narrow

ranges of K. The maximum Lyapunov exponent (MLE) diagram is shown in Figure 2.5.1b . The system exhibits stable periodic solutions if the MLE is negative, quasiperiodic if it is zero, and chaotic if it is positive. The algorithm used for finding maximum Lyapunov exponents is based on the program provided in Wolf *et al.* [33]. We have written explicit code in MATLAB to find the value of Lyapunov exponents. We have used 100000 iterations in obtaining the Lyapunov exponents. Even if we considered more than 100000 iterations, the results derived from the MLE remains same. The system is periodic for $9.2 < K < 9.455$ as $MLE < 0$, quasiperiodic for $9.455 < K < 10.1$ as $MLE = 0$ and chaotic for $K \in (10.1, 10.2)$ as $MLE > 0$. The dynamics of the system becomes very complex as K increases beyond 10.2. The quasiperiodic behavior continues, but in between, periodic windows of different periods appear. The first periodic window is of period-29 which appears for $K \in (10.01121, 10.01135)$. There is a period-adding sequence of period-30, 31, 32, and so on, between the quasiperiodic region for $K < 10.126$. We have identified the period-bubbling and periodic-doubling phenomena in Figure 2.5.1c. A complicated sequence of periodic and quasiperiodic behavior is observed for $K < 10.125$. One of the complicated sequences existing for $K \in (10.1058, 10.1118)$ is: period-40 $\rightarrow$ quasiperiodicity $\rightarrow$ period-81 $\rightarrow$ quasiperiodicity $\rightarrow$ period-41 $\rightarrow$ quasiperiodicity $\rightarrow$ period-82 $\rightarrow$ period-41 $\rightarrow$ period-83. Many such complex sequences are observed for $K \in (9.46, 10.125)$. The onset of chaos is around $K \approx 10.126$. The identical complex sequences are present with chaos and periodic windows. The periodic windows of period sequence-45, 90, 46, 91, 92 can be seen between chaotic regions when $K \in (10.1284, 10.13484)$. These complicated sequences of chaos and periodic windows vanish for $K > 10.19938$. The chaotic behavior continues when $10.169938 < K < 10.2$.

We have already plotted a bifurcation diagram in Figure 2.5.1a with initial condition $(4.87, 30.43)$. Now, we would like to examine the existence of multistability with increasing K. For this purpose, we choose a different initial condition $(1.83, 4.84)$. We draw the bifurcation diagram using both the initial conditions in the same figure to distinguish them. The bifurcation diagram for initial condition $(4.87, 30.43)$ is shown in Figure 2.5.2a in red color and the bifurcation diagram for $(1.83, 4.84)$ in blue color. The blue bifurcation diagram overshadows the red one where the dynamics are the same but the bifurcation curves do not merge at many values of K. This non-merging of bifurcation curves clearly indicates the presence of multistability. We detected the existence of multistability from

$K = 10.1$ to $K = 10.2$ for different values of K. From the maximum Lyapunov exponent plot in Figure 2.5.2b for both the initial conditions, we can observe that the red and blue plot are also not overlapping at many values of K which confirms that both the initial conditions have different dynamics for same value of K. A more clear visualization of multistability is shown in Figure 2.5.2c by zooming the bifurcation diagram. Hence, the system shows various multistable modes for $K \in (10.11, 10.12)$ and $(10.16, 10.175)$ but has different dynamic modes. As an example we have provided a phase portrait for these two initial conditions in Figure 2.5.2d for $K = 10.1655$ which shows that the coexistence of period-53 and period-106. Further, we could verify the coexistence of periodicity and chaos for $K = 10.1711$.

We would like to determine how the basin of attraction looks like for different values of K especially when the system is multistable. We have plotted the basin of attraction within the region $[0, 14] \times [0, 40]$. We used step-size 0.01 along $x-$ and y-axis to create a meshgrid of 1400×4000 grid points (x_0, y_0). For each grid point (x_0, y_0), we have computed a total of 100000 iterations and checked the periodicity after removing the transient part. We checked which initial conditions exhibit cycle of same period and plotted those value of initial conditions in a specific color. For the initial conditions which lead to non-periodic attractors, we used the MLE to differentiate between quasiperiodic and chaotic behavior. In Figure 2.5.3a , the system is monostable, and the coexisting fixed point is stable. As shown in Figure 2.5.3b , a multistable state occurs at $K = 10.1655$, where two stable periodic orbits of period-53 and period-106 coexist. Figure 2.5.3c shows multistability at $K = 10.1711$ where a stable period-54 cycle and chaotic attractor coexist. Finally, the system is attracted to a chaotic attractor at $K = 10.2$ and becomes monostable again as shown in Figure 2.5.3d. The size and shape of the basin is same for all four values of K. In Figure 2.5.4a and Figure 2.5.4b , we show more clearly the geometry of basins of attraction by magnifying some portion of Figure 2.5.3b and Figure 2.5.3c respectively. The basins have a very complicated structure as the set of initial conditions going to period-53 and period-106 are collection of many disjoint sets in Figure 2.5.3b . The structure is even more complicated in Figure 2.5.3c.

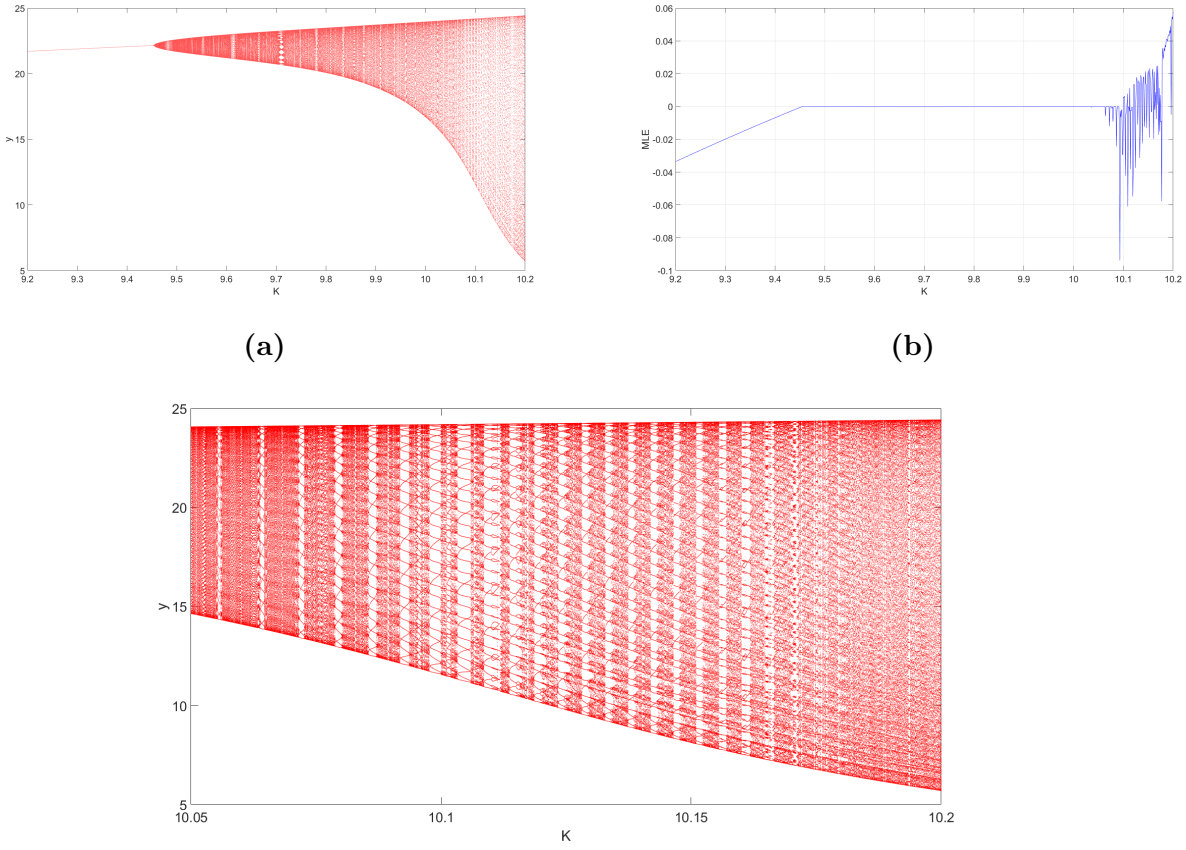

(a) **(b)**

(c)

Figure 2.5.1: (a) Bifurcation diagram with predator population for varying K from 9.2 to 10.2, (b) Maximum Lyapunov exponents corresponding to $K \in (9.2, 10.2)$, and (c) magnification of the bifurcation diagram varying K from 10.05 to 10.2.

2.5.2 Prey harvesting

We incorporate prey harvesting into the system to study its influence on the dynamic modes. We consider the different dynamic modes of the unharvested system with fixed ecological parameters, and explore the variation in dynamics with harvesting effort on the prey.

Let us consider the parameters as $r = 3.2, K = 9.2, \alpha = 0.5, \beta = 0.3, h = 2$, and $m = 0.2$. For this parameter set, the unharvested system showed stable behaviour of the coexisting equilibrium. Without loss of generality, we set $q_1 = 1$ and varying prey harvesting effort $e_1 \leq 1.8$ so that the coexisting equilibrium exists. The predator population decreases with increase in effort as shown in the bifurcation diagram (Figure 2.5.5a). We observed that the coexisting equilibrium maintains its stability under prey harvesting.

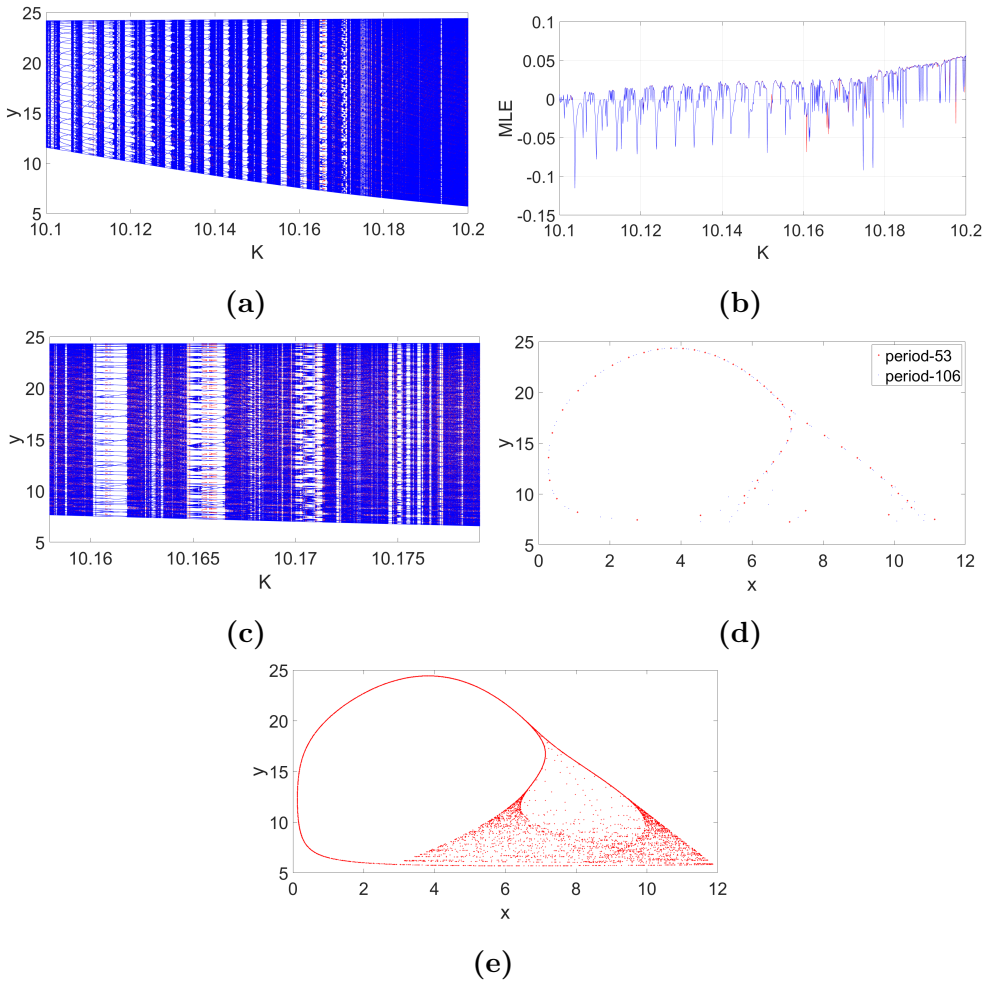

Figure 2.5.2: (a) Bifurcation diagram with two different initial conditions: red curve corresponding to initial condition $(4.87, 30.43)$ and blue curve corresponding to initial condition $(1.83, 4.84)$, (b) Maximum Lyapunov exponents corresponding to $(4.87, 30.43)$ in red and $(1.83, 4.84)$ in blue, (c) A part of the bifurcation diagram with $K \in (10.158, 10.179)$, and (d) Phase portraits of the two initial conditions at $K = 10.1655$ and (e) chaotic attractor for $K = 10.2$.

As effort is increased further beyond 1.8, the predator population goes extinct. The prey population starts decreasing as e_1 increased in $(1.8, 3.2)$ and eventually dies out when $e_1 = 3.2$.

We now consider a different dynamics of the unexploited system with $K = 10.1655$. We have already observed multistability for different initial conditions in this unharvested system. Now, the coexisting equilibrium exists when $e_1 \leq 1.94$. For the initial condition $(1.83, 4.84)$, the unharvested system exhibits periodic behavior of period-106. The bifurcation diagrams in Figure 2.5.5b - 2.5.5d show that the predator population experiences

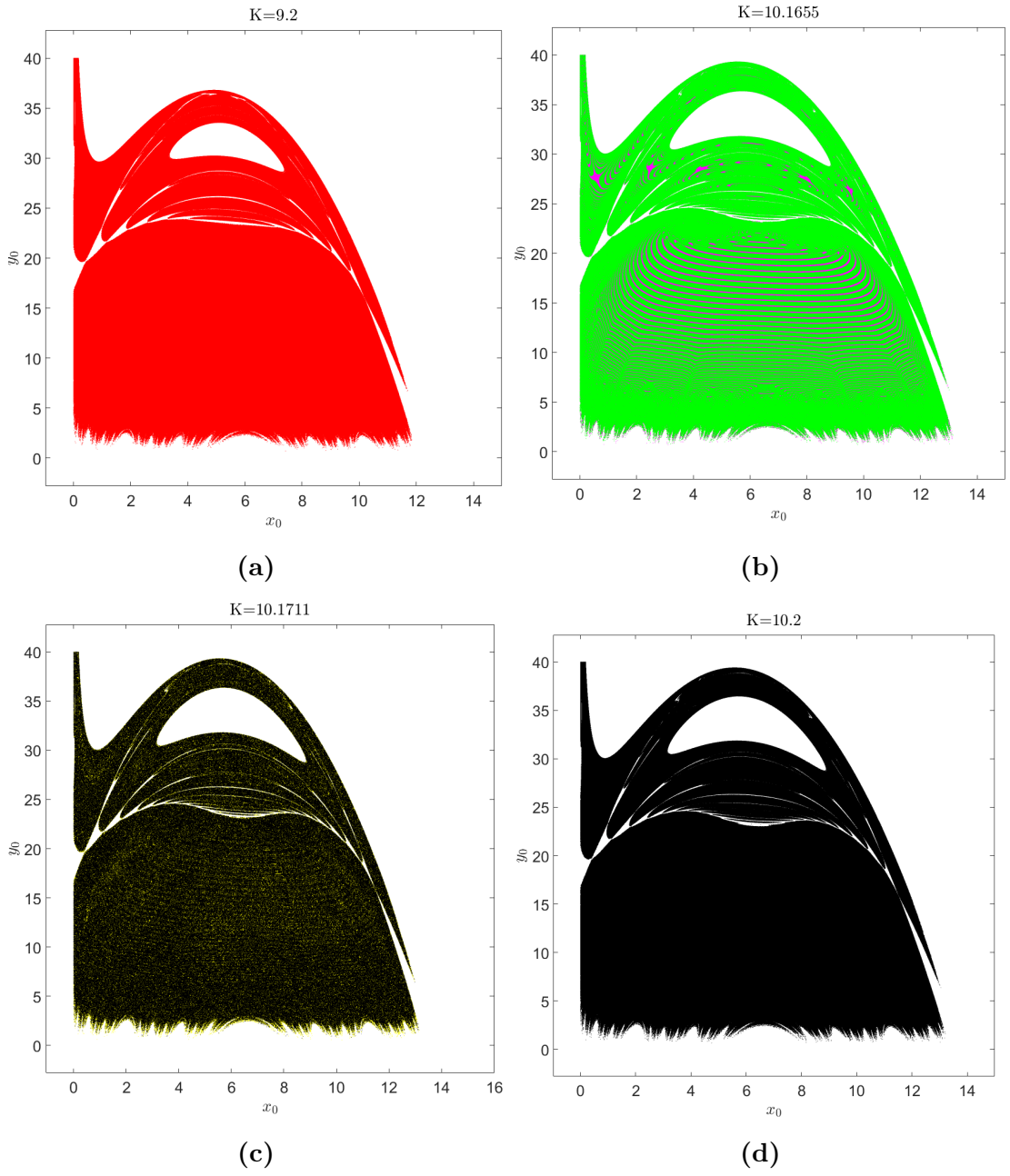

Figure 2.5.3: Basin of attraction for different values of K (white region is for all the initial conditions which lead to unbounded trajectories) (a) basin for equilibrium point (red region), (b) basin of period-53 (magenta region) and period-106 (green region), (c) basin of : period-54 (yellow region) and chaos (black region), and (d) chaos(black region).

periodic, chaotic and quasiperiodic oscillations for $e_1 \in (0, 0.223)$. Further increase in effort stabilizes the system and predator population decreases. There are also many periodic windows between chaotic and quasiperiodic regions as shown in Figure 2.5.5c . The system exchanges dynamics between chaos and periodic windows for $e_1 \in (0, 0.0208)$. The

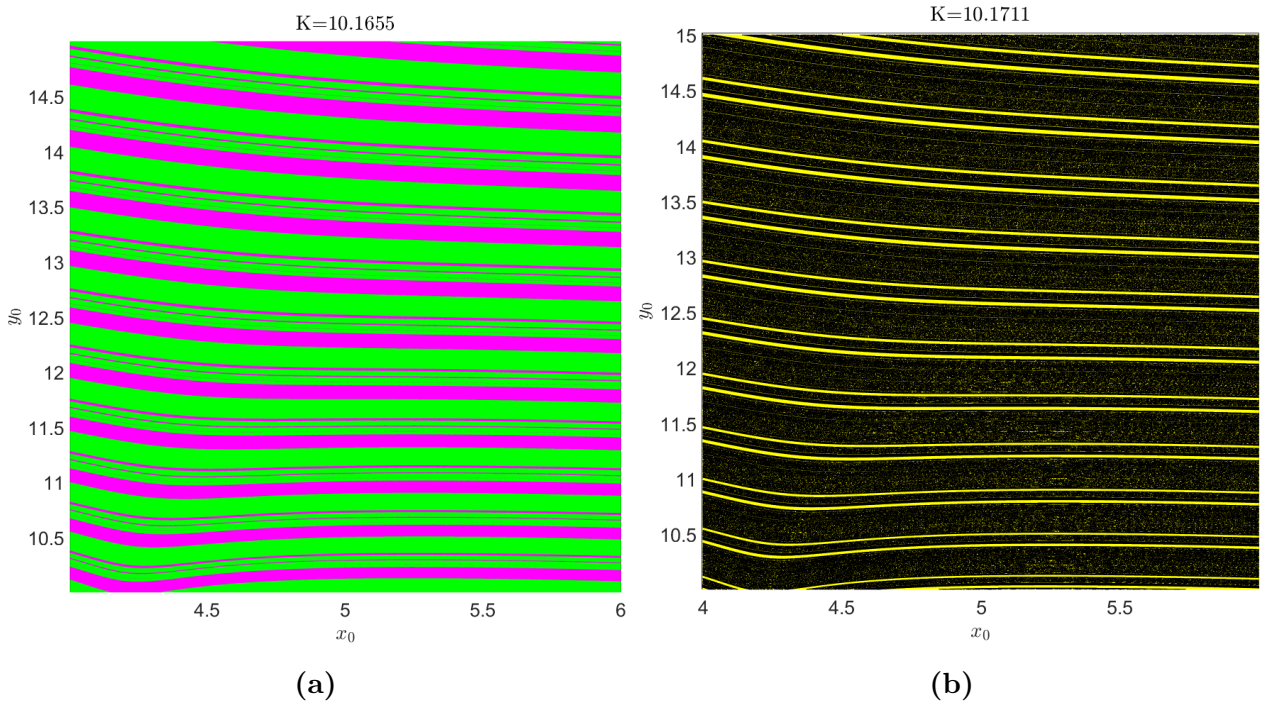

Figure 2.5.4: (a) zoomed part of the basin in Figure 2.5.3b , and (b) zoomed part of the basin in Figure 2.5.3c .

chaotic region with periodic windows disappears leading to the birth of a quasiperiodic orbit around $e_1 \approx 0.0209$. The dynamics again starts shifting between quasiperiodic orbit and periodic windows in the interval $(0.0209, 0.04)$. The quasiperiodic behavior continues for a wide range of parameter value for $e_1 \in (0.04, 0.224)$. This orbit is destroyed around $e_1 = 0.224$ through a Neimark-Sacker bifurcation and the coexisting equilibrium becomes stable for $e_1 > 0.224$. The stable coexisting equilibrium decreases as e_1 increases and hence the predator population goes to extinction for $e_1 > 1.94$. We plotted the magnification of bifurcation diagram for $0 < e_1 < 0.045$ in Figure 2.5.5c to see more clearly how the dynamics change from periodic to chaos and then to quasiperiodic. The system also exhibits period-bubbling phenomenon for many intervals of e_1 which can be concluded from the magnified bifurcation diagram (Figure 2.5.5c). Each intervals contains many period bubbles. Figure 2.5.5e captures the period-bubbling in the interval $(0.0162, 0.0172)$. The maximum Lyapunov exponents (Figure 2.5.5d) clearly state that the system continuously jumps back and forth from chaos to periodic mode and then from periodic to quasiperiodic mode in a very narrow range of e_1 before stabilizing in the equilibrium state.

The system also shows multistability for various values of effort. We analyze the behaviour exhibited by the two initial conditions $(1.83, 4.84)$ and $(4.2, 22.12)$ as the effort is increased. These two initial conditions show periodic behaviour (period-106) in the unharvested system. In Figure 2.5.6a , the bifurcation curves for the two initial conditions $(1.83, 4.84)$ and $(4.2, 22.12)$ indicated in red and blue colour respectively, are plotted. This figure also indicates the existence of multisabilities in the range $(0.014, 0.015)$, $(0.01625, 0.01645)$ and $(0.0175, 0.179)$. One of the multistabilities, we detected, between a stable period-85 orbit and chaotic oscillations when $e_1 = 0.01465$. The phase portrait (Figure 2.5.6b) for $e_1 = 0.01465$ shows that period-85 orbit and a multiband chaotic attractor coexist. It can be seen from the maximum Lyapunov exponents in Figure 2.5.6c that the dynamics for the two initial conditions are not the same for many values of e_1 in the interval $(0.0145, 0.0179)$. In fact for other values of K such as $K = 10.1711$ and $K = 10.2$, we can obtain similar kind of dynamics as e_1 increases as shown for $K = 10.1655$. For $K = 10.1711$, we take two initial conditions $(4.52, 12.90)$ and $(10.36, 4.83)$ which lead to chaotic trajectories in the unharvested system. These again show multistability for various values of e_1 with chaos, periodicity, and quasiperiodicity existing in the similar manner. Hence harvesting the prey leads to the stabilization of both population.

If we consider another initial condition $(4.87, 30.43)$ which leads to a period-53 orbit in the natural system then we notice similar kind of dynamics. It also marks its way to stabilization through chaos, periodic windows, period-bubbling, and quasiperiodicity. The only difference is that for $e_1 \in (0.12, 0.36)$, the system diverges and then stable coexisting equilibrium appears(Figure 2.5.6d). It diverges completely for $e_1 > 0.639$. The initial conditions play an important role in how the dynamics will appear as e_1 increases.

2.5.3 Predator harvesting

Introducing predator harvesting to the system, we will analyze the impacts of predator harvesting on both species. The different dynamic modes were obtained in the unharvested system for $K = 9.2, 10.1655, 10.1711$, and 10.2. Now, the alteration occurring in the dynamics with varying e_2 will be concluded for each of the value of K. The value of q_2 is fixed to be 0.01.

When $K = 9.2$, the coexisting equilibrium can be obtained for $e_2 \leq 4.6$. The coexisting equilibrium remains stable for $e_2 \leq 2.66$ and the trajectories diverge for $e_2 \in (2.66, 4.6)$

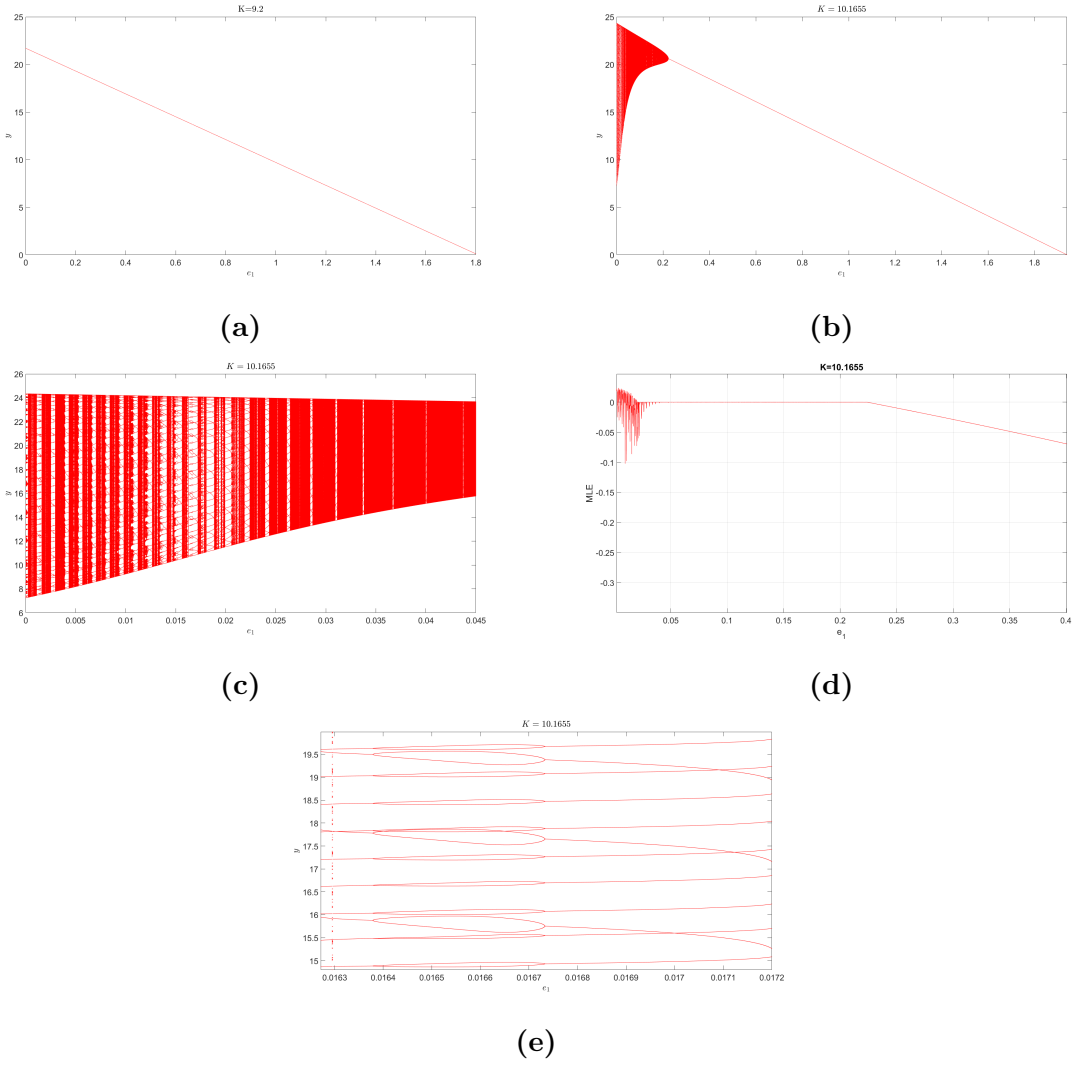

Figure 2.5.5: (a) Bifurcation diagram of predator population with e_1 as bifurcation parameter for $K = 9.2$ with initial condition $(1.83, 4.84)$, (b) Bifurcation diagram of predator population with bifurcation parameter e_1 for $K = 10.1655$, (c) magnification of bifurcation diagram in (b), (d) maximum Lyapunov exponents for $e_1 \in (0, 0.4)$, and (e) period-bubbling phenomenon.

for the initial condition $(1.83, 4.84)$. The predator population decreases with increase in e_2 while the prey population increases.

We focus on $K = 10.1711$ for showing the different complex dynamics arising with increase in e_2. The unharvested system displayed multistability with stable periodic and chaotic behavior coexisting for different initial conditions. We can obtain the coexisting equilibrium for $e_2 \leq 5$. The bifurcation diagram in Figure 2.5.7a reveals that the system commences with chaotic behavior along with periodic windows ($0 < e_2 < 0.0664$), then

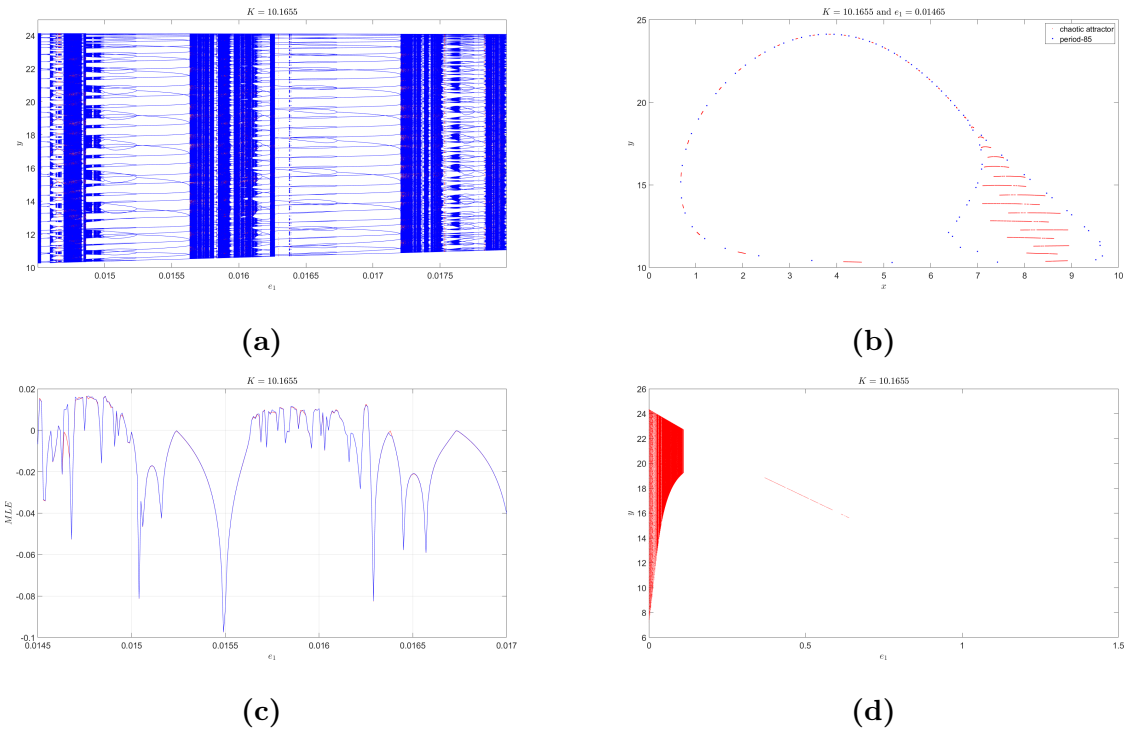

Figure 2.5.6: (a) Bifurcation diagram with two different initial conditions: red curve corresponding to initial condition $(1.83, 4.84)$ and blue curve corresponding to initial condition $(4.2, 22.12)$, (b) phase portrait for coexistence of period-85 (blue color) and chaotic attractor (red color), (c) maximum Lyapunov exponent corresponding to the bifurcation curves in (a), and (d) Bifurcation diagram of predator population with e_1 as bifurcation parameter for $K = 10.1655$ with initial condition $(4.87, 30.43)$.

exhibits quasiperiodic behavior with periodic windows $(0.664 < e_2 < 0.57525)$, and finally achieves stability at equilibrium for $e_2 \in (0.57525, 2.86)$. The change in dynamics from quasiperiodic orbit to stable equilibrium is a result of Neimark-Sacker bifurcation which occurs around $e_2 = 0.57525$. As we zoom in to have a clearer look at the dynamics between $e_2 = 0$ and 0.08 (Figure 2.5.7b), a complex network of criss-cross period-bubbles, chaos, quasiperiodic and periodic windows appears. The complex criss-cross period-bubbling phenomenon is shown in Figure 2.5.7c . The maximum Lyapunov exponents, plotted in Figure 2.5.7d , also confirm the complicated behaviour of trajectories with increase in effort.

Figure 2.5.8a demonstrates the existence of multistability as the two bifurcation diagrams with different initial conditions don't overlap each other for various values of e_2. We determine the specific type of multistabilities occurring at different values as e_2 is

increased. One of these multistabilities exists when $e_2 = 0.00087$ for which the initial condition $(1.83, 4.84)$ is attracted to a stable multi-band chaotic attractor while the other initial condition $(4.2, 22.12)$ moves on a period-54 orbit (Figure 2.5.8b). Other multistabilities, which we detected, are for $e_2 = 0.0169$ (period-50 and period-200) indicated in Figure 2.5.8c and $e_2 = 0.04724$ (chaos and period-170). The different behaviour of the two initial conditions for same value of effort can also be comprehended from the maximum Lyapunov exponents. The Lyapunov exponents are not same for many values of effort, and hence solidify our claim of multistability. Consider the interval $(0.0051, 0.0052)$ in Figure 2.5.8d where the maximum Lyapunov exponents are not coinciding for many values of e_2. As a particular case, the maximum Lyapunov exponents at $e_2 = 0.005126$ for initial conditions $(1.83, 4.84)$ and $(4.2, 22.12)$ are -0.07467982 (periodic) and 0.0035566 (chaos), respectively.

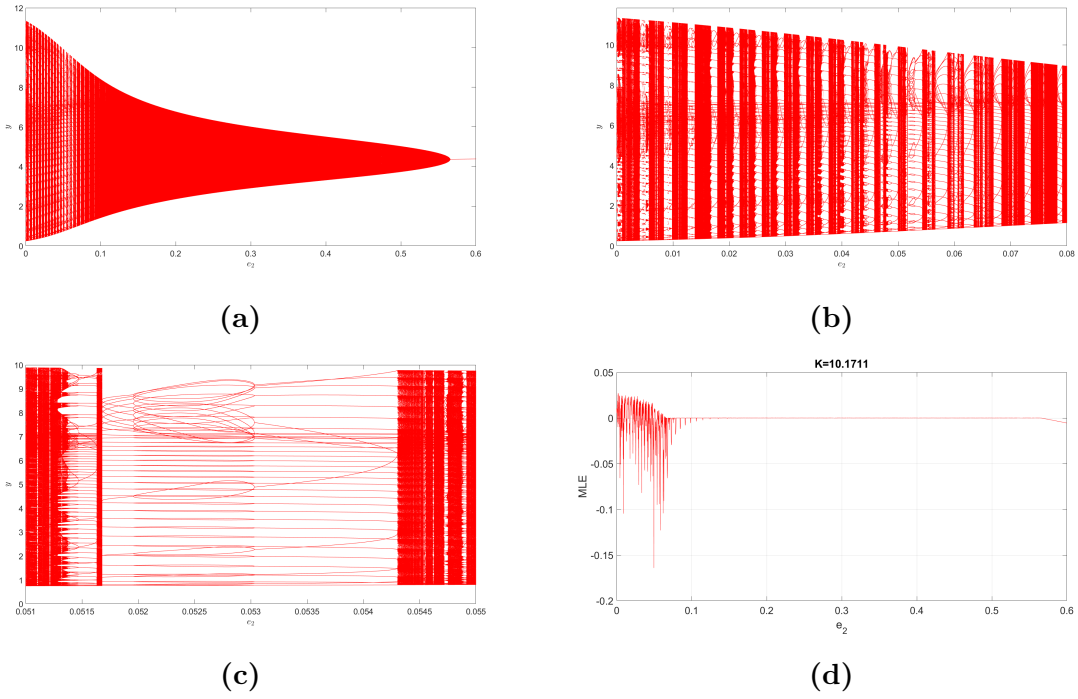

Figure 2.5.7: (a) Bifurcation diagram of the system in (y, e_2) plane for $0 \leq e_2 \leq 0.6$, (b) Bifurcation diagram of the system in (y, e_2) plane for $0 \leq e_2 \leq 0.08$, (c) Complex structure of periodic bubbles, (d) Maximum Lyapunov exponents with respect to the bifurcation diagram in (a).

The increment of carrying capacity of prey species may lead to predator extinction. This phenomenon is called as the paradox of enrichment [43–47]. Weide *et al.* [46] reported

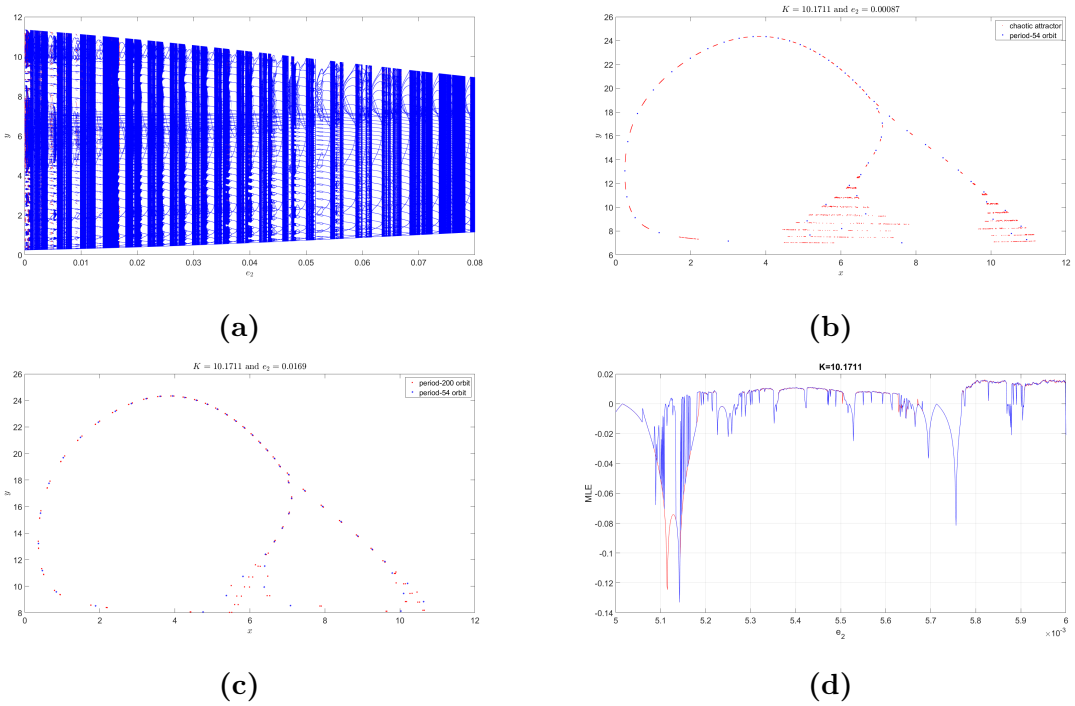

Figure 2.5.8: (a) Bifurcation diagram in (y, e_2) plane with two different initial conditions: red curve corresponding to initial condition $(1.83, 4.84)$ and blue curve corresponding to initial condition $(4.2, 22.12)$, (b) phase portrait for coexistence of period-54 (blue colour) and multi-band chaotic attractor (red colour), (c) Phase portrait for coexistence of period-54 (blue colour) and period-200 (red colour) orbits, and (d) Maximum Lyapunov exponent corresponding to the bifurcation curves in (e).

that in a Nicholson-Bailey framework based discrete-time predator-prey model, increase in carrying capacity destabilizes the system. Recently, Pattanayak *et al.* [47] observed that increasing carrying capacity of the resource level species results in extinction of species at higher trophic level (bottom-up effect). They showed that varying the carrying capacity induced bistability into the system. The ecological implications stemming from an increase in carrying capacity are highly intriguing. The paradox of enrichment, as described by Rosenzweig [43], Abrams and Roth [44], Wollrab *et al.* [45], Weide *et al.* [46], and Pattanayak *et al.* [47] refers to the phenomenon where the increment in the carrying capacity of prey species (i.e., increase in food supply to the predator) can lead to the extinction of their predators.

The paradoxical phenomenon known as the "hydra effect" describes the counter-intuitive increase in a species' population with an enhancement in its death rate. This phenomenon has been noted to occur in continuous-time as well as discrete-time models

[44,46,49,53–56]. Pal [57] showed that the positive density-dependent effects of predators, such as grouping behavior or cooperation in trophic functions, exhibit a hydra effect within the prey species. Conversely, the negative density-dependent effects of predators, such as interference, manifest a hydra effect within the predator species. Legović *et al.* [58] reported that harvesting of prey will lead to extinction of predator in continuous-time model. To assess nonequilibrium dynamics over extended periods, the mean population density is commonly used as a measure of the population level (Liz and Ruiz-Herrera [48]and Sieber and Hilkar [53]). Using mean density, we answer the following questions:

(i) What are the ecological implications of increase in food supply to predator species?

(ii) What will be the effect of increasing mortality rate of the predator population?

First, let us define mean population density for the discrete-time models.

2.6 Mean population in a Discrete-time model

If the trajectories approach an equilibrium, then it is not difficult to determine the population size over a long period of time. When the equilibrium is unstable (for nonequilibrium dynamics), measuring the stock level is challenging. A time-averaged stock could be a reasonable estimate to quantify the population level. We consider continuous and discrete systems, and represent the formula to calculate the same for both systems.

First consider a continuous system,

$$\frac{dX}{dt} = f(X),$$

where $f : D \subseteq \mathbb{R}^m \to \mathbb{R}^m$. Let $X(t)$ be the solution of the system with initial condition $X(0) = X_0$. Then, the mean value map ([53, 59]) is defined by

$$\phi(X_0) = \lim_{t\to\infty} \frac{1}{t} \int_0^t X(s)\, ds,$$

where X_0 is a fixed initial condition, $\phi : M \to \mathbb{R}^m$ and M is the subset of initial conditions for which the limit exists. In a similar manner, Liz and Ruiz-Herrera [48] proposed the mean density for a discrete map

$$X_{n+1} = f(X_n),$$

as

$$\phi(X_0) = \lim_{n\to\infty} \frac{1}{n} \sum_{i=0}^{n-1} X_i, \text{ provided the limit exists.}$$

Now, for system (5), we define

$$\overline{x}((x_0, y_0)) = \lim_{n\to\infty} \frac{1}{n} \sum_{i=0}^{n-1} x_i,$$

$$\overline{y}((x_0, y_0)) = \lim_{n\to\infty} \frac{1}{n} \sum_{i=0}^{n-1} y_i,$$

where $\overline{x}$ and $\overline{y}$ are the mean population densities of prey and predator species, respectively.

2.6.1 Paradox of enrichment

Many researchers have investigated the effects of increase in the carrying capacity of prey (species enrichment) in various models. The paradox of enrichment in population models was defined as the destabilization of the coexisting equilibrium resulting in birth of cyclic dynamics. The extinction of predator population becomes more likely as carrying capacity is increased sufficiently. The above phenomenon was first discussed by Rosenzweig [43]. The paradox of enrichment became more popular after Abrams [44] studied a continuous tri-trophic food chain model. They shed some light on the response of food chains or ecosystems to enrichment, which could lead to chaos. The key conclusion was that the mean population density of the dominant species initially rises, but eventually decreases as the carrying capacity increases beyond a certain threshold. The supply of additional nutrient (enhancement of carrying capacity) to the bottom species, which influences a food chain including the top species is known as bottom-up effect. Pattanayak *et al.* [47] observed the bottom-up effect in the same model studied by Abrams [44] as the top predator leads to extinction.

However, the discussion of the paradox of enrichment in discrete-time population models has rarely been reported. Very recently, Weide *et al.* [46] have studied a discrete-time Nicholson-Bailey model, and they uncovered that the nonequilibrium dynamics arise due to increase in carrying capacity. The limit cycles generated by Neimark-Sacker bifurcation tend towards the axes in the phase portrait as the carrying capacity is increased, which could result in extinction of the predator. They have described destabilization of the equilibrium by quasiperiodic motion, and we further take the opportunity to estimate mean density of population in the nonequilibrium dynamics of our model.

For the parameter set: $r = 3.2, \alpha = 0.5, \beta = 0.3, h = 2,$ and $m = 0.2,$ we already discussed the destabilizing effect of increasing the carrying capacity in the unharvested

system. Now, we enhance carrying capacity K of the prey species in the system (2.2.2) to capture the changes in mean population density. The main advantage of the RM model is that we can obtain explicit form of the equilibrium biomass of the species. The equilibrium prey biomass is independent of K whereas the equilibrium predator biomass is dependent. The prey (respectively predator) equilibrium state remains constant (respectively increases) with increase in carrying capacity. The mean prey (predator) density coincides with prey (predator) equilibrium for $K \leq 9.454$. It is expected that if more nutrients are provided to the prey population, it would enhance its own population size and the sustainability of predator species is also anticipated. Both curve separate as the system undergoes a Neimark-Sacker bifurcation for an intermediate carrying capacity. The mean prey (respectively predator) density increases (respectively decreases) while prey (respectively predator) equilibrium continue to remain constant (respectively increase) with increment of nutrient supply to the prey species (Figure 2.6.1a -2.6.1b). The figures are generated by making code in MATLAB using the theory mentioned above. Theoretically, the value of number of iterations is very large as $n \to \infty$ in the definition. From computation point of view, we calculated 5000000 iterations to compute mean density for a fixed parameter value. We have also examined the mean density value by taking iterations more than 5000000 which gave the same results. Our results for discrete-time framework for two species are in accordance with those of Abrams [44] as claimed for the continuous tri-trophic system.

We already know that the system shows multistability for various values of K. It is necessary and interesting to examine the effect of initial conditions in estimating mean density. Figure 2.6.1a and Figure 2.6.1b are generated using a fixed initial condition $(1.83, 4.84)$. However, many other initial conditions demonstrate the same estimate. For example, the initial conditions $(1.83, 4.84)$ and $(4.87, 30.43)$ showed chaotic and periodic dynamics, respectively, for $K = 10.1711$, but mean density of the respective species is the same for both of these initial conditions.

2.6.2 Mean population with prey harvesting

Next, we will examine the effects of prey harvesting on the mean population size of both species. Legović *et al.* [58] asserted that harvesting only the prey population results in the extinction of the predator in a continuous predator-prey system. In the systems they

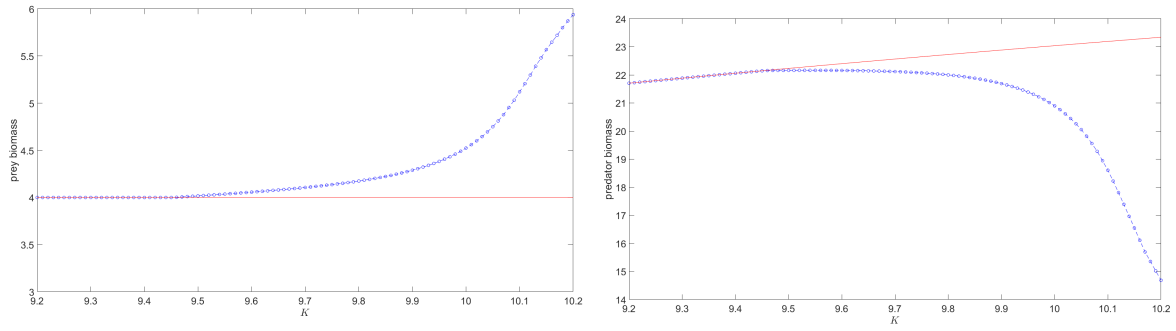

(a) **(b)**

Figure 2.6.1: Carrying capacity vs Mean density population (blue coloured) and equilibrium state (red coloured) using initial condition $(1.83, 4.84)$ (a) mean prey density with prey equilibrium state, and (b) mean predator density with predator equilibrium state.

studied, the yield from the prey species is a linear function of the harvesting effort, and therefore, it does not exhibit a maximum. Harvesting towards the maximum yield causes the extinction of predator population. Ghosh *et al.* [60] and Tromeur and Loeuille [61] also revealed similar behavior in terms of yield and predator extinction while harvesting prey in the continuous Rosenzweig-MacArthur model. We can obtain the coexisting equilibrium explicitly from the system (6). The equilibrium prey biomass is independent of harvesting effort e_1, while equilibrium predator biomass is dependent on effort. As the harvesting effort on prey population is increased, one might expect the reduction of both prey and predator biomass.

However, it is already established [58, 60, 61] that equilibrium prey biomass is constant as exploitation of prey species is increased . In our discrete-time model, we also come across the constant equilibrium prey biomass with increase in harvesting effort. We detect that the mean prey density decreases with increase in effort when nonequilibrium dynamics exist in the system (Figure 2.6.2a). On the other hand, the mean predator density increases for relatively smaller effort and then decreases when the system is unstable (Figure 2.6.2b). The increase in mean predator size when prey decreases for small efforts seems very uncommon in theoretical ecology. This indicates a very complex stock pattern in terms of mean population density between prey and predator while prey is harvested. However, mean population densities of both the species decrease in some other interval of prey harvesting effort which is more acceptable and evident in ecological systems. The

system becomes stable after the occurrence of a Neimark-Sacker bifurcation and the mean population densities coincide with the equilibrium densities of both the species under prey harvesting.

We already reported that the mean prey density is a decreasing function of the harvesting effort $e_1 \in (0, 0.224)$. We now examine if the mean yield $(q_1 e_1 \overline{x})$, produces a maximum from the prey in nonequilibrium dynamics. In Figure 2.6.2a, the small section in the upper left corner reveals that the yield is an increasing function of the harvesting effort. Thus, the yield increases approximately linearly with prey exploitation and lacks a maximum. Our results are consistent with those provided by [58, 60, 61] at equilibrium. The multistable states do not affect the mean population densities of both species under consideration, as also observed in the case of species enrichment.

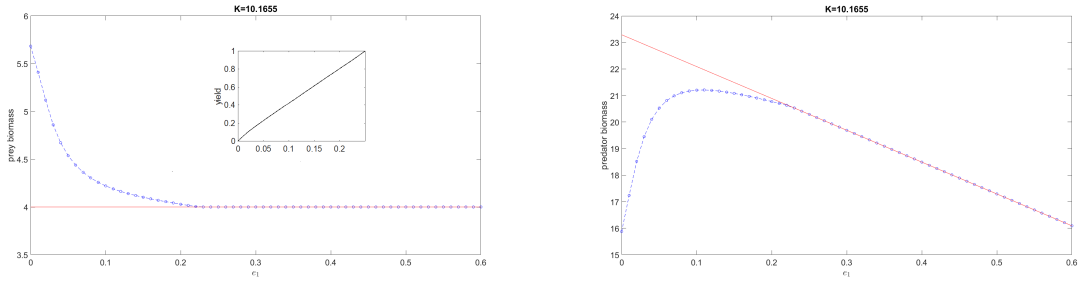

(a) **(b)**

Figure 2.6.2: Prey harvesting effort vs mean population density (blue colored) and equilibrium state (red colored) (a) mean prey density with prey equilibrium state for $K = 10.1655$ with e_1 vs yield (black colored) in the small subplot, and (b) mean predator density with predator equilibrium state for $K = 10.1655$.

2.6.3 Hydra effect

The hydra effect, or hydra paradox, is inspired by the Greek myth of the "Lernaean Hydra", which grew two heads for every one that was cut off. Ecological systems can display a hydra effect when an increase in the death rate of a particular species ultimately leads to a growth in its population size. Mathematically, a species is considered to exhibit a hydra effect, if there exist an initial condition $x_0 \in D \geq 0$ and mortality rates $m_1 < m_2$ so that $\phi(x_0, m_1) < \phi(x_0, m_2)$, where ϕ is the mean value map [53]. Recalling the model (2.2.2),

$$x_{n+1} = x_n + r x_n \left(1 - \frac{x_n}{K}\right) - \frac{\alpha x_n y_n}{h + x_n} - q_1 e_1,$$
$$y_{n+1} = y_n + \frac{\beta x_n y_n}{h + x_n} - m y_n - q_2 e_2.$$

Figure 2.6.3: The mythical creature Hydra. (Source:https://en.wikipedia.org/wiki/File:Hydra.png)

We examine the effect of increase in exploitation of the predator in terms of mean population densities. Typically, as the harvesting effort on the predator increases, the prey population grows while the predator population declines. When the predator is harvested, predator population decreases resulting in increase of prey population in a Lotka-Volterra predator-prey model [58] and in a stable system [45]. On the contrary, Sieber and Hilkar [53] and Ghosh et al. [60] reported that the time-averaged predator density increases with increase in predator mortality when the Rosenzweig-MacArthur model is in cyclic mode. Such an increase in mean (or stable) stock of the target species is a paradoxical phenomenon called the hydra effect. The mean prey density increases with increase in predator exploitation to decrease again as harvesting effort is increased further (see Table 1 in [60]). A discrete-time Nicholson-Bailey model was analyzed by Weide *et al.* [46] which also showed hydra effect in the targeted species.

In the model currently under consideration, the equilibrium prey biomass increases with harvesting effort. However, the mean prey population decreases when the system is unstable (Figure 2.6.4a). When system is stable, the equilibrium prey biomass and mean prey density increase together as an outcome of Neimark-Sacker bifurcation as the exploitation of predator increases. Figure 2.6.4b suggests that the equilibrium predator density decreases with increase in predator exploitation. On the other hand, the mean predator density increases with harvesting effort where the system exhibits nonequilibrium behaviour. Hence, the mean predator stock increases (hydra effect) but then the stable stock decreases with increased effort. In continuous RM model, mean density of the

harvested species increases only when unstable equilibrium biomass of the same species increases. However, there is opposite relation between the mean predator density and the equilibrium predator biomass when the system is unstable. When the system becomes stable, the mean predator density merges with the equilibrium predator stock and decreases for further increment in harvesting effort on predator. The predator harvested system behaves in agreement with the results of Legović *et al.* [58] and Wollrab *et al.* [45], when it is in stable mode. The maximum sustainable yield can't be achieved in the nonequilibrium dynamics, but only when the system is stable. Stocks are not influenced by changing the initial conditions.

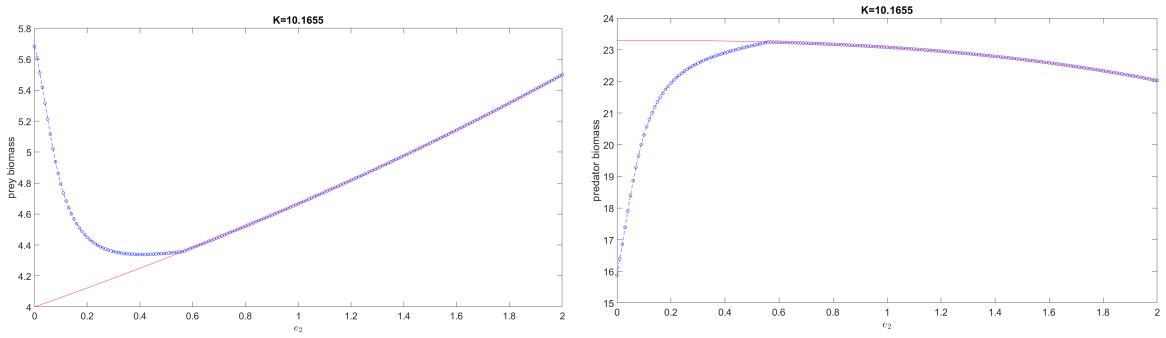

(a) **(b)**

Figure 2.6.4: Predator harvesting effort vs Mean density population (blue coloured) and equilibrium state (red coloured) (a) mean prey density with prey equilibrium state, and (b) mean predator density with predator equilibrium state.

2.7 Conclusion

In this chapter, we applied the forward Euler's scheme with a unit step size to discretize the continuous-time RM model. Conditions for the existence and stability of fixed points are obtained for both unharvested and harvested systems. Using bifurcation theory, we showed that the system undergoes a Neimark-Sacker bifurcation around the interior equilibrium under carrying capacity (K), harvesting effort on prey (e_1), and predator exploitation rate (e_2).

For further analysis, we examined dynamical changes in the unharvested system by varying the prey's carrying capacity. After a Neimark-Sacker bifurcation, the system exhibited complex dynamics, including period-bubbling, quasiperiodicity, chaos, and high-periodic windows. Notably, periodic solutions were embedded in quasiperiodic and chaotic

windows (Figure 2.5.1c). Multistability was prevalent, with coexisting periodic cycles of different periods and periodic-chaotic attractors. The basin of attraction, containing several disjoint sets (see Figure 2.5.3b-2.5.4b), was plotted. The mean prey density increased while mean predator stock declined in the non-equilibrium dynamics with increase in prey nutrient quotient, ultimately leading to predator on the verge of extinction which is a counter-intuitive phenomenon called the paradox of enrichment.

Next, we analyzed independent harvesting of prey and predator. Increasing prey harvesting effort led to system stabilization by eradicating chaotic, periodic, and quasiperiodic windows via a Neimark-Sacker bifurcation. Similar dynamics occurred when only the predator was harvested.While Wikan and Kristensen [62] and Jiménez López and Liz [63] observed harvesting-induced instability, we found that harvesting stabilizes the coexisting equilibrium.

In the unstable regime, mean predator stock increased with prey harvesting but later declined, aligning with equilibrium densities upon stabilization of the equilibrium point. When predators were harvested, prey increased while predator density declined at the stable state, as seen in continuous RM models [45, 58]. Our model exhibited the hydra effect [46, 53, 60], where mean predator density increased despite declining unstable equilibrium (Figure 2.6.4b), a feature not observed in continuous-time RM models. While mean prey density declined in the unstable regime, stable prey biomass increased, whereas predator stock declined with further exploitation.

CHAPTER 3

A discretized Rosenzweig-MacArthur model with harvesting using method of piecewise constant argument

3.1 Introduction

In this chapter *, we explore a discrete-time Rosenzweig-MacArthur (RM) model incorporating harvesting, demonstrating its complex dynamical behavior compared to the continuous-time counterpart. Using the method of piecewise constant argument [9], we discretize the continuous model and examine stability of fixed points under variations of key parameters such as prey carrying capacity and harvesting efforts. We derive conditions for the occurrence of a Neimark-Sacker bifurcation and explore how multistability influences the system dynamics.

The method of piecewise constant arguments (semi-discrete method) for differential equations [9] serves as an alternative to the forward Euler's scheme for discretizing continuous-time predator-prey models, ensuring non-negativity of solutions. Fang *et al.* [64] demonstrated global attractivity in a discrete system with Beddington-DeAngelis response. Din [39] established boundedness, equilibrium uniqueness, and bifurcations in a Leslie-Gower model, while Din *et al.* [65] studied persistence and existence of equilibrium in a Nicholson-Bailey model. Recent works, Naik *et al.* [66] and Sharma *et al.* [67] explored bifurcations, including codimension-1 and codimension-2 cases.

A key parameter in ecological dynamics is the carrying capacity of prey, influencing system stability [44, 47, 68]. The paradox of enrichment [43] suggests that increasing prey resources can drive predator extinction. Weide *et al.* [46] found that increasing carrying capacity destabilizes discrete-time systems, while Pattanayak *et al.* [47] highlighted multistability due to resource augmentation. Rajni and Ghosh [68] demonstrated bistability, where different initial conditions lead to distinct stable states. This work examines system dynamics under fluctuating nutrient supply for prey.

Phase portraits and bifurcation diagrams are fundamental tools in analyzing nonlinear systems, but two-parameter bifurcation analysis provides deeper insights. Other studies [42, 69–72] revealed organized periodic structures like Arnold tongues and shrimp structures. Li *et al.* [73] explored two-parameter bifurcation diagrams, demonstrating resonant phenomena.

* This chapter based on the following article: **Rajni, Bapan Ghosh**, Arnold tongues, shrimp structures, multistability, and ecological paradoxes in a discrete-time predator-prey System, *Chaos: An Interdisciplinary Journal of Nonlinear Science,* 34.12 (2024).

Harvesting significantly impacts population models, requiring sustainable strategies to balance yield and ecological stability. Increased harvesting can stabilize chaotic attractors [46, 48]. Eskandari *et al.* [74] investigated harvesting-induced bifurcations, while Neverova *et al.* [49] reported multistability under age-specific harvesting. The hydra effect, where increased mortality counterintuitively boosts population levels, has been observed in various models [44, 54–56]. Pal [57] noted that predator grouping fosters a hydra effect in prey, while interference induces the effect in predators.

This chapter is divided into six major sections. In the section 3.2, we formulate discrete-time RM model incorporating independent harvesting of both predator and prey species derived using the method of piecewise constant argument (semi-discrete scheme). Moving to the section 3.3, we determine the equilibrium points and providing insights into stability characteristics of those steady points of the system. In the section 3.4, we employ the center manifold theorem and bifurcation theory to derive the normal forms associated with flip and Neimark-Sacker bifurcations. The section 3.5 primarily focuses on the dynamical effects and ecological implications of varying the carrying capacity (increase in nutrient supply) of the prey species. Additionally, we conduct a bi-parameter analysis of the system, exploring how simultaneous variations in prey and predator harvesting efforts affect the system's behavior in the section 3.6. Finally, in the section 3.7, we provide the key findings and their significance in the broader context of the study.

3.2 Model formulation

We discretize the model (2.2.1) by using the method of piecewise constant argument [9]. System (2.2.1) can be written as,

$$\begin{aligned} \frac{1}{x(t)}\frac{\mathrm{d}x(t)}{\mathrm{d}t} &= r\left(1-\frac{x([t])}{K}\right)-\frac{\alpha y([t])}{h+x([t])}-q_1e_1,\\ \frac{1}{y(t)}\frac{\mathrm{d}y(t)}{\mathrm{d}t} &= \frac{\beta x([t])}{h+x([t])}-m-q_2e_2, \end{aligned} \tag{3.2.1}$$

where $[t]$ is the integer part of t, and $t \in (0,\infty)$. Then $[t] = n$, for $t \in [n, n+1)$. Hence, $(x([t]), y([t])) = (x(n), y(n))$.

In view of the above, the system (3.2.1) could be written as

$$\frac{1}{x(t)}\frac{\mathrm{d}x(t)}{\mathrm{d}t} = r\left(1-\frac{x(n)}{K}\right)-\frac{\alpha y(n)}{h+x(n)}-q_1e_1,$$

$$\frac{1}{y(t)}\frac{\mathrm{d}y(t)}{\mathrm{d}t} = \frac{\beta x(n)}{h + x(n)} - m - q_2 e_2.$$

Now the RHS of the above systems is constant.

Integrating the system on the intervals $t \in [n, n+1)$ with $n = 0, 1, 2, ...$, we obtain

$$\ln(x(t))\Big|_n^t = \left(r\left(1 - \frac{x(n)}{K}\right) - \frac{\alpha y(n)}{h + x(n)} - q_1 e_1\right)(t - n),$$
$$\ln(y(t))\Big|_n^t = \left(\frac{\beta x(n)}{h + x(n)} - m - q_2 e_2\right)(t - n).$$

which gives,

$$\begin{aligned} x(t) &= x(n)\exp\left(\left[r\left(1 - \frac{x(n)}{K}\right) - \frac{\alpha y(n)}{h + x(n)} - q_1 e_1\right](t - n)\right), \\ y(t) &= y(n)\exp\left(\left[\frac{\beta x(n)}{h + x(n)} - m - q_2 e_2\right](t - n)\right). \end{aligned} \tag{3.2.2}$$

By taking $t \to n + 1$, we derive the discretized model,

$$x(n+1) = x(n)\exp\left(r\left(1 - \frac{x(n)}{K}\right) - \frac{\alpha y(n)}{h + x(n)} - q_1 e_1\right),$$
$$y(n+1) = y(n)\exp\left(\frac{\beta x(n)}{h + x(n)} - m - q_2 e_2\right).$$

Using the notation $x(n) = x_n$ and $y(n) = y_n$, we obtain,

$$\begin{aligned} x_{n+1} &= x_n\exp\left(r\left(1 - \frac{x_n}{K}\right) - \frac{\alpha y_n}{h + x_n} - q_1 e_1\right), \\ y_{n+1} &= y_n\exp\left(\frac{\beta x_n}{h + x_n} - m - q_2 e_2\right). \end{aligned} \tag{3.2.3}$$

More details on this discretization is provided in many papers such as Hu *et al.* [75], Cui *et al.* [76], Banerjee *et al.* [77], Garai *et al.* [78], and Han and Lei [79]. The discrete-time system (3.2.3) will be analyzed for various dynamical changes and qualitative states of the system in this paper.

The mapping form of system of difference equations (3.2.3) is as follows:

$$\begin{pmatrix} x \\ y \end{pmatrix} \longmapsto \begin{pmatrix} x\exp\left(r\left(1 - \frac{x}{K}\right) - \frac{\alpha y}{h+x} - q_1 e_1\right) \\ y\exp\left(\frac{\beta x}{h+x} - m - q_2 e_2\right) \end{pmatrix}. \tag{3.2.4}$$

We can clearly see that system (3.2.3) always has positive solution if we take initial conditions positive. We will now discuss the stability of the equilibria of the system (3.2.3) .

3.3 Equilibrium points and their stability

Within this section, we identify the equilibrium points of the map (3.2.4) and analyze their stability and instability behaviors. The equilibria of the system (3.2.3) are given by

$$x \exp\left(r\left(1-\frac{x}{K}\right)-\frac{\alpha y}{h+x}-q_1e_1\right)=x$$
$$y \exp\left(\frac{\beta x}{h+x}-m-q_2e_2\right)=y$$

i.e.,

$$r\left(1-\frac{x}{K}\right)-\frac{\alpha y}{h+x}-q_1e_1=0$$
$$\frac{\beta x}{h+x}-m-q_2e_2=0.$$

Clearly, $E_0=(0,0)$ is trivial equilibrium point of the system (3.2.3) which always exists. The boundary equilibrium is $E_B=\left(K(1-\frac{q_1e_1}{r}),0\right)$ which exists if $r>q_1e_1$. The unique coexisting equilibrium is

$$E_*=(x^*,y^*)=\left(\frac{h(m+q_2e_2)}{\beta-m-q_2e_2},\frac{h\beta((m+q_2e_2)(Kq_1e_1-(h+K)r)+K\beta(r-q_1e_1))}{K\alpha(\beta-m-q_2e_2)^2}\right).$$

For existence of positive equilibrium, following three conditions should be satisfied:

$$\beta-m>q_2e_2 \text{ and } K>\frac{(m+q_2e_2)hr}{(r-q_1e_1)(\beta-m-q_2e_2)}.$$

Therefore, the equilibrium points of system (3.2.3) are same as the equilibrium points of continuous-time RM model. In the absence of harvesting of both the species, the equilibrium points are $(0,0)$, $(K,0)$, and $\left(\frac{mh}{\beta-m},\frac{h\beta r(K\beta-Km-hm)}{\alpha K(\beta-m)^2}\right)$.
Now we direct our focus on the local dynamic behavior of the system (3.2.3).
The Jacobian matrix system (3.2.3) at any arbitrary point is

$$J(x,y)=\begin{bmatrix}\left(1+x\left(-\frac{r}{K}+\frac{\alpha y}{(h+x)^2}\right)\right)e^{r(1-\frac{x}{K})-\frac{\alpha y}{h+x}-q_1e_1} & -\frac{\alpha x}{h+x}e^{r\left(1-\frac{x}{K}\right)-\frac{\alpha y}{h+x}-q_1e_1}\\ \frac{\beta hy}{(h+x)^2}e^{\frac{\beta x}{h+x}-m-q_2e_2} & e^{\frac{\beta x}{h+x}-m-q_2e_2}\end{bmatrix}.$$

The stability of the equilibria $(0,0)$ and $\left(K(1-\frac{q_1e_1}{r}),0\right)$, depends on the eigenvalues of the matrices

$$J(0,0)=\begin{bmatrix} e^{r-q_1e_1} & 0 \\ 0 & e^{-m-q_2e_2} \end{bmatrix}$$

and

$$J\left(K(1-\frac{q_1e_1}{r}),0\right)=\begin{bmatrix} 1-r+q_1e_1 & \frac{K\alpha(r-q_1e_1)}{K-q_1e_1-(h+K)r} \\ 0 & e^{-m-q_2e_2+\frac{K\beta(r-q_1e_1)}{hr+K(r-q_1e_1)}} \end{bmatrix}, \text{ respectively.}$$

Examining the matrices obtained, we state the following propositions:

Proposition 3.1. *The fixed point* $(0,0)$ *is always a saddle.*

Proposition 3.2. *The fixed point* E_B *is locally asymptotically stable if* $0<r-q_1e_1<2$ *and* $K<\dfrac{hr(m+q_2e_2)}{(r-q_1e_1)(\beta-m-q_2e_2)}$.

One can note that when $K<\dfrac{hr(m+q_2e_2)}{(r-q_1e_1)(\beta-m-q_2e_2)}$, the system has only two fixed points viz trivial and boundary fixed points. The positive equilibrium comes into existence when $K>\dfrac{hr(m+q_2e_2)}{(r-q_1e_1)(\beta-m-q_2e_2)}$. Without harvesting efforts, the coexisting equilibrium exists iff $\beta>m$ and $K>\dfrac{hrm}{r(\beta-m)}$.
Hereafter, we discuss the stability of the interior equilibrium point. Consider the Jacobian matrix of the system (3.2.3) evaluated at $E_*=(x^*,y^*)$ given by

$$V(x^*,y^*)=\begin{bmatrix} \left(1+x^*\left(-\frac{r}{K}+\frac{\alpha y^*}{(h+x^*)^2}\right)\right) & -\dfrac{\alpha x^*}{h+x^*} \\ \dfrac{\beta h y^*}{(h+x^*)^2} & 1 \end{bmatrix}. \tag{3.3.1}$$

The characteristic polynomial corresponding to the matrix (3.3.1) at (x^*,y^*) is given by,

$$C(\Lambda)=\Lambda^2-\mathcal{P}(x^*,y^*)\Lambda+\mathcal{Q}(x^*,y^*), \tag{3.3.2}$$

where

$$\mathcal{P}(x^*,y^*)=2-\frac{rx^*}{K}+\theta(x^*,y^*),$$

$$\mathcal{Q}(x^*,y^*)=1-\frac{rx^*}{K}+(1+\phi(x^*,y^*))\theta(x^*,y^*),$$

$$\theta(x^*, y^*) := \frac{\alpha x^* y^*}{(h + x^*)^2},$$

and

$$\phi(x^*, y^*) := \frac{\beta h}{h + x^*}.$$

This notation will be useful in the next section.

The following proposition states the stability conditions of the positive equilibrium of system (3.2.3).

Proposition 3.3. *The unique coexisting equilibrium point of system (3.2.3) is locally asymptotically stable if*

$$\left|2 + x^*\left(-\frac{r}{K} + \frac{\alpha y^*}{(h + x^*)^2}\right)\right| < 2 + x^*\left(-\frac{r}{K} + \frac{\alpha y^*}{(h + x^*)^2}\right) + \frac{\alpha\beta h x^* y^*}{(h + x^*)^3} < 2.$$

The proposition mentioned above can be derived using the result from Luo [30], Let (x^*, y^*) be a fixed point of the system (4). Then we say (x^*, y^*) is asymptotically stable iff

$$|\text{Trace}(J(x^*, y^*))| < 1 + \text{Det}(J(x^*, y^*)) < 2.$$

Next, we turn our attention to the bifurcation analysis around the positive equilibrium point of system (3.2.3) using bifurcation theory.

3.4 Bifurcation analysis

3.4.1 Neimark-Sacker bifurcation

We study the Neimark-Sacker (N-S) bifurcation of the system (3.2.3) around the positive fixed point by taking the carrying capacity of the prey population as bifurcation parameter. The similar bifurcation analysis of normal form of the Neimark-Sacker bifurcation in discrete-time systems can be found in Hu *et al.* [36], Salman *et al.* [34], Din [39], Khan [51], and Ajaz *et al.* [6].

Consider the characteristic polynomial (3.3.2) from the section 3.3. The equation $C(\lambda) = 0$ will possess two complex conjugate roots with a modulus of unity if the conditions mentioned below are satisfied:

$$K = \frac{rx^*}{(1 + \phi)\theta}$$

and

$$\left|2-\frac{rx^*}{K}+\theta\right|<2.$$

Choose the parameters $(r,K,\alpha,h,\beta,m,q_1,e_1,q_2,e_2)$ from the set

$$\Omega_{NS}=\left\{(r,K,\alpha,h,\beta,m,q_1,e_1,q_2,e_2):K=\frac{rx^*}{(1+\phi)\theta},\left|2-\frac{rx^*}{K}+\theta\right|<2\right\}.$$

An invariant closed curve bifurcates around the unique coexisting equilibrium of the system when parameters vary in a small neighborhood of Ω_{NS}. The system (3.2.3) with parameters $(r,K,\alpha,h,\beta,m,q_1,e_1,q_2,e_2)$ becomes

$$\begin{pmatrix}X\\Y\end{pmatrix}\longmapsto\begin{pmatrix}X\,\mathrm{e}^{r\left(1-\frac{X}{K}\right)-\frac{\alpha Y}{h+X}-q_1e_1}\\Y\,\mathrm{e}^{\frac{\beta X}{h+X}-m-q_2e_2}\end{pmatrix}. \tag{3.4.1}$$

The perturbation of equation (3.4.1) by taking $\widetilde{K}$ as bifurcation parameter can be written as follows:

$$\begin{pmatrix}X\\Y\end{pmatrix}\longmapsto\begin{pmatrix}X\,\mathrm{e}^{r\left(1-\frac{X}{(K+\widetilde{K})}\right)-\frac{\alpha Y}{h+X}-q_1e_1}\\Y\,\mathrm{e}^{\frac{\beta X}{h+X}-m-q_2e_2}\end{pmatrix}, \tag{3.4.2}$$

where $|\widetilde{K}|\ll 1$ is a small perturbation parameter. Introducing the transformations $x=X-x^*(\widetilde{K})$ and $y=Y-y^*(\widetilde{K})$, where (x^*,y^*) is positive equilibrium of system (3.2.3), we using Taylor's expansion about (x^*,y^*), the map (3.4.2) can be expressed as,

$$\begin{pmatrix}x\\y\end{pmatrix}\longmapsto\begin{pmatrix}\rho_{11}&\rho_{12}\\\rho_{21}&\rho_{22}\end{pmatrix}\begin{pmatrix}x\\y\end{pmatrix}+\begin{pmatrix}\mathcal{F}_1(x,y)\\\mathcal{G}_1(x,y)\end{pmatrix}, \tag{3.4.3}$$

where

$$\mathcal{F}_1(x,y)=\rho_1x^2\rho_2xy+\rho_3y^2+\rho_4x^3+\rho_5x^2y+\rho_6xy^2+\rho_7y^3+\mathcal{O}((|x|+|y|)^4),$$
$$\mathcal{G}_1(x,y)=\sigma_1x^2+\sigma_2xy+\sigma_3y^2+\sigma_4x^3+\sigma_5x^2y+\sigma_6xy^2+\sigma_7y^3+\mathcal{O}((|x|+|y|)^4),$$

and

$$\rho_{11} = \frac{(h+x^*)^2((K+\widetilde{K}) - rx^*) + \alpha x^* y^*}{(K+\widetilde{K})(h+x^*)^2},$$

$$\rho_{12} = -\frac{\alpha x^*}{h+x^*}, \quad \rho_{21} = \frac{\beta h y^*}{(h+x^*)^2}, \quad \rho_{22} = 1,$$

$$\rho_1 = -\frac{r^2 x^*}{(K+\widetilde{K})^2} - \frac{\alpha y^*(2h(h+x^*) + \alpha x^* y^*)}{(h+x^*)^4} + \frac{2r((h+x^*)^2 + \alpha x^* y^*))}{(K+\widetilde{K})(h+x^*)^2},$$

$$\rho_2 = \frac{(h+x^*)(-h(K+\widetilde{K}) + hrx^* + rx^{*^2}) - (K+\widetilde{K})\alpha x^* y^*}{(K+\widetilde{K})(h+x^*)^3}, \quad \rho_3 = \frac{\alpha^2 x^*}{(h+x^*)^2},$$

$$\begin{aligned}\rho_4 = -\frac{1}{(K+\widetilde{K})^3(h+x^*)^6)}[&(-6(K+\widetilde{K})^3 x^*(h+x^*)^2 y^*\alpha + 6(K+\widetilde{K})^3(h+x^*)^3 y^*\alpha - \\ &6(K+\widetilde{K})^2 x^*(h+x^*) y^*\alpha(r(h+x^*)^2 - (K+\widetilde{K}) y^*\alpha) + \\ &x^*(r(h+x^*)^2 - (K+\widetilde{K}) y^*\alpha)^3 - 3(K+\widetilde{K})(r(h+x^*)^3 - \\ &(K+\widetilde{K})(h+x^*) y^*\alpha)^2)]\end{aligned}$$

$$\begin{aligned}\rho_5 = \frac{\alpha}{(K+\widetilde{K})^2(h+x^*)^5}[&(-(h+x^*)^2(-2h(K+\widetilde{K})((K+\widetilde{K}) + hr) + hr(-2(K+\widetilde{K}) + hr) \\ &x^* + 2hr^2 x^{*^2} + r^2 x^{*^3}) + 2(K+\widetilde{K})(h+x^*)(h(-(K+\widetilde{K}) + rx^*) + \\ &x^*((K+\widetilde{K}) + rx^*)) y^*\alpha - (K+\widetilde{K})^2 x^* y^{*^2}\alpha^2)]\end{aligned}$$

$$\rho_6 = \frac{\alpha^2(-(h+x^*)(h(-(K+\widetilde{K}) + rx^*) + x^*((K+\widetilde{K}) + rx^*)) + (K+\widetilde{K})x^* y^*\alpha)}{(K+\widetilde{K})(h+x^*)^4},$$

$$\rho_7 = -\frac{\alpha^3 x^*}{(h+x^*)^3}, \ \sigma_1 = \frac{h\beta y^*(-2(h+x^*) + h\beta)}{(h+x^*)^4},$$

$$\sigma_2 = \frac{h\beta}{(h+x^*)^2}, \ \sigma_4 = \frac{h\beta y^*(6(h+x^*)^2 - 6h\beta(h+x^*) + h^2\beta^2)}{(h+x^*)^6},$$

$$\sigma_5 = \frac{h\beta(-2(h+x^*) + h\beta)}{(h+x^*)^4}, \text{ and } \sigma_3 = \sigma_6 = \sigma_7 = 0.$$

The characteristic equation of the linearized system with perturbation $\widetilde{K}$ of the system (3.4.3) can be written as,

$$\Lambda^2 - \mathcal{P}(\widetilde{K}) - \mathcal{Q}(\widetilde{K}) = 0, \tag{3.4.4}$$

where

$$\mathcal{P}(\widetilde{K}) = 2 - \frac{rx^*}{K+\widetilde{K}} + \theta(\widetilde{K}),$$

$$\mathcal{Q}(\widetilde{K}) = 1 - \frac{rx^*}{K+\widetilde{K}} + (1+\phi)\theta(\widetilde{K})$$

and

$$\theta(\widetilde{K}) = \frac{\alpha x^* y^*(\widetilde{K})}{(h+x^*)^2}$$

The roots of the characteristic equation are complex conjugate with modulus unit as the parameters lie in the neighborhood of the set Ω_{NS} given by

$$\Lambda_1, \Lambda_2 = \frac{\mathcal{P}(\widetilde{K})}{2} \pm \frac{i}{2}\sqrt{4\mathcal{Q}(\widetilde{K}) - \mathcal{P}^2(\widetilde{K})}.$$

Then

$$|\Lambda_1| = |\Lambda_2| = \sqrt{\mathcal{Q}(\widetilde{K})}.$$

Also,

$$\left(\frac{\mathrm{d}|\Lambda_1|}{\mathrm{d}\widetilde{K}}\right)_{\widetilde{K}=0} = \left(\frac{\mathrm{d}|\Lambda_2|}{\mathrm{d}\widetilde{K}}\right)_{\widetilde{K}=0} = \left(\frac{\mathrm{d}\sqrt{\mathcal{Q}(\widetilde{K})}}{\mathrm{d}\widetilde{K}}\right)_{\widetilde{K}=0}. \tag{3.4.5}$$

We have

$$\begin{aligned}
\frac{\mathrm{d}\sqrt{\mathcal{Q}(\widetilde{K})}}{\mathrm{d}\widetilde{K}} &= \frac{1}{2\sqrt{\mathcal{Q}(\widetilde{K})}}\frac{\mathrm{d}\mathcal{Q}(\widetilde{K})}{\mathrm{d}\widetilde{K}} \\
&= \frac{1}{2\sqrt{\mathcal{Q}(\widetilde{K})}}\left[\frac{rx^*}{(K+\widetilde{K})^2} + (1+\theta)\frac{\mathrm{d}\phi}{\mathrm{d}\widetilde{K}} + \phi\frac{\mathrm{d}\theta}{\mathrm{d}\widetilde{K}}\right] \\
&= \frac{1}{2\sqrt{\mathcal{Q}(\widetilde{K})}}\left[\frac{rx^*}{(K+\widetilde{K})^2} + \phi\frac{\mathrm{d}\theta}{\mathrm{d}\widetilde{K}}\right] \\
&= \frac{1}{2\sqrt{\mathcal{Q}(\widetilde{K})}}\left[\frac{rx^*}{(K+\widetilde{K})^2} + \frac{h^2(m+q_2e_2)r\beta^2x^*}{(h+x^*)^2(K+\widetilde{K})^2(m+q_2e_2-\beta)^2}\right].
\end{aligned}$$

Hence, from equation (3.4.5),

$$\left(\frac{\mathrm{d}|\Lambda_1|}{\mathrm{d}\widetilde{K}}\right)_{\widetilde{K}=0} = \left(\frac{\mathrm{d}|\Lambda_2|}{\mathrm{d}\widetilde{K}}\right)_{\widetilde{K}=0} = \frac{1}{2\sqrt{\mathcal{Q}(0)}}\left[\frac{rx^*}{K^2} + \frac{h^2(m+q_2e_2)r\beta^2x^*}{(h+x^*)^2K^2(m+q_2e_2-\beta)^2}\right].$$

It is difficult to analyze the sign of transversality condition analytically for the above expression. We will calculate the value of transversality condition for some fixed parameter set in the example provided in later of this section.

Assume that $\mathcal{P}(0) = 2 - \dfrac{rx^*}{K} + \theta(0) \neq 0, -1$, and since $(r, K^*, \alpha, h, \beta, m, q_1, e_1, q_2, e_2) \in \Omega_{NS}$, we can conclude that $-2 < \mathcal{P}(0) < 2$. Then $\mathcal{P}(0) \neq \pm 2, -1, 0$ implies $\Lambda_1^m, \Lambda_2^m \neq 1\, \forall m = 1, 2, 3, 4$ at $\widetilde{K} = 0$. When $\widetilde{K} = 0$ and if the following conditions are satisfied:

$$2 - \frac{rx^*}{K} + \theta(0) \neq 0 \text{ and } 2 - \frac{rx^*}{K} + \theta(0) \neq -1, \tag{3.4.6}$$

the solutions of equation (3.4.4) do not lie on the real or imaginary axes of the unit circle (i.e., they are not equal to ± 1 or $\pm i$).

The normal form of equation (12) at $\widetilde{K} = 0$ is obtained by taking $\kappa = \dfrac{\mathcal{P}(0)}{2}$ and $\eta = \dfrac{1}{2}\sqrt{4\mathcal{Q}(0) - \mathcal{P}^2(0)}$. Consider the following transformation:

$$\begin{pmatrix} x \\ y \end{pmatrix} = \begin{pmatrix} 0 & \rho_{12} \\ \eta & \kappa - \rho_{11} \end{pmatrix} \begin{pmatrix} \mu \\ \nu \end{pmatrix}. \tag{3.4.7}$$

The normal form of equation (3.4.3) using transformation (3.4.7) can be written as:

$$\begin{pmatrix} \mu \\ \nu \end{pmatrix} \longmapsto \begin{pmatrix} \kappa & -\eta \\ \eta & \kappa \end{pmatrix} \begin{pmatrix} \mu \\ \nu \end{pmatrix} + \begin{pmatrix} \mathcal{F}_2(\mu, \nu) + (O)((|\mu| + |\nu|)^4) \\ \mathcal{G}_2(\mu, \nu) + \mathcal{O}((|\mu| + |\nu|)^4) \end{pmatrix}, \tag{3.4.8}$$

where

$$\mathcal{F}_2(\mu, \nu) = \frac{\rho_{11} - \kappa}{\rho_{12}\eta}\mathcal{F}_1(\rho_{12}\nu, \eta\mu + (\kappa - \rho_{11})\nu) + \frac{1}{\eta}\mathcal{G}_1(\rho_{12}\nu, \eta\mu + (\kappa - \rho_{11})\nu)$$

$$\mathcal{G}_2(\mu, \nu) = \frac{1}{\rho_{12}}\mathcal{F}_1(\rho_{12}\nu, \eta\mu + (\kappa - \rho_{11})\nu).$$

Now, the Lyapunov coefficient [31] can be defined as follows:

$$L = \left(\left[-Re\left(\frac{(1-2\Lambda_1)\Lambda_2^2}{1-\Lambda_1}\tau_{20}\tau_{11}\right) - \frac{1}{2}|\tau_{11}|^2 - |\tau_{02}|^2 + Re(\Lambda_2\tau_{21})\right]\right)_{\widetilde{K}=0},$$

where

$$\tau_{20} = \frac{1}{2}[\mathcal{F}_{2\mu\mu} - \mathcal{F}_{2\nu\nu} + 2\mathcal{G}_{2\mu\nu} + i(\mathcal{G}_{2\mu\mu} - \mathcal{G}_{2\nu\nu} - 2\mathcal{F}_{2\mu\nu})],$$
$$\tau_{11} = \frac{1}{4}[\mathcal{F}_{2\mu\mu} + \mathcal{F}_{2\nu\nu} + i(\mathcal{G}_{2\mu\mu} + \mathcal{G}_{2\nu\nu})],$$
$$\tau_{02} = \frac{1}{8}[\mathcal{F}_{2\mu\mu} - \mathcal{F}_{2\nu\nu} - 2\mathcal{G}_{2\mu\nu} + i(\mathcal{G}_{2\mu\mu} - \mathcal{G}_{2\nu\nu} + 2\mathcal{F}_{2\mu\nu})],$$
$$\tau_{21} = \frac{1}{16}[\mathcal{F}_{2\mu\mu\mu} + \mathcal{F}_{2\mu\nu\nu} + \mathcal{G}_{2\mu\mu\nu} + \mathcal{G}_{2\nu\nu\nu} + i(\mathcal{G}_{2\mu\mu\mu} + \mathcal{G}_{2\mu\nu\nu} - \mathcal{F}_{2\mu\mu\nu} - \mathcal{F}_{2\nu\nu\nu})].$$

Utilizing the analysis provided above, we present the subsequent theorem.

Theorem 3.4. *[31] When $L \neq 0$, the system (2) experiences a Neimark-Sacker bifurcation around the singular positive equilibrium point (x^*, y^*) as the parameter K undergoes variation within the vicinity of Ω_{NS}. In cases where $L < 0$ (respectively, $L > 0$), an attracting (or repelling) closed curve that is invariant undergoes bifurcation from the point (x^*, y^*).*

Example 3.5. Setting $r = \frac{5}{2}, \alpha = \frac{9}{10}, \beta = \frac{7}{10}, h = 4$, and $m = \frac{2}{10}$, the Neimark-Sacker bifurcation occurs at the equilibrium point $(x^*, y^*) = \left(\frac{8}{5}, \frac{98}{9}\right)$ at $K^* = \frac{16}{3}$ in the unharvested system. At the positive equilibrium (x^*, y^*), the eigenvalues of the Jacobian matrix are

$$\lambda_1 = \frac{7 - i\sqrt{15}}{8}, \ \lambda_2 = \frac{7 + i\sqrt{15}}{8}.$$

Here, $|\lambda_1| = |\lambda_2| = 1$, at the bifurcation point K^*. The value of transversality condition is calculated as,

$$\left(\frac{d|\Lambda_{1,2}|}{d\widetilde{K}}\right)_{\widetilde{K}=0} = \frac{9}{64} = 0.81667.$$

A positive derivative value of the absolute eigenvalue signifies the system's instability subsequent to the Neimark-Sacker bifurcation. When $K < K^*$, the eigenvalues will reside within the interior of the unit circle. As $K > K^*$, the eigenvalues will escape from the unit circle. The Lyapunov coefficient

$$L = \frac{295893}{14049280} \approx 0.02106108$$

which means that a repelling invariant curve bifurcates at the interior equilibrium point.

3.4.2 Period-doubling bifurcation

In this subsection, we deal with the period-doubling bifurcation of the system (3.2.3) around the positive equilibrium point as the carrying capacity of the prey species is varied. If the Jacobian matrix at the coexisting equilibrium point (x^*, y^*) has one of the eigenvalues is -1 (say λ_1) and other one is not equal to ± 1 (say λ_2).The period-doubling bifurcation emerges when the parameters undergo slight variations within a small vicinity of

$$\Omega_{PD} = \{(r, K, \alpha, h, \beta, m, q_1, e_1, q_2, e_2): \ \frac{8x^*}{K} + \left(2 - \frac{rx^*}{K} + \theta\right)^2 > 4(1 + \theta + \theta\phi), \\ K = \frac{(2+r)x^*}{4 + 2\theta + \theta\phi} \}.$$

The above set is derived using the characteristic polynomial of the Jacobian matrix at coexisting equilibrium and $\theta(x^*, y^*)$ and $\phi(x^*, y^*)$ have same meaning as taken in eq (3.4.4). Consider $\widehat{K}$ as bifurcation parameter, then system (3.2.3) becomes

$$\begin{aligned} x_{n+1} &= x_n \exp\left(r\left(1 - \frac{x_n}{(K + \widehat{K})}\right) - \frac{\alpha y_n}{h + x_n} - q_1 e_1\right), \\ y_{n+1} &= y_n \exp\left(\frac{\beta x_n}{h + x_n} - m - q_2 e_2\right), \end{aligned} \tag{3.4.9}$$

where $|\widehat{K}| \ll 1$. Let $u_n = x_n - x^*$ and $v_n = y_n - y^*$. Using this transformation, we transformed the coexisting equilibrium (x^*, y^*) to origin. By Taylor's expansion around $(0, 0)$, we get

$$\begin{aligned} u_{n+1} &= \Gamma_{11}u_n + \Gamma_{12}v_n + \Gamma_{13}u_n^2 + \Gamma_{14}u_n v_n + \Gamma_{15}v_n^2 \\ &\quad + \gamma_{01}u_n\widehat{K} + \gamma_{02}u_n^2\widehat{K} + \gamma_{03}v_n^2\widehat{K} + \gamma_{04}v_n^2\widehat{K}, \\ v_{n+1} &= \Gamma_{21}u_n + \Gamma_{22}v_n + \Gamma_{23}u_n^2 + \Gamma_{24}u_n v_n + \Gamma_{25}v_n^2, \end{aligned} \tag{3.4.10}$$

where

$$\Gamma_{11} = \frac{(h+x^*)^2(K-rx^*)+\alpha K x^* y^*}{K(h+x^*)^2},$$

$$\Gamma_{12} = -\frac{\alpha x^*}{h+x^*},\ \ \Gamma_{21} = \frac{\beta h y^*}{(h+x^*)^2},\ \ \Gamma_{22} = 1,$$

$$\Gamma_{13} = \frac{1}{2}\left(\frac{r^2 x^*}{K^2} + \frac{\alpha y^*(2h(h+x^*)+\alpha x^* y^*)}{(h+x^*)^4} - \frac{2r((h+x^*)^2+\alpha x^* y^*))}{K(h+x^*)^2}\right),$$

$$\Gamma_{14} = \frac{(h+x^*)(-hK+hrx^*+rx^{*^2})-K\alpha x^* y^*}{K(h+x^*)^3},$$

$$\Gamma_{15} = \frac{\alpha^2 x^*}{(h+x^*)^2},$$

$$\gamma_{01} = \frac{rx^*\left((h+x^*)^2(2K-rx^*)+Kx^* y^*\alpha\right)}{K^3(h+x^*)^2},$$

$$\gamma_{02} = \frac{r}{2K^4(h+x^*)^4}\Big((h+x^*)^4(2K^2-4Krx^*+r^2x^{*^2})+$$
$$2Kx^*(h+x^*)(x^*(K-rx^*)+h(2K-rx^*)y^*\alpha+K^2\alpha^2x^{*^2}y^{*^2})\Big),$$

$$\gamma_{03} = -\frac{r\alpha x^{*^2}}{K^2(h+x^*)},\ \ \gamma_{04} = \frac{r\alpha^2 x^{*^2}}{2K^2(h+x^*)^2},$$

$$\Gamma_{23} = \frac{h\beta y^*(-2(h+x^*)+h\beta)}{(h+x^*)^4},\ \ \Gamma_{24} = \frac{h\beta}{(h+x^*)^2},\quad \Gamma_{25} = 0.$$

Constructing the invertible matrix T

$$T = \begin{pmatrix} \Gamma_{12} & \Gamma_{12} \\ -1-\Gamma_{11} & \lambda_2-\Gamma_{11} \end{pmatrix}$$

and use the transformation

$$\begin{pmatrix} u_n \\ v_n \end{pmatrix} = \begin{pmatrix} \Gamma_{12} & \Gamma_{12} \\ -1-\Gamma_{11} & \lambda_2-\Gamma_{11} \end{pmatrix}\begin{pmatrix} X_n \\ Y_n \end{pmatrix}.$$

From (3.4.10), we get

$$\begin{pmatrix} X_{n+1} \\ Y_{n+1} \end{pmatrix} = \begin{pmatrix} -1 & 0 \\ 0 & \lambda_2 \end{pmatrix}\begin{pmatrix} X_n \\ Y_n \end{pmatrix} + \begin{pmatrix} \Phi_1(u_n, v_n, \widehat{K}) \\ \Phi_2(u_n, v_n, \widehat{K}) \end{pmatrix}, \tag{3.4.11}$$

where

$$\phi_1(u_n, v_n, \widehat{K}) = \frac{\Gamma_{13}(\lambda_2 - \Gamma_{11}) - \Gamma_{12}\Gamma_{23}}{\Gamma_{12}(1+\lambda_2)}u_n^2 + \frac{\Gamma_{14}(\lambda_2 - \Gamma_{11}) - \Gamma_{12}\Gamma_{24}}{\Gamma_{12}(1+\lambda_2)}u_n v_n +$$
$$\frac{\Gamma_{15}(\lambda_2 - \Gamma_{11}) - \Gamma_{12}\Gamma_{25}}{\Gamma_{12}(1+\lambda_2)}v_n^2 + \frac{\gamma_{01}(\lambda_2 - \Gamma_{11})}{\Gamma_{12}(1+\lambda_2)}u_n\widehat{K} + \frac{\gamma_{03}(\lambda_2 - \Gamma_{11})}{\Gamma_{12}(1+\lambda_2)}v_n\widehat{K} +$$
$$\frac{\gamma_{02}(\lambda_2 - \Gamma_{11})}{\Gamma_{12}(1+\lambda_2)}u_n^2\widehat{K} + \frac{\gamma_{04}(\lambda_2 - \Gamma_{11})}{\Gamma_{12}(1+\lambda_2)}v_n^2\widehat{K},$$

$$\phi_2(u_n, v_n, \widehat{K}) = \frac{\Gamma_{13}(1 + \Gamma_{11}) + \Gamma_{12}\Gamma_{23}}{\Gamma_{12}(1+\lambda_2)}u_n^2 + \frac{\Gamma_{14}(1 + \Gamma_{11}) + \Gamma_{12}\Gamma_{24}}{\Gamma_{12}(1+\lambda_2)}u_n v_n +$$
$$\frac{\Gamma_{15}(1 + \Gamma_{11}) + \Gamma_{12}\Gamma_{25}}{\Gamma_{12}(1+\lambda_2)}v_n^2 + \frac{\gamma_{01}(1 + \Gamma_{11})}{\Gamma_{12}(1+\lambda_2)}u_n\widehat{K} + \frac{\gamma_{03}(1 + \Gamma_{11})}{\Gamma_{12}(1+\lambda_2)}v_n\widehat{K} +$$
$$\frac{\gamma_{02}(1 + \Gamma_{11})}{\Gamma_{12}(1+\lambda_2)}u_n^2\widehat{K} + \frac{\gamma_{04}(1 + \Gamma_{11})}{\Gamma_{12}(1+\lambda_2)}v_n^2\widehat{K},$$

$$u_n^2 = \Gamma_{12}^2(X_n^2 + 2X_nY_n + Y_n^2)$$
$$u_n v_n = (-\Gamma_{12} - \Gamma_{12}\Gamma_{11})X_n^2 + (\Gamma_{12}\lambda_2 - \Gamma_{12}\Gamma_{11} - \Gamma_{12}(1+\Gamma_{11}))X_nY_n + \Gamma_{12}(\lambda_2 - \Gamma_{11})Y_n^2,$$
$$u_n\widehat{K} = \Gamma_{12}X_n\widehat{K} + \Gamma_{12}Y_n\widehat{K},$$
$$u_n^2\widehat{K} = \Gamma_{12}^2(X_n^2\widehat{K} + 2X_nY_n\widehat{k} + Y_n^2\widehat{K}).$$

Hence, there exists a center manifold $\mathcal{M}^c(0,0)$ of the map (3.4.11) about $(0,0)$ in a small neighborhood of $\widehat{K}$ (using center manifold theorem that is represented as:

$$\mathcal{M}^c(0,0) = \{(X_n, Y_n) : Y_n = c_0X^2 + c_1X\widehat{K} + c_2\widehat{K}^2 + \mathcal{O}((|X_n| + |\widehat{K}|)^3)\},$$

where

$$c_0 = \frac{(1+\Gamma_{11})^3\Gamma_{15} - \Gamma_{12}^3\Gamma_{23} - (1+\Gamma_{11})\Gamma_{12}^2(\Gamma_{13} - \Gamma_{24}) + (1+\Gamma_{11})^2\Gamma_{12}(\Gamma_{14} + \Gamma_{25})}{\Gamma_{12}(1+\lambda_2)(2+\lambda_2)}$$
$$c_1 = \frac{(1+\Gamma_{11})(-\gamma_{01}\Gamma_{12} + \gamma_{03}(1+\Gamma_{11}))}{\Gamma_{12}(1+\lambda_2)^2}, \quad c_2 = 0.$$

Then, we derive map (3.4.11) restricted to the center manifold $\mathcal{M}^c(0,0)$ as follows:

$$\mathcal{F}(\tilde{x}_n) = -\tilde{x}_n + d_1\tilde{x}_n^2 + d_2\tilde{x}_n\widehat{K} + d_3\tilde{x}_n^2\widehat{K} + d_4\tilde{x}_n\widehat{K}^2 + d_5\tilde{x}_n^3 + \mathcal{O}((|\tilde{x}_n| + |\widehat{K}|)^4) \quad (3.4.12)$$

where

$$d_1 = \frac{1}{1+\lambda_2}(-\Gamma_{12}(\Gamma_{13}(\Gamma_{11}-\lambda_2)+\Gamma_{12}\Gamma_{23})+(1+\Gamma_{11})(\Gamma_{14}(\Gamma_{11}-\lambda_2)+\Gamma_{12}\Gamma_{24}))$$
$$-\frac{(1+\Gamma_{11})^2(\Gamma_{15}(\Gamma_{11}-\lambda_2)+\Gamma_{12}\Gamma_{25})}{\Gamma_{12}(1+\lambda_2)}, \quad d_2 = \frac{(\Gamma_{11}-\lambda_2)(-\gamma_{01}\Gamma_{12}+\gamma_{03}(1+\Gamma_{11}))}{\Gamma_{12}(1+\lambda_2)},$$

$$d_3 = -\frac{1}{\Gamma_{12}(1+\lambda_2)}\left(\gamma_{02}\Gamma_{12}^2(\Gamma_{11}-\lambda_2)+\gamma_{04}(\Gamma_{11}-\lambda_2)(1+\Gamma_{11})^2+c_0\gamma_{01}\Gamma12(\Gamma_{11}-\lambda_2)-c_0\gamma_{03}(\Gamma_{11}-\lambda\right.$$
$$2c_1\Gamma_{12}^2(\Gamma_{11}\Gamma_{13}+\Gamma_{12}\Gamma_{23}-\Gamma_{13}\lambda_2)+c_1\Gamma_{12}(1+2\Gamma_{11}-\lambda_2)(\Gamma_{11}\Gamma_{14}+\Gamma_{12}\Gamma_{24}-\Gamma_{14}\lambda_2)+$$
$$\left.2c_1(1+\Gamma_{11})(\Gamma_{11}-\lambda_2)(\Gamma_{11}\Gamma_{15}+\Gamma_{12}\Gamma_{25}-\Gamma_{15}\lambda_2)\right),$$

$$d_4 = \frac{c_1(\lambda_2-\Gamma_{11})(\gamma_{01}\Gamma_{12}+\gamma_{03}(\lambda_2-\Gamma_{11}))}{\Gamma_{12}(1+\lambda_2)},$$

$$d_5 = c_0\left(\frac{-2\Gamma_{12}(\Gamma_{11}\Gamma_{13}+\Gamma_{12}\Gamma_{23}-\Gamma_{13}\lambda_2))}{1+\lambda_2}+\frac{(1+2\Gamma_{11}-\lambda_2)(\Gamma_{11}\Gamma_{14}+\Gamma_{12}\Gamma_{24}-\Gamma_{14}\lambda_2)}{1+\lambda_2}+\right.$$
$$\left.\frac{2(1+\Gamma_{11})(\Gamma_{11}-\lambda_2)(\Gamma_{11}\Gamma_{15}+\Gamma_{12}\Gamma_{25}-\Gamma_{15}\lambda_2)}{\Gamma_{12}(1+\lambda_2)}\right).$$

For map (3.4.12) to show occurrence of period-doubling bifurcation, the following two discriminatory quantities α_1 and α_2 are non-zero:

$$\alpha_1 = \left(\frac{\partial^2\mathcal{F}}{\partial\tilde{x}_n\partial\widehat{K}}+\frac{1}{2}\frac{\partial\mathcal{F}}{\partial\widehat{K}}\frac{\partial^2\mathcal{F}}{\partial\tilde{x}_n^2}\right)\Bigg|_{(0,0)} = d_2$$

and

$$\alpha_2 = \left(\frac{1}{6}\frac{\partial^3\mathcal{F}}{\partial\tilde{x}_n^3}+\left(\frac{1}{2}\frac{\partial^2\mathcal{F}}{\partial\tilde{x}_n^2}\right)^2\right)\Bigg|_{(0,0)} = d_1^2+d_5.$$

From above analysis and the theorem in Kuznetsov [31] and Guckenheimer [80], we have the theorem as follows:

Theorem 3.6. *If $\alpha_2 \neq 0$, then the map (3.4.9) undergoes a Period-doubling bifurcation about the unique positive equilibrium point (x^*, y^*) when the parameter $\widehat{K}$ varies slightly in the vicinity of Ω_{PD}. If $\alpha_2 > 0$ (resp. $\alpha_2 < 0$), then an attracting (resp. repelling) period-2 orbit bifurcates from (x^*, y^*).*

Example 3.7. Setting $r = 4, \alpha = \dfrac{6}{10}, \beta = \dfrac{5}{10}, h = 20$, and $m = \dfrac{1}{10}$, the period-doubling bifurcation occurs at the equilibrium $(x^*, y^*) = \left(5, \dfrac{6250}{93}\right)$ at $K^* = \dfrac{310}{37}$ in the unharvested system. The eigenvalues of the Jacobian matrix at (x^*, y^*) are -1 and $\dfrac{29}{31}$. After the normal form analysis, we obtain

$$\alpha_2 = \frac{19259}{888671875} > 0.$$

Hence, using Theorem 3.6, an attracting period-2 orbit bifurcates at bifurcation point K^* indicating the occurrence of period-doubling bifurcation.

3.5 Dynamical behavior without harvesting

We analyze the unharvested system ($e_1 = e_2 = 0$) by varying the carrying capacity of prey species, and we report the dynamical changes in the system. We show the existence of period-doubling (or flip) and Neimark-Sacker bifurcations, and we make an order in which those bifurcations occur.

3.5.1 Existence and order of the bifurcations

First we discuss the existence of only one of the bifurcations with respect to K. Considering $r = 2.5$, $\alpha = 0.9$, $\beta = 0.7$, $h = 4$, and $m = 0.2$, the coexisting equilibrium for $K = \frac{16}{3}$ is $\left(\frac{8}{5}, \frac{98}{9}\right)$. The eigenvalues of the Jacobian matrix of the system 3.2.3 at the coexisting equilibrium are $\dfrac{1}{8}(7 \pm i\sqrt{15})$ which are unity in absolute value. From the normal form analysis done in Section 3.4 , we obtain the value of the Lyapunov coefficient $L = 0.02106108$. Hence, a stable invariant closed orbit bifurcates for increasing K through $K = \frac{16}{3}$ (Theorem 3.4). This validates the presence of Neimark-Sacker bifurcation.

Next, we input the values of parameter as $r = 4$, $\alpha = 0.6$, $\beta = 0.5$, $h = 20$, and $m = 0.1$ in the unharvested system. The eigenvalues of the Jacobian matrix at coexisting equilibrium $(5, \frac{6250}{93})$ corresponding to $K = \frac{310}{37}$ are -1 and $\frac{29}{31}$. Therefore, the system experiences a period-doubling (or flip) bifurcation under the considered parameter set.

Now, one might ask the question: can flip and Neimark-Sacker bifurcations occur for the same parameter set while varying K? If yes, then which bifurcation will occur first

followed by the other one? Further, one might be interested to investigate the successive change of dynamic modes while K is varied.

To address the above questions, we consider the first parameter set. When K is significantly small, the trivial and boundary equilibria exist which are unstable. The coexisting equilibrium exists at $K = 1.6$ and it is in unstable mode for $K < 1.87$. The coexisting equilibrium becomes stable for $K > 1.87$ and maintains its stability for $K < \frac{16}{3}$. Figure 3.5.1a shows that the system destabilizes through a Neimark-Sacker bifurcation at $K = \frac{16}{3}$. A stable quasiperiodic orbit exists which loses its stability giving rise to a series of periodic windows and period-bubbling phenomenon as K is varied. The system finally settles in chaotic mode through the route of quasiperiodicity. This complicated behaviour is also evident from the maximum Lyapunov exponents plotted with respect to K in Figure 3.5.1b . The positive value of maximum Lyapunov exponent validates the existence of chaotic behaviour, negative values imply periodicity, and quasiperiodicity is exhibited if its value is zero. We plotted the real part of the eigenvalues of the Jacobian matrix at the coexisting equilibrium in Figure 3.5.1c for $K \leq 40$. The red and blue curve represents the real part of the two corresponding eigenvalues. We can observe that the real part of both eigenvalues is different for $K < 3.27$, but both are less than unity. As K increases further the eigenvalues become complex and the real part of both eigenvalues is the same. The real part of eigenvalues increases and remains greater than unity with increase in K after the emergence of Neimark-Sacker bifurcation at $K = \frac{160}{7}$. There is no possibility of the eigenvalues to be -1 which indicates the presence of flip bifurcation. Consequently, there is no flip bifurcation for further increase in K.

In case of the second parameter set, only the trivial and boundary equilibria exist for $K < 5.1$, but both of those are unstable. The coexisting equilibrium exists for $K > 5.1$ which is also unstable as the system exhibits stable chaotic behaviour. The coexisting equilibrium becomes stable via a flip bifurcation at $K = \frac{310}{37}$ (Figure 3.5.2a- 3.5.2b). The system is in stable mode for $K > \frac{310}{37}$ and remains stable for $K \in (\frac{310}{37}, \frac{160}{7})$. The Jacobian matrix has eigenvalues $\frac{1}{80}(79 \pm i\sqrt{159})$ with absolute value unity corresponding to $K = \frac{160}{7}$. The stable coexisting equilibrium loses its stability to an invariant closed orbit due to the Neimark-Sacker bifurcation. This bifurcation causes chaotic behaviour via quasiperiodicity. The instance of emergence of Neimark-Sacker bifurcation after the flip bifurcation is

shown in bifurcation diagrams (Figure 3.5.2c- 3.5.2d). The complex behaviour can also be examined using maximum Lyapunov exponents as shown in Figure 3.5.2e .

We considered different parameter sets which lead to either a Neimark-Sacker bifurcation, or both a flip followed by Neimark-Sacker bifurcation. Another question that may be asked whether it is possible to exhibit only a flip bifurcation for a certain parameter set. We checked many parameter sets, but didn't find any such situation which could lead to only flip bifurcation without any Neimark-Sacker bifurcation. We also couldn't find any parameter configuration where Neimark-Sacker bifurcation occurs followed by flip bifurcation of the coexisting equilibrium. One might be interested to investigate this in other population models.

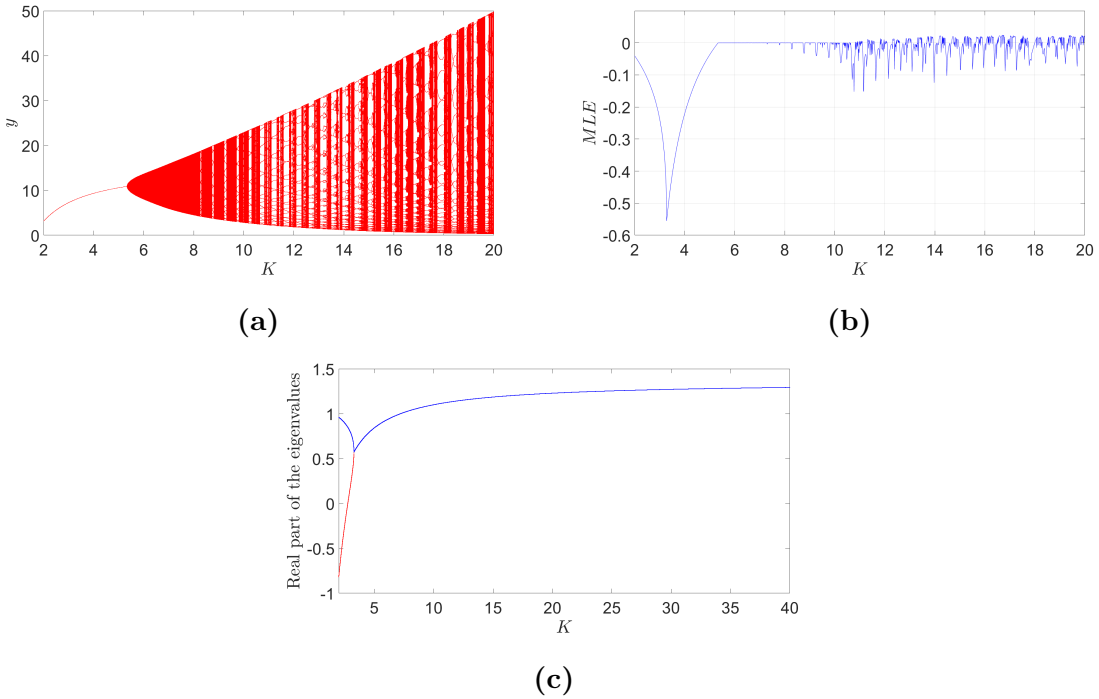

Figure 3.5.1: (a) Bifurcation diagram with varying K for the first parameter values: $r = 2.5$, $\alpha = 0.9$, $\beta = 0.7$, $h = 4$, and $m = 0.2$. (b) Corresponding maximum Lyapunov exponents. (c) Real part of the eigenvalues corresponding to Jacobian matrix at coexisting equilibrium for $2 \leq K \leq 40$.

3.5.2 Multistability

If more than one attractors exist for different initial conditions for the fixed values of the parameters, the system is said to be multistable. Multistability can be of different types, viz, periodic-periodic, periodic-chaotic, periodic-quasiperiodic, chaotic-quasiperiodic, and

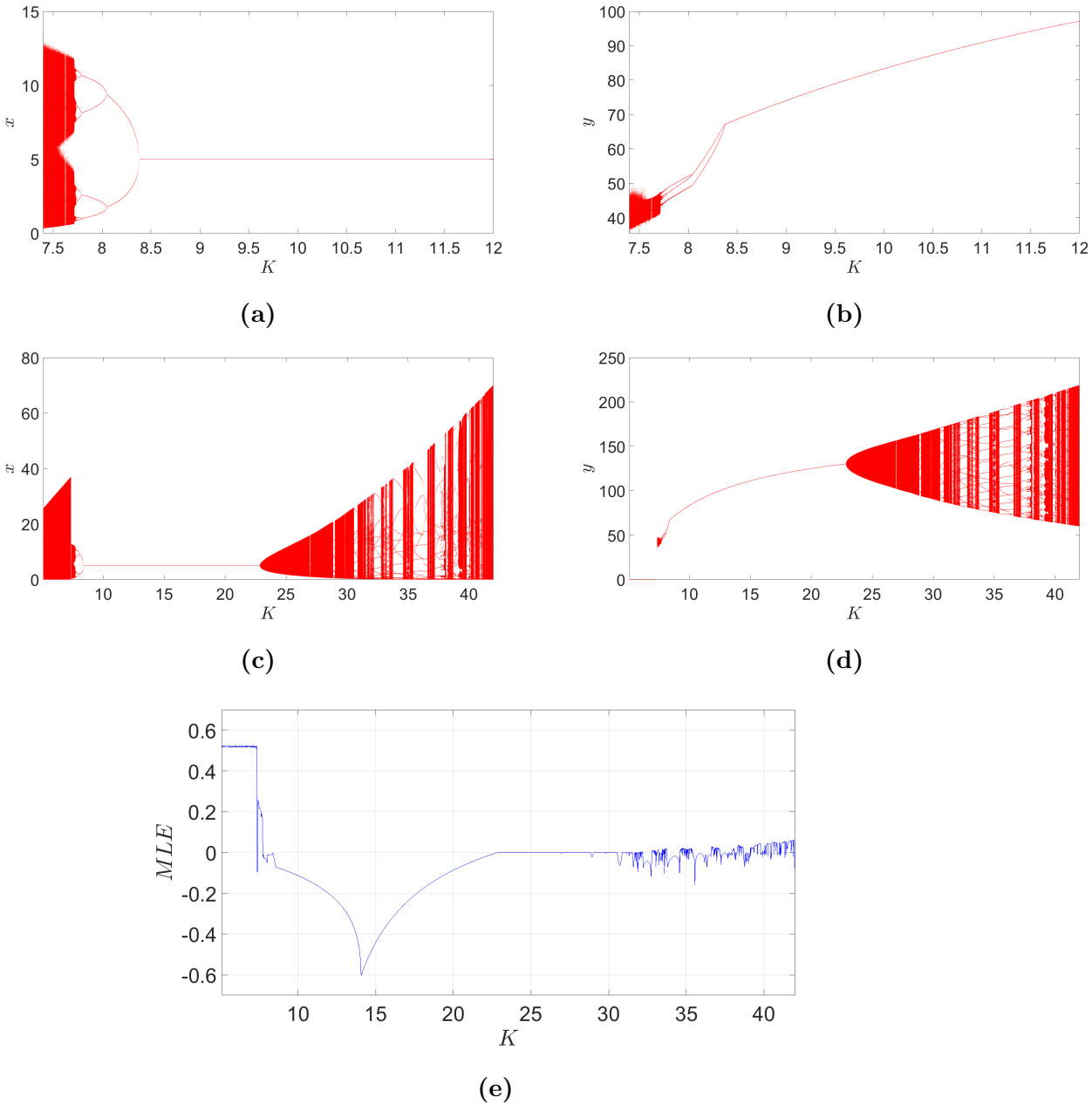

Figure 3.5.2: Existence of flip bifurcation with respect to K and fixing other parameter values as: $r = 4$, $\alpha = 0.6$, $\beta = 0.5$, $h = 20$, and $m = 0.1$, (a) for predator population and (b) for prey population. Emergence of both the period-doubling and Neimark-Sacker bifurcation by varying K (c) for predator population and (d) for prey population. (e) Maximum Lyapunov exponents corresponding to K.

many more. System (4) exhibits different multistable stable modes for various values of K for the second parameter set. We plotted red bifurcation diagram by first taking the initial condition $(2.8, 134.13)$, and then using the initial condition $(2.8, 130.4)$ in blue

color in the same figure window (Figure 3.5.3a). The two initial conditions show different dynamical behavior. The red and blue curves in the Figure 3.5.3a are not overlapping for some values K which shows that the initial conditions are attracted to different attractors for the same value of K. We also obtained the different maximum Lyapunov exponents for these two initial conditions (Figure 3.5.3b). It is clear from the MLE curves also that the dynamics behaviour of the system don't match for various values of K. It is possible to have more than two attractors for the values of K where the red and blue bifurcation curve are not coinciding. We will determine the different stable coexisting attractors for different initial conditions using phase portraits and basins of attraction.

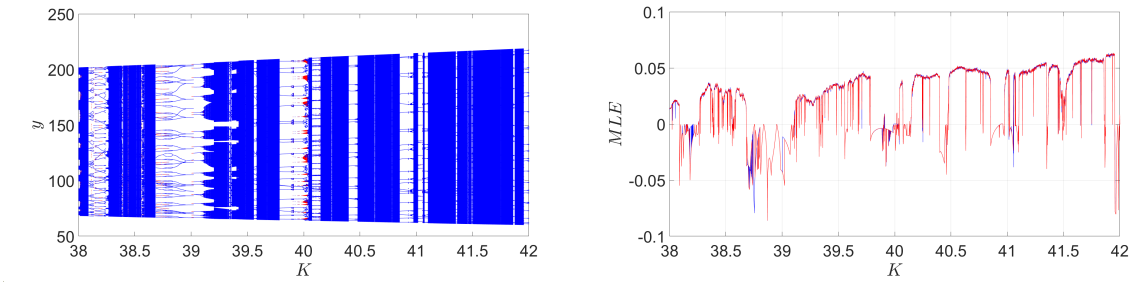

(a) **(b)**

Figure 3.5.3: (a) Bifurcation diagram of predator population by varying K and using the initial conditions $(2.8, 134.13)$ in blue and $(2.8, 130.4)$ in red. (b) Maximum Lyapunov exponent for $38 \leq K \leq 42$ using the initial conditions $(2.8, 134.13)$ in blue and $(2.8, 130.4)$ in red.

Two attractors: (periodic-periodic): When two attractors coexist for two different initial conditions, we say that the system is bistable. We observed that the system exhibits periodic-periodic bistability for $K = 38.186$ where period-20 and period-41 coexist for different initial conditions. Similar kind of periodic-periodic multistability can be observed for $K = 38.244$ (period-82 and period-100), $K = 39.019$ (period-21 and period-84), and $K = 40.039$ (period-43 and period-231). Figure 3.5.4a shows the basins of attraction for $K = 38.186$ with period-41 (green region) and period-20 (magenta region). The initial conditions converging to period-100 cycles are represented by black color while period-82 are indicating by yellow color for $K = 38.244$ (Figure 3.5.4b).

Three attractors (periodic-periodic-periodic): Any system is tristable if three different attractors coexist with three initial conditions. These attractors can be periodic,

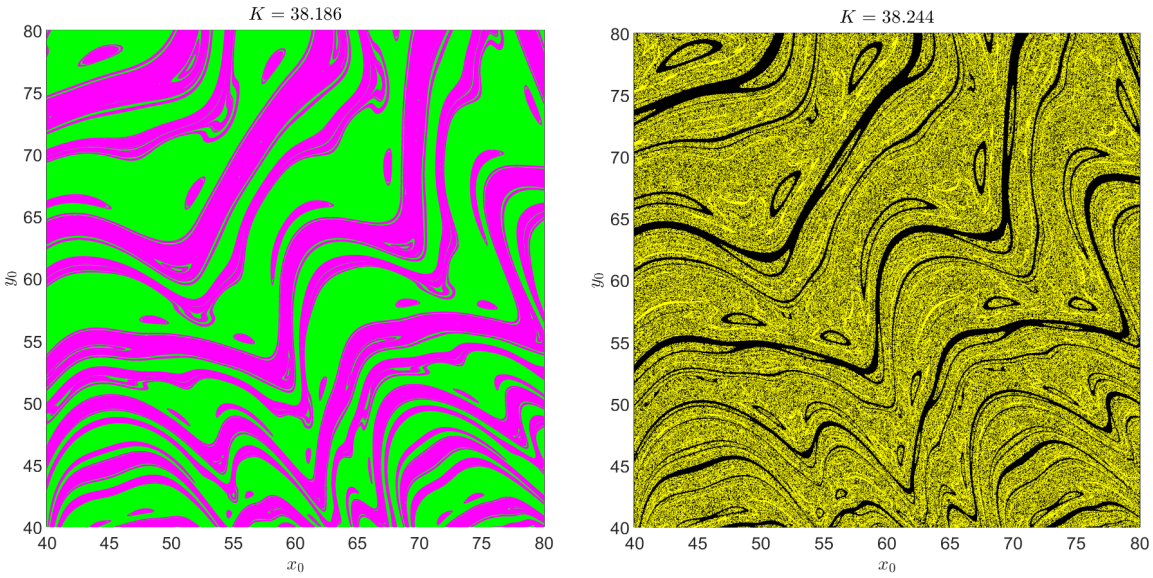

(a) **(b)**

Figure 3.5.4: (a) Basin of attraction for $K = 38.186$: period-20 (magenta colored region) and period-41 (green colored region). (b) Basin of attraction for $K = 38.244$: period-82 (yellow colored region) and period-100 (black colored region).

quasiperiodic, chaotic, or any combination of those. In our system, we come across three stable periodic cycles such as period-43, 66, and 231 orbits for $K = 40.039$. In Figure 3.5.5a- 3.5.5b , the black region is made up of the initial conditions which lead to period-43 cycle, period-66 behavior is exhibited by the initial conditions shown in cyan color, and red region contains the initial conditions converging to period-231 cycle. In the zoomed part as shown in Figure 3.5.5b , we observe that the initial conditions leading to period-66 and period-231 cycles are very densely spread and its difficult to separate the values of (x_0, y_0) for either of the periodic cycles.

Four attractors (periodic-periodic-quasiperiodic-chaotic): The more interesting kind of multistability is exhibited when a quasiperiodic, chaotic attractors, and periodic-orbits coexist. For $K = 40.02$, the initial conditions $(2.8, 134.13)$ converges to a quasiperiodic attractor, the initial condition $(10, 26.125)$ leads to a chaotic attractor, a stable period-44 cycle is observed when the initial condition is set to $(3, 2.02)$ and the initial condition $(3.48, 23.83)$ exhibits a stable period-132 orbit. We also calculated the maximum Lyapunov exponent for both initial conditions to be sure of the behavior of the system. We used 50 million iterations to quantify the maximum Lyapunov exponent.

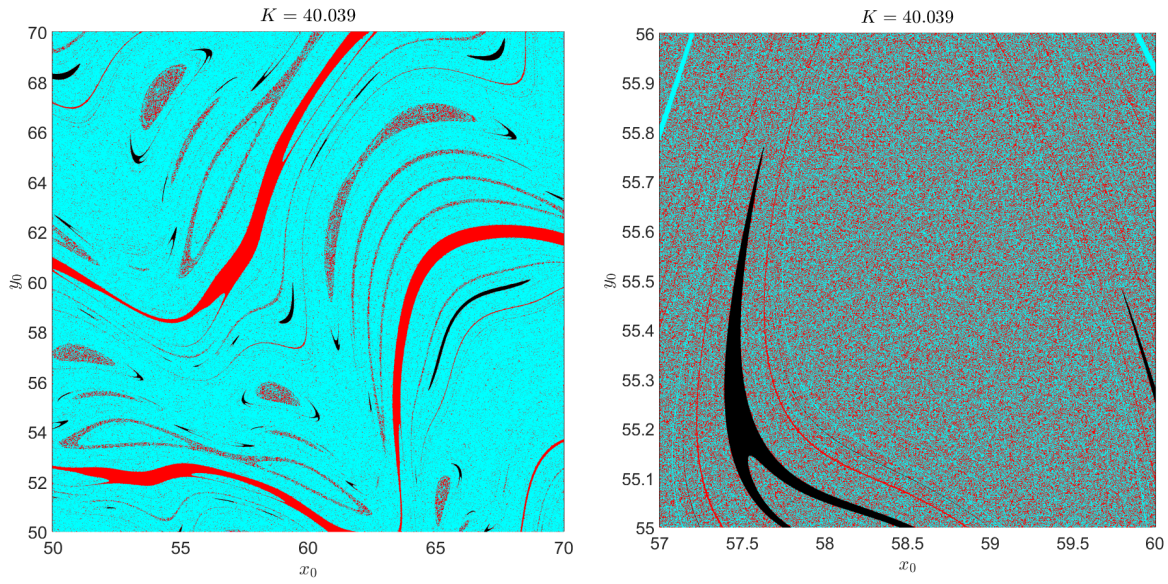

(a) **(b)**

Figure 3.5.5: (a) Basin of attraction for period-43 (black region), 66 (cyan region), and 231 (red region) orbits respectively when $K = 40.039$. (b) Enlarged part of basin of attraction for $K = 40.039$.

The values of maximum Lyapunov exponent for $(2.8, 134.13)$, $(10, 26.125)$, $(3, 2.02)$, and $(3.48, 23.83)$ are 0.00000009 (quasiperiodic), 0.01007792(chaotic), -0.01452989 (period-44), and -0.00397646 (period-132), respectively. Figure 3.5.6 shows the four coexisting attractors: quasiperiodic attractor in blue, chaotic attractor in red, green dots represents period-44 orbit, and black dots made up the period-132 orbit. We can see that the blues is the closed orbit and hence we say that it is quasiperiodic.

Next, we take a region of initial conditions in x_0y_0-plane and draw the basin of attraction for $K = 40.02$. We plotted the basin of attraction by differentiating between periodic and non-periodic behavior and further, dividing the non-periodic behavior into chaotic and quasiperiodic mode using maximum Lyapunov exponents using MATLAB. For the dividing the periodic and non-periodic behavior, we took a grid consisting of $0.1 \leq x_0 \leq 20$ and $20 \leq y_0 \leq 30$ and calculated the period and maximum Lyapunov exponent at each value of the grid by moving a distance of 0.01 in both horizontal and vertical direction. Figure 3.5.7a comprises of the basin of attraction for the quadruple [72, 81] attractors: quasiperiodic (magenta), chaotic (black), period-44 (yellow), and period-132 (green). The magnification of the basin of attraction is represented by the

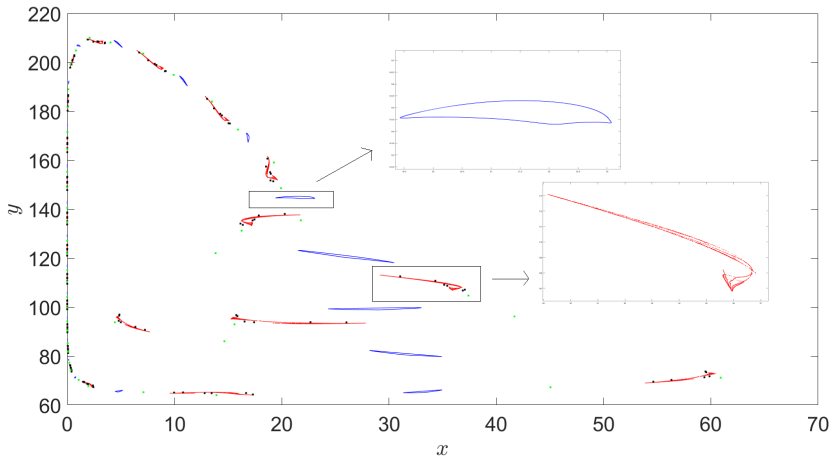

Figure 3.5.6: For $K = 40.02$, stable quasiperiodic (blue colored), chaotic (red colored), period-44 (green colored) and period-132 (black colored) attractors coexisting for different initial conditions.

Figure 3.5.7b. We have thoroughly examined the dynamical modes of the system when nutrient supply (carrying capacity) of the prey species is varied till now. In the next subsection, we will study the change in overall stocks of the predator and prey population when the prey species is enriched.

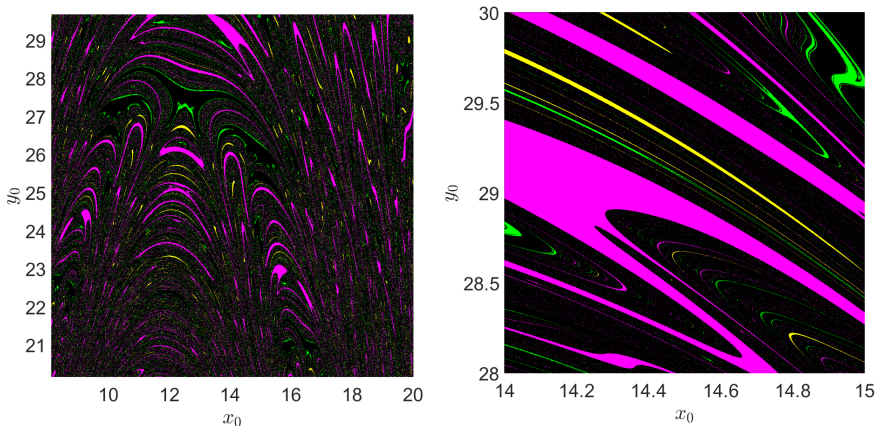

(a) **(b)**

Figure 3.5.7: (a) Basin of attraction for the quadruple attractors: quasiperiodic (magenta), chaotic (black), period-44 (yellow), and period-132 (green) for $K = 40.02$. (b) Magnified part of basin of attraction in (a).

3.6 Dynamical behavior with harvesting

Harvesting (of fishes) and culling (of pest) are two common practices in fishery and cropping systems, respectively. Both the human induced activities reduce the abundance of the target species, and hence the stocks of the other species of ecosystems also get changed. In fishery, industries employ efforts to catch predatory fishes because of their higher economic values, and catches some prey fish as a bycatch. Often two different fishery industries exert effort on two different tropic levels following independent effort policy. We here study the impacts of independent harvesting of predator and prey species in the context of stability and stock pattern. Generally, the ecological parameters ($r, K, \alpha, h, \beta,$ and m) are inherent, and we should not vary those in a mathematical model. However, we are free to regulate efforts e_1 and e_2 as these are the control parameters induced by human activity directly. Immediately, we are interested in exploring the effect on the structure of (in)stability zones of the coexisting equilibrium under harvesting of both the species in the e_1e_2-plane, and soon after we estimate population abundance under harvesting.

3.6.1 Stability region

Our main aim is to analyze the dynamical behavior of the system in the bi-parameter space, i.e., e_1e_2-plane. We define the region in e_1e_2-plane where both species can have stable coexistence or unstable mode. This is a specialist predator-prey system, therefore, the predator gets extinct first then the prey do so. Under harvesting, the coexistence equilibrium (x^*, y^*) can be calculated from the Section 3.3. We set the parameter values as $r = 2.5$, $K = 20$, $\alpha = 0.9$, $\beta = 0.7$, $h = 4$, $m = 0.2$, $q_1 = 0.1,$ and $q_2 = 0.01$. We determine the positive equilibrium point for the aforementioned parameter set given by

$$(x^*, y^*) = \left(\frac{4\,(e_2 + 20)}{(50 - e_2)}, \frac{280(1150 + e_1(e_2 - 50) - 30e_2)}{9(e_2 - 50)^2} \right).$$

When prey is harvested only then extinction of predator happens at $e_1 = 23$. Similarly, when only predator is harvested the predator extincts at $e_2 = \frac{115}{3}$. Hence, the region of interest to investigate (in)stability will be

$$R := \left\{ (e_1, e_2) : 0 \leq e_1 \leq 23,\, 0 \leq e_2 \leq \frac{115}{3} \right\}.$$

We obtain the predator extinction curve at equilibrium by plotting

$$F(e_1, e_2) := 280(1150 + e_1(e_2 - 50) - 30e_2) = 0.$$

Note that $F(0,0) > 0$. Hence the prey and predator must coexist in the absence of harvesting. The coexistence region is bounded by e_1-axis, e_2-axis and the curve $F(e_1, e_2) = 0$. The predator extinction region must lie above the extinction curve.

The coexistence region can be further divided into two parts by stability and instability behaviors of the coexisting equilibrium. We extract the stability region by calculating the eigenvalues (λ) of the Jacobian matrix (3.3.1) at the coexisting equilibrium. We find that Neimark-Sacker bifurcation occurs (for $|\lambda| = 1$) producing a bifurcation curve which leads to the blue curve. The gray region below the blue curve in the Figure 3.6.1 shows the values of e_1 and e_2 for which the equilibrium is in unstable mode ($|\lambda| > 1$). The increase in any of the harvesting effort leads to stabilization of the coexisting equilibrium via a Neimark-Sacker bifurcation. The yellow region represents stability zone where the coexisting equilibrium is stable ($|\lambda| < 1$). The coexisting equilibrium loses its stability again via a flip bifurcation (black curve) where one of the eigenvalues is -1. The green zone is the region of instability of coexisting equilibrium. We will analyze explicitly the dynamic modes present in the green region later section when effect of predator harvesting on mean population size is discussed.

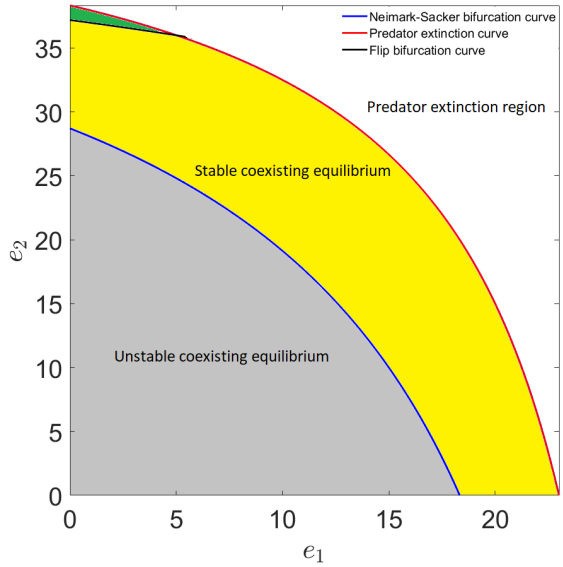

Figure 3.6.1: The Neimark-Sacker bifurcation curve (blue) and predator extinction curve (red) in e_1e_2-plane.

3.6.2 Two-parameter space analysis

Arnold tongues and Period-adding sequence

Now in unstable regions (gray), we quantify whether the system experiences either mode: a periodic with period more than 1, quasiperiodic, or chaotic. The maximum Lyapunov exponent (MLE) is an useful measure to distinguish between periodic (MLE<0), quasiperiodic (MLE$=0$), and chaotic (MLE>0) behavior of the system. For plotting the maximum Lyapunov exponents, we calculated the MLE for all $(e_1, e_2) \in [0, 8] \times [0, 25]$. These exponents are calculated for each value of (e_1, e_2) in the parameter space divided into a mesh-grid of 25000×8000 equidistant points. Figure 3.6.2a shows the values of MLE for different values of e_1 and e_2 revealing three topologically nonequivalent dynamical behavior. The color map indicates the range of obtained MLEs. The parameter values which are colored light-dark yellow leads to periodic behavior, black ones indicate quasiperiodic dynamics, and the green-blue ones demonstrate chaotic motion.

We further classify the periodic behavior by finding the period of the trajectories for different values of e_1 and e_2. Figure 3.6.2b depicts the isoperiodic diagram with varying both harvesting rates simultaneously. The white region represents non-periodic behaviour (quasiperiodic or chaotic) while the colored region is for periodic windows engulfed in the quasiperiodic and chaotic regions. The red region on the upper right corner of the Figure 3.6.2b shows the stable region which is separated from the unstable region of coexisting equilibrium (or period-1) by Neimark-Sacker bifurcation curve in e_1e_2-plane. The colored regions (apart from the red one) are the values of (e_1, e_2) for which the system exhibits periodic behaviour. The periodic regime with period-26, 27, 28, 29, 30, 31, 32, 33, 34, and so on are clearly marked using different colors in the isoperiodic diagram. These periodic structures collide with each other which correspond to occurrence of phase-locking (or frequency locking) phenomenon in the quasiperiodic regime. When two frequencies interact nonlinearly (or commensurate) and the ratio of the two is a rational number then we say that the frequencies are phase-locked [14]. This occurrence of phase-locking leads to formation of organized periodic structures called Arnold tongues. These Arnold tongues are similar to structures observed in circle maps [14], and these are associated with rotation numbers 1/26, 1/27, 1/28, 1/29, 1/30, 1/31, 1/32, 1/33, 1/34, and so on. An infinite collection of periodic structures is organized in a period-adding sequence,

where the period increases by one as e_2 decreases. The head of the Arnold tongues lies in the chaotic region while the V-shaped tail is immersed in the quasiperiodic regime. Self-similarity is observed in these organized periodic structures.

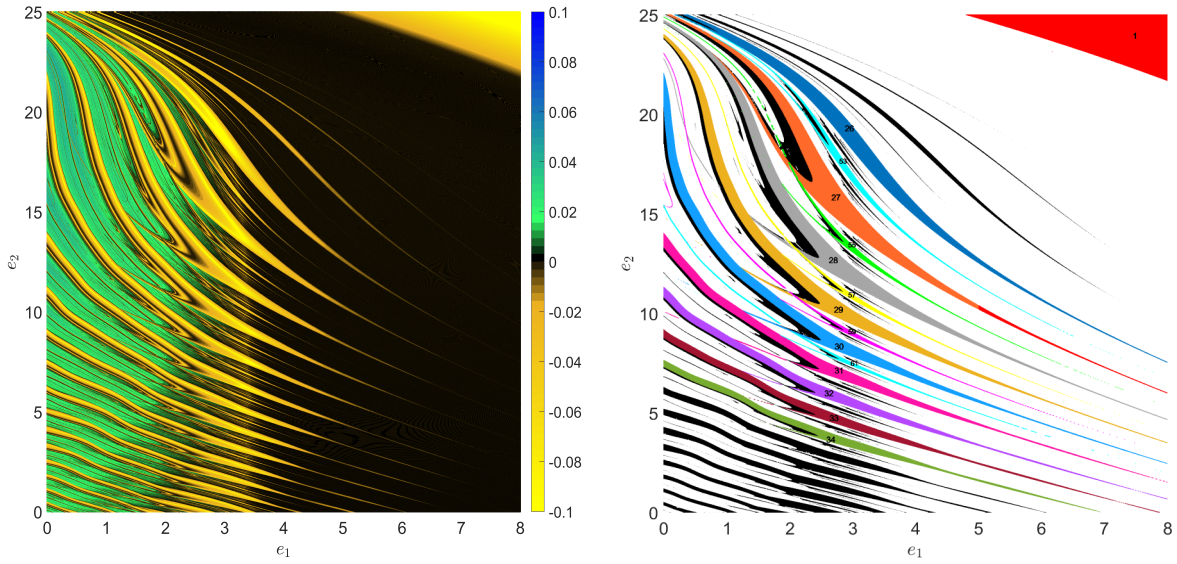

(a) **(b)**

Figure 3.6.2: (a) Maximum Lyapunov exponent diagram in e_1e_2-plane for $0 \leq e_1 \leq 8$ and $0 \leq e_2 \leq 25$. The values of MLE for associated color represented in the colorbar. (b) Isoperiodic diagram for e_1e_2-plane for $0 \leq e_1 \leq 8$ and $0 \leq e_2 \leq 25$. The colored structures represent the periodic regime while the white region can be either quasiperiodic or chaotic. The colored tongues with rotation number $1/p$ are labeled by p. The black colored tongues correspond to other rotation number tongues.

Between two adjacent tongues with rotation numbers p/r and q/s, there is a tongue with rotation number $(p+q)/(r+s)$. Here for example, a tongue of rotation number $2/53$ is present between tongues of rotation numbers $1/26$ and $1/27$, $2/55$ rotation numbered tongue between tongues with rotation number $1/27$ and $1/28$, and so on. There is an infinite sequence of such alignment of these tongues. Also, there are infinite number of such two Arnold tongues with different rotation numbers where the similar kind of layout exists. One of those sequence is,

$$\frac{1}{26}, \frac{2}{53}, \frac{1}{27}, \frac{2}{55}, \frac{1}{28}, \frac{2}{57}, \frac{1}{29}, \cdots$$

which can be written in a sequence $\{a_k\}$ as follows,

$$a_k = \frac{2}{k+51}, \text{ with } k = 1, 2, 3, \ldots .$$

This is a small part of the Farey tree that consists of rational numbers between 0 and 1.

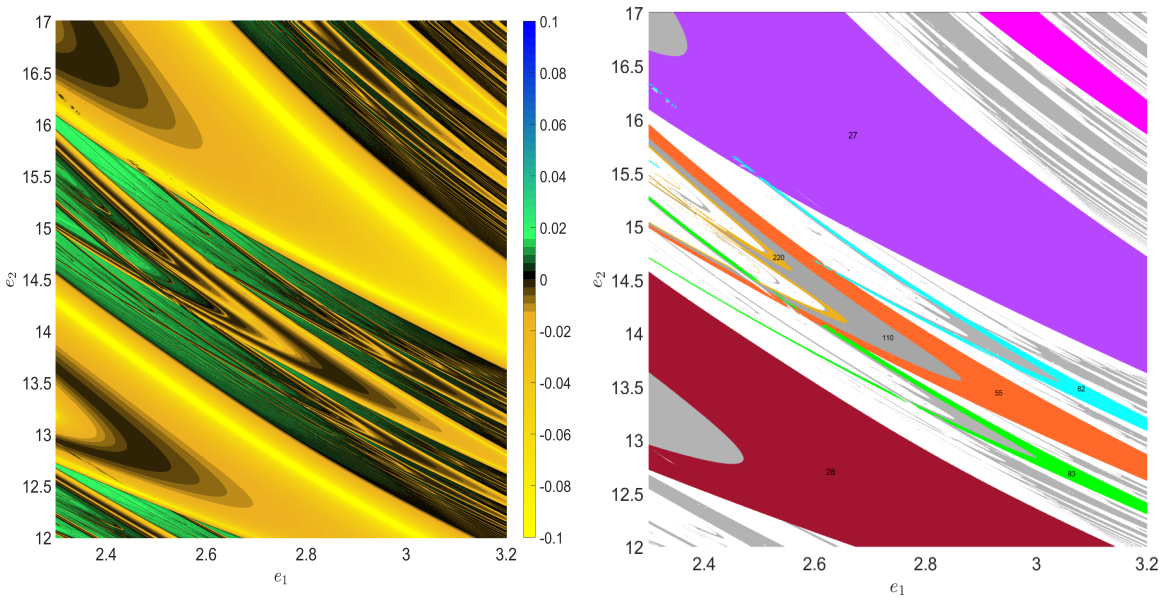

(a) **(b)**

Figure 3.6.3: (a) Magnification of Figure 3.6.2b : MLE diagram. (b) The colored part represent the Arnold tongues of rotation number as marked in the picture. The gray part represents the Arnold tongue with other rotation numbers.

We now magnify some part of Figure 3.6.2b to visualize different organized periodic structures. Figure 3.6.3a (respectively Figure 3.6.3b) are an enlargement of Figure 3.6.2a (respectively Figure 3.6.2b) for $2.3 \leq e_1 \leq 3.2$ and $12 \leq e_2 \leq 17$. The largest tongue between the period-26 and period-27 tongues corresponds to period-53, between the period-27 and period-28 tongues to period-55, and so forth. The pattern is repeated and we obtain a Fibonacci-like sequence $\{b_k\}_{k=1}^{\infty} = \{26, 27, 53, 80, 133, 213, ...\}$ generated with decreasing e_1 in e_1e_2-plane. The interesting fact is that the ratio of consecutive terms $\left(\frac{b_{k+1}}{b_k}\right)$ of the sequence tends to $\phi = \frac{1+\sqrt{5}}{2} \approx 1.61803$, called the Golden ratio (or Golden mean).

Shrimp Structures

Other important periodic structures are Shrimp structures which are engulfed in the chaotic region. From the maximum Lyapunov exponent diagram, we observed that the

head of the Arnold tongues is embedded in the chaotic region while the tail is immersed in the quasiperiodic region. Another important periodic structure submerged in the chaotic regime is a shrimp-like structure with a head and four tails named shrimp structure [82]. A magnification of a part of Figure 3.6.2b is shown in Figure 3.6.4b . The head of the shrimp structure colored orange corresponds values of (e_1, e_2) which exhibit period-84 orbits. As we move towards tail of the structure, the period-84 $\times$ 2 (period-168) oscillations are observed. This is a part of the period-bubbling cascade leading to chaos.

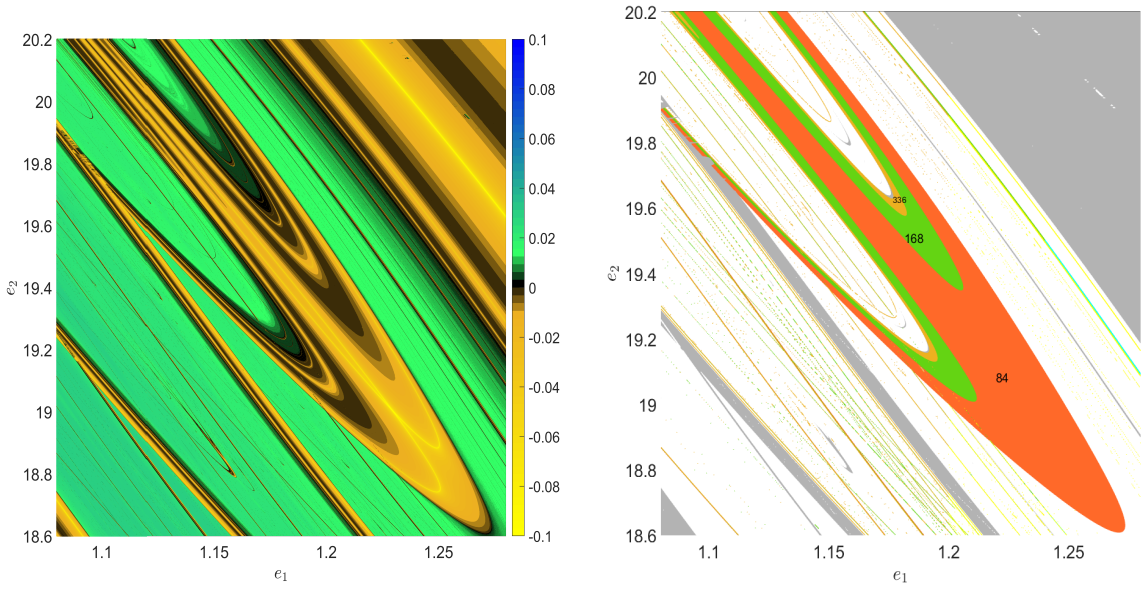

(a) **(b)**

Figure 3.6.4: (a) Magnification of Figure 3.6.2a . (b) Magnification of Figure 3.6.2b . The colored part represent the Shrimp structure. The gray part represents the other periodic orbits.

3.6.3 Paradox of enrichment

We can write the model (3.2.3), without harvesting as

$$\begin{aligned} x_{n+1} &= x_n \exp\left(r\left(1-\frac{x_n}{K}\right) - \frac{\alpha y_n}{h+x_n}\right), \\ y_{n+1} &= y_n \exp\left(\frac{\beta x_n}{h+x_n} - m\right). \end{aligned} \tag{3.6.1}$$

The increase in K (increasing nutrient supply) to prey species should have a positive impact on prey population size. The overall predator population is also expected to be benefited by the prey enrichment. By computing mean population size of both species, we

shall verify that this increase in population size with carrying capacity is in well agreement or any counter-intuitive situations arise.

The mean population size with species enrichment are illustrated in Figure 3.6.5a - 3.6.5c corresponding to the parameter set $r = 4$, $\alpha = 0.6$, $\beta = 0.5$, $h = 20$, and $m = 0.1$. The red curve represents the coexisting equilibrium and the black one corresponds the mean population size. We know from the previous subsection 3.5.1, for the considered parameter set the system undergoes a flip bifurcation which stabilizes the coexisting equilibrium. As K is increased further, the system exhibits a Neimark-Sacker bifurcation contributing to emergence of non-equilibrium dynamics. The mean population of the prey species rises in the non-equilibrium state prior to flip bifurcation occurring for $K = \frac{310}{37}$, then the mean population matches with the stable coexisting equilibrium. The prey component of the stable coexisting equilibrium is independent of the carrying capacity, hence the prey stocks remain constant when the system exhibits stable equilibrium state. Further, the mean prey stocks increase with species enrichment as the system exhibits non-equilibrium dynamics with occurrence of the Neimark-Sacker bifurcation for $K \leq \frac{160}{7}$ (Figure 3.6.5a). In the equilibrium states, the mean predator population increases with species enrichment. When the equilibrium becomes unstable followed by the Neimark-Sacker bifurcation, the average predator population shows a significant decrease for a small interval $(27, 36)$ of K (Figure 3.6.5b). This decrease in the predator population with prey enrichment is called as paradox of enrichment [44, 46]. The rate of decrease in the mean predator population is not significant as the nutrient supply to prey species is increased further. We found that the mean population values lie between 111.43 and 109.67 when $K \in (200, 500)$. The mean stocks show a sudden jump with a discontinuity towards zero for $K > 513$. We can conclude from Figure 3.6.5c that the decrease in mean predator population is not smooth. Due to positivity of the map (3.2.3), as proved in section 3.2, the predator population never goes extinct but its is on the verge of extinction. Hence, paradox of enrichment is very evidently present in our system.

We can check the mean population for the other parameter set which produced different bifurcation and dynamics. We found that similar kind of changes in both prey and predator population were observed in the second parameter set $r = 2.5$, $\alpha = 0.9$, $\beta = 0.7$, $h = 4$, and $m = 0.2$ (Figure 3.6.5d - 3.6.5f). We have plotted all these figures in

MATLAB using 5 million iterations. We also obtained the same values of the mean population with 50 million iterations.

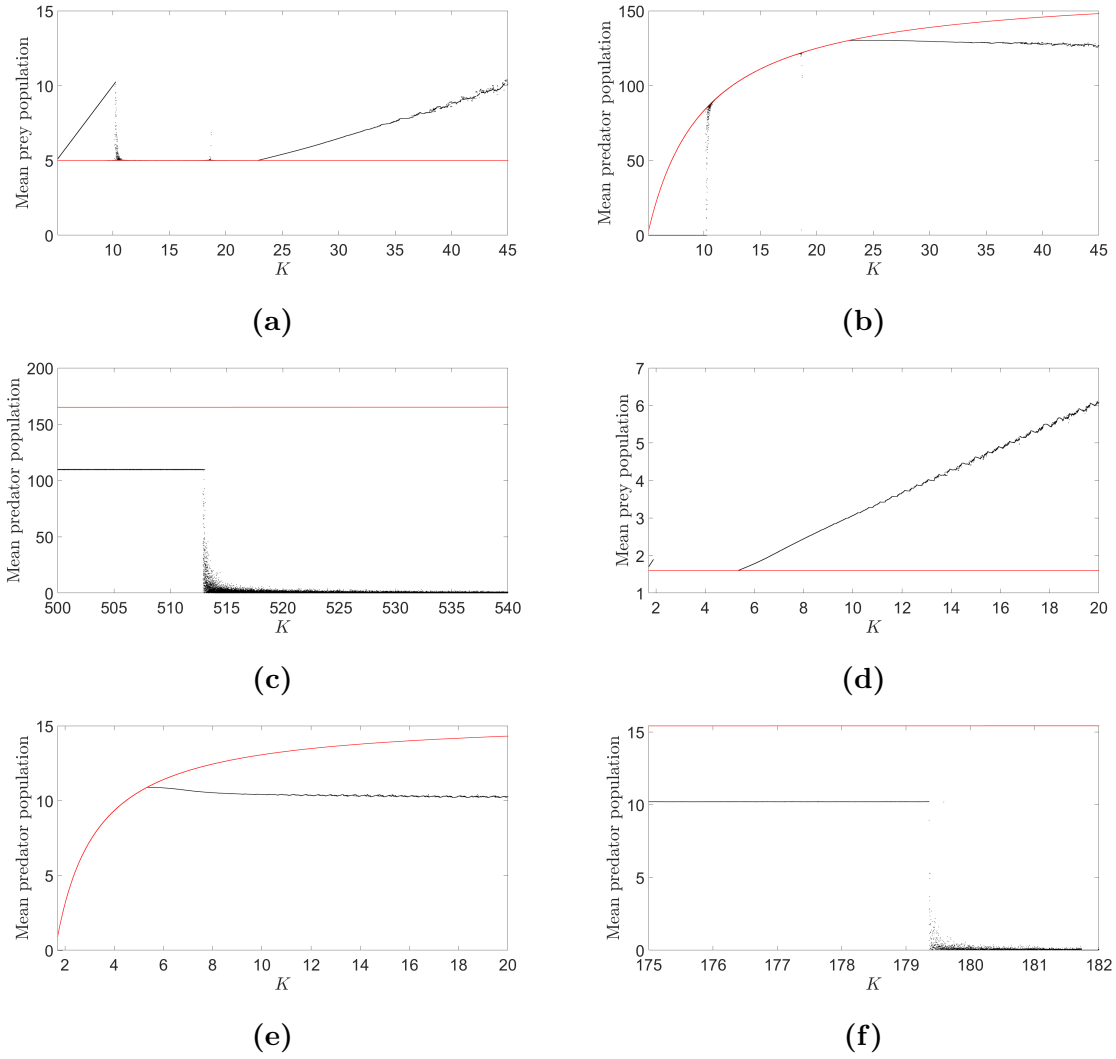

Figure 3.6.5: For parameter values $r = 4$, $\alpha = 0.6$, $\beta = 0.5$, $h = 20$, and $m = 0.1$: (a) mean prey population for $5.1 < K < 45$, (b) mean predator population for $5.1 < K < 45$, and (c) mean predator population for $500 < K < 540$. For parameter values $r = 2.5$, $\alpha = 0.9$, $\beta = 0.7$, $h = 4$, and $m = 0.2$: (d) mean prey population for $1.6 < K < 20$, (e) mean predator population for $1.6 < K < 20$, and (f) mean predator population for $175 < K < 182$.

3.6.4 Hydra effect

Recalling the model (3.2.3),

$$\begin{aligned} x_{n+1} &= x_n \exp\left(r\left(1-\frac{x_n}{K}\right) - \frac{\alpha y_n}{h+x_n} - q_1 e_1\right), \\ y_{n+1} &= y_n \exp\left(\frac{\beta x_n}{h+x_n} - m - q_2 e_2\right). \end{aligned} \tag{3.6.2}$$

We examine the effect on the population stocks by inducing constant prey harvesting effort while increasing predator harvest rate. The coexisting equilibrium exists for $e_2 \leq 38.3333$ in the absence of prey harvesting (i.e., $e_1 = 0$). Using the eigenvalues approach, the positive equilibrium is unstable for $e_2 \in (0, 28.7142)$. The system exhibits complex phenomenon such as periodic windows,period-doubling, period-bubbling, quasiperiodicity, and chaos when the coexisting equilibrium is unstable as show in the bifurcation diagram Figure 3.6.6a. A Neimark-Sacker bifurcation leads to the stabilization of the coexisting equilibrium at $e_2 = 28.7142$. Consequently, predator harvesting stabilizes the coexisting equilibrium for $e_2 \in (28.7142, 33.2218)$. The coexisting equilibrium again loses stability via a flip bifurcation at $e_2 = 33.2218$. We will discuss the dynamics of the system for $e_2 \in (33.2218, 38.3333)$ in detail soon after in the same subsection.

The red curve in Figure 3.6.6a represents the coexisting equilibrium. When the system is stable, we can clearly interpret the decreasing behaviour of the predator population. However understanding the population stock is difficult from Figure 3.6.6a for unstable mode. Now, we estimate the mean stock for $e_2 \in (0, 28.7142)$. We calculated the mean and equilibrium population size of both species with increasing predator harvesting. In a Lotka-Volterra predator-prey model the predator population decreases while prey population increases when predator exploitation is increased ([83]). In our model, the equilibrium prey size (red colored) increases (Figure 3.6.6b) which is in well agreement with the result of Legović *et al.* [83]. However, the equilibrium predator population (blue colored) shows a paradoxical behaviour. From Figure 3.6.7a, mean prey population maintains opposite relation in terms of increment and decrement with predator population size. The most important result in our discrete-time model is that the mean prey population size decreases in a small interval of effort.

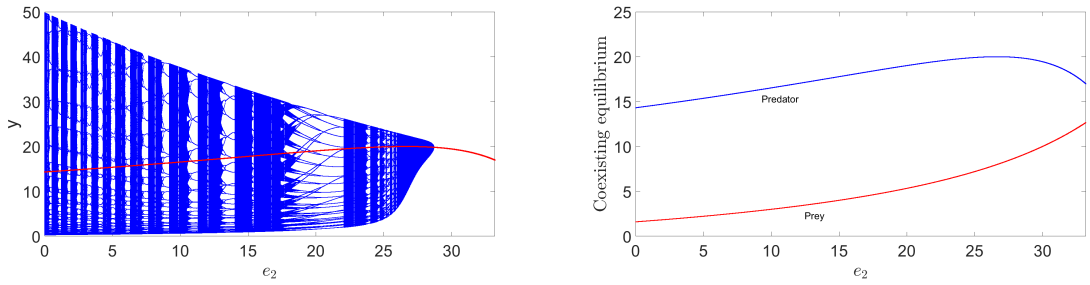

(a) **(b)**

Figure 3.6.6: (a) Bifurcation diagram for the predator (blue colored) and the predator part of coexisting equilibrium (red colored) with varying predator harvesting rate. (b) Coexisting prey (red color) and predator (blue color) equilibrium with varying e_2.

Ecologically, it is expected that the population of any species must decline with increase in their exploitation rate. Contrary to this, many models show a positive response on the targeted species when they are culled or removed. This paradoxical behaviour is known as hydra effect [46, 53]. The black colored curve in Figure. 3.6.7b represents the mean predator population with varying predator harvesting effort. When the harvesting rate is relatively low, the mean stocks are somewhat decreasing while the equilibrium is increasing. The mean predator population starts showing positive growth around $e_2 = 17.57$. Between the lines L_1 ($e_2 = 22.06$) and L_2 ($e_2 = 27.69$), the mean predator population and equilibrium stocks both show a prominent increase leading to the conclusion that the discrete-time system (3.2.3) exhibits the hydra effect. The equilibrium population in the unstable states is monotonically decreasing while mean population keeps on increasing with increment of harvesting effort in the narrow interval (L_2, L_3). In the unstable mode, the mean population is always less than the equilibrium size. The stock pattern is very complex with increment in exploitation rate of the predator in non-equilibrium states.

The coexisting equilibrium becomes unstable again in courtesy of a flip bifurcation with predator get on the verge of extinction while prey population exists in the unstable mode (Figure 3.6.7c). Although the coexisting equilibrium exists but the dynamics are driven by fluctuation mode in the green region shown in the Figure 3.6.1 in the previous chapter (3.6.1). However, there is sudden jump in predator size after destabilization of the coexisting equilibrium leading to extinction of the predator population (Figure 3.6.7d). For $e_2 > 33.2$, the coexisting equilibrium becomes unstable and predator population

extincts while the prey population is existing in the unstable mode. If we fix $e_1 = 10$, there is a very smooth decrement of the predator population to extinction as shown in Figure 3.6.7e . The coexisting equilibrium decreases continuously and tend to zero maintaining the stable mode.

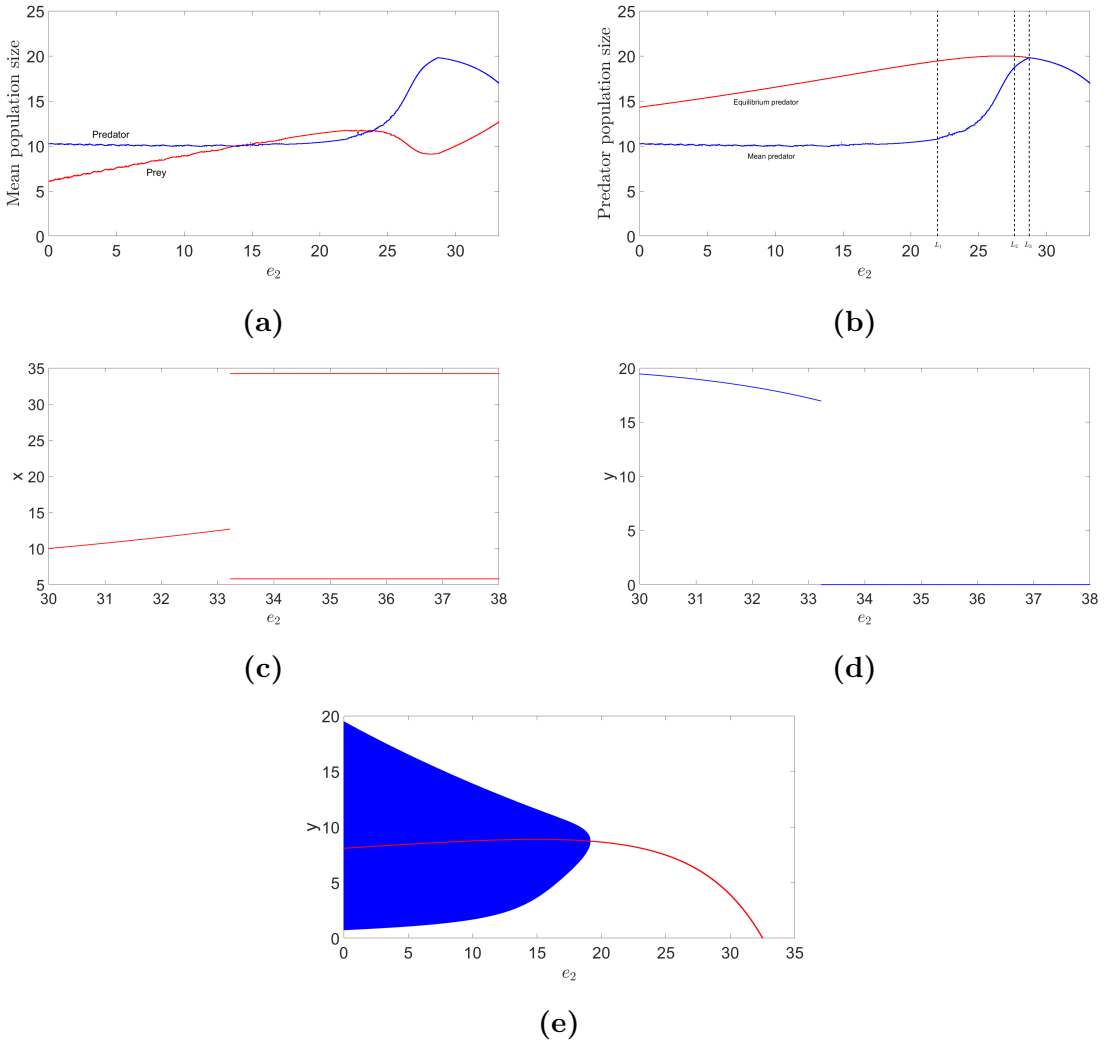

Figure 3.6.7: (a) Mean population size of prey (red color) and predator (blue color) with e_2. (b) Predator population size : mean population in blue color and predator part of the coexisting equilibrium in red color with varying e_2. (c) Bifurcation diagram for the prey (red colored) with varying predator harvesting rate. (d) Bifurcation diagram for the predator (blue colored). (e) Bifurcation diagram for the predator (blue colored) and the predator part of coexisting equilibrium (red colored) with varying predator harvesting rate when $e_1 = 10$.

3.7 Conclusion

This study investigated the dynamical behavior of a discrete-time RM model derived using the method of piecewise constant argument. Unlike the Euler-discretized RM model [68], which does not guarantee positivity, our formulation ensures positive populations. We analyzed the stability of equilibrium points and examined Neimark-Sacker and flip bifurcations under variations in carrying capacity (K). In one scenario, Neimark-Sacker bifurcation destabilized the coexisting equilibrium without flip bifurcation, whereas in an another case, both bifurcations occurred, stabilizing the equilibrium before eventual destabilization. Unlike the continuous RM model, where stability loss leads to a unique limit cycle, our discrete model exhibited periodicity, quasiperiodicity, and chaos. Multistability was evident, featuring coexisting periodic and chaotic attractors with intricate basins of attraction.

The system also demonstrated the paradox of enrichment, where increased K caused sudden predator extinction (Figure 3.6.5b). Under two-parameter harvesting analysis, we identified stability, instability, and extinction regions. The Neimark-Sacker bifurcation curve delineated stability loss, while the predator extinction curve marked population collapse. The unstable regime displayed organized periodic structures, including Arnold tongues (Figure 3.6.2b) and shrimp structures (Figure 3.6.4b), revealing a period-adding sequence and self-similar patterns.

Examining predator harvesting effects, we observed the hydra effect, where mean predator density initially increased with harvesting before declining (Figure. 3.6.7b). Unlike the continuous RM model, where prey biomass remains constant, our discrete model exhibited declining mean prey density under harvesting. Increased harvesting eventually led to predator extinction, though prey culling smoothed this decline.

CHAPTER 4

A Discrete-time predator-prey model with dispersal in a two-patch environment

4.1 Introduction

In this chapter *, we investigate a discrte-time predator-prey model in two patch environment incorporating both prey and predator dispersal. The coupled maps play a vital role in the nonlinear dynamics [84–91]. The use of coupled map is widespread in neurophysiology [13, 92], nonlinear oscillator systems [93, 94], and population models [95, 96]. In a coupling of three discrete-time quadratic maps, Rech [93] showed that the quasiperiodic behavior is obtained from a chaotic attractor by virtue of a Neimark-Sacker bifurcation as the coupling parameter increases. Their coupled system also showed hyperchaos with an increase in coupling strength. Rech [97] and Kuznetsov *et al.* [13] have also reported the existence of hyperchaos in the bidirectional coupling of two chaotic Lorenz systems and two coupled Chialvo maps, respectively. Bashkirtseva *et al.* [94] showed that in coupled discrete-time logistic maps, the increase in coupling leads to the coexistence of periodic, quasiperiodic, and chaotic attractors.

The coupling of predator-prey models is used to feature dispersal factors in population models. Many researchers have studied the continuous [98–101] as well as discrete-time [102–104] predator-prey models in a two-patch environment with dispersal. The effect of including dispersal in various well-established predator-prey models such as Lotka-Volterra model [98] and Rosenzweig-MacArthur model [96, 98, 99, 105–107] have been explored thoroughly. Kang *et al.* [99] formulated a Rosenzweig-MacArthur predator-prey model in a two-patch environment with the dispersal of only the predator species. They showed that dispersal can have both stabilizing and destabilizing effects in the system. While considering both prey and predator dispersal in a Rosenzweig-MacArthur model distributed over discrete patches, Kon et al. [96] reported that the positive equilibrium of the system can be stabilized or destabilized by the non-diffusive population dispersal on a non-regular network. The coupled logistic maps show quasiperiodic behavior through a Neimark-Sacker bifurcation [85, 95]. Al-Kaff *et al.* [104] observed the emergence of transcritical, period-doubling, and Neimark-Sacker bifurcations that arise from coexisting positive fixed points in a discrete-time predator-prey model based on logistic maps.

* This chapter based on the following article: **Rajni, Bapan Ghosh**, Dispersal induced catastrophic bifurcations, Arnold tongues, shrimp structures, and stock patterns in an ecological system, *Chaos: An Interdisciplinary Journal of Nonlinear Science,* 34.12 (2024).

In ecological systems, the path to chaos often progresses through quasi-periodic behavior, with frequency-locking leading to chaotic dynamics [14]. Structured regions between quasi-periodic and chaotic states, such as Arnold tongues and shrimp-like structures, have been observed in many coupled systems [13, 95, 97, 108, 109]. These organized periodic structures result in complex patterns and period-adding sequences in parameter spaces.

In this regard, we realize that a patchy model can be formulated from the classical predator-prey models coupled in a two-patch environment. We consider a four-dimensional system with prey and predator moving from one patch to another. The growth rate of both populations follows the logistic map. The predator-prey interaction in an isolated patch is defined by a Holling type-II functional response. We explore the answer to the following points:

(i) As previously shown in the literature that coupling can both stabilize and destabilize the predator-prey system [99], does our system also have the same property?

(ii) Rech *et al.* [108] showed that by decreasing the coupling factor, a flip bifurcation occurs first, followed by a Neimark-Sacker, which transforms both fixed points to limit cycles in pairs of coupled maps. A key question is if a similar sequence of bifurcations occurs and how these bifurcations contribute to the stabilization or destabilization of our spatial population model.

(iii) Takashina *et al.* [110], Ujjwal *et al.* [89], and Ghosh *et al.* [111] show alternate stable states in continuous-time patchy models. We are interested in examining multiple stable modes in our discrete-time model.

(iv) How the periodic, quasiperiodic, and chaotic regimes exist in the two-parameter space when both dispersal rates are varied simultaneously?

(v) Many studies highlight the hydra effect due to species mortality in the uncoupled systems using the mean population [43, 44, 47, 59, 68]. Vortkamp *et al.* [112] showed that the dispersal can have positive and negative effects on the net population size in a heterogeneous environment. In a heterogeneous environment, Bajeux *et al.* [105] found that the hydra effect occurs and yield could be enhanced in RM model, whereas Doanh *et al.* [113], in the Lotka-Volterra model, showed that the total catch could be enhanced due to connectivity. We are interested to know if the dispersal-induced hydra effects could occur in our homogeneous environment.

This chapter comprises six distinct sections. Section 4.2 focuses on model formulation, with the significance and interpretation of all the model parameters. Section 4.3 is dedicated to the exploration of the existence and stability of the equilibrium points. In section 4.4, we investigate the dynamic behavior arising from varying dispersal rates individually. In particular, we deal with different bifurcations, chaos, and bistability. We vary both prey and predator dispersal rates simultaneously in section 4.5 to explore the possibility of the existence of organized periodic structures such as Arnold tongues and shrimp structures. Section 4.6 discusses the ecological implications of these dynamical changes via mean population. Section 4.7 encompasses a comprehensive and insightful discussion of our results.

4.2 Model formulation

In this study, we explore the dynamics of a predator-prey model in a patchy environment, aiming to understand the impact of varying dispersal rates on system stability. Many researchers have investigated dynamical changes in a continuous-time predator-prey model that incorporates dispersal within a two-patch environment [99,100,103,114–117]. Patchy models based on the frameworks of the Lotka–Volterra and Rosenzweig–MacArthur models are investigated by Cressman *et al.* [98]. A typical continuous-time model with two patches can be proposed as:

$$\begin{aligned}
\dot{x} &= rx\left(1-\frac{x}{K}\right)-\frac{\alpha xu}{h+x}+d_1(y-x),\\
\dot{u} &= su\left(1-\frac{u}{L}\right)+\frac{\beta xu}{h+x}+d_2(v-u),\\
\dot{y} &= ry\left(1-\frac{y}{K}\right)-\frac{\alpha yv}{h+y}+d_1(x-y),\\
\dot{v} &= sv\left(1-\frac{v}{L}\right)+\frac{\beta yv}{h+y}+d_2(u-v),
\end{aligned} \tag{4.2.1}$$

with initial population $x(0) > 0$, $u(0) > 0$, $y(0) > 0$ and $v(0) > 0$. The prey (and predator) species, denoted by x (and u) and y (and v) represent population densities in patch 1 and 2, respectively. We assume that the prey and predator in each patch evolve following a logistic growth rate. Therefore, the predator is generalist in nature. The intrinsic growth rates of the prey and predator species are denoted by r and s, respectively; while K and L represent the carrying capacities of the prey and predator species. The predation coefficient is denoted by α, and the conversion coefficient of prey biomass to

predator biomass is given by $\beta = \alpha c$. Here, c serves as an amplification factor reflecting the efficiency of biomass conversion. The half-saturation constant is denoted by h, a parameter that influences the functional response in the Holling type-II interaction. All the ecological parameters ($r, s, K, L, \alpha, \beta$, and h) are positive.

Apart from the reaction term (predation), the system is also coupled due to dispersal. The dispersal rates of the prey and predator species between patches are denoted by $d_1(>0)$ and $d_2(>0)$, respectively. These dispersal rates capture the movement of individuals between patches and play a crucial role in determining the spatial dynamics in ecological systems. The patches can be homogeneous or heterogeneous. Researches have studied both types of patches. Aly *et al.* [118], Mchich *et al.* [119], and Kon *et al.* [96] analyzed homogeneous patchy environments, while studies related to heterogeneous patches can be found in the works of Kuang *et al.* [120], Poggiale [121], Kang *et al.* [122], Sun *et al.* [123], and Choi *et al.* [124]. Some researchers also focused on comparing the results by considering both the cases of homogeneous and heterogeneous patchy habitats [125]. We made assumptions on homogeneity of both patches, meaning that within a given patch, ecological conditions such as resource availability, habitat quality, and climatic factors are assumed to be same. While this simplification may not fully capture the complexity of real-world ecosystems, it provides a tractable framework for studying the influence of spatial structure on population dynamics. The main focus of this model lies in investigating the stability of the system when dispersal rates vary. The dispersal rate of prey (and predator) between patches is equal.

The dynamics exhibited by discrete models, particularly in lower dimensional systems, surpass the complexity and richness observed in their continuous-time counterparts. Notably, discrete systems excel in describing intricate patterns and chaotic behaviors inherent in nonlinear dynamics, underscoring their suitability for capturing the intricate nature of ecological processes. Erm *et al.* [126] investigated a logistic map, which is the discretized form (using the forward Euler's scheme with a unit step size) of the continuous-time logistic equation. We formulate a discretized version of the continuous-time ecological system (4.2.1) as follows:

$$\begin{aligned} x_{n+1} &= x_n + r x_n \left(1 - \frac{x_n}{K}\right) - \frac{\alpha x_n u_n}{h + x_n} + d_1(y_n - x_n), \\ u_{n+1} &= u_n + s u_n \left(1 - \frac{u_n}{L}\right) + \frac{\beta x_n u_n}{h + x_n} + d_2(v_n - u_n), \end{aligned} \tag{4.2.2}$$

$$y_{n+1} = y_n + ry_n\left(1 - \frac{y_n}{K}\right) - \frac{\alpha y_n v_n}{h + y_n} + d_1(x_n - y_n),$$
$$v_{n+1} = v_n + sv_n\left(1 - \frac{v_n}{L}\right) + \frac{\beta y_n v_n}{h + y_n} + d_2(u_n - v_n),$$

with initial population $x_0 > 0,\ u_0 > 0,\ y_0 > 0$ and $v_0 > 0$.

We now delve into the further analysis of system (4.2.2). In the next section, we discuss the existence and stability of the equilibrium points of the system.

4.3 Existence and stability of the equilibria

In this section, we find the equilibrium points of the model (4.2.2). First, the conditions for the existence of equilibrium points are derived and then we delve into the stability of these points.

4.3.1 Existence of the equilibria

The equilibrium points of system (4.2.2) can be obtained by solving the following system of algebraic equations:

$$\begin{aligned}
rx\left(1 - \frac{x}{K}\right) - \frac{\alpha xu}{h + x} + d_1(y - x) &= 0,\\
su\left(1 - \frac{u}{L}\right) + \frac{\beta xu}{h + x} + d_2(v - u) &= 0,\\
ry\left(1 - \frac{y}{K}\right) - \frac{\alpha yv}{h + y} + d_1(x - y) &= 0,\\
sv\left(1 - \frac{v}{L}\right) + \frac{\beta yv}{h + y} + d_2(u - v) &= 0.
\end{aligned} \tag{4.3.1}$$

Clearly, the trivial equilibrium $(0, 0, 0, 0)$ is a solution of the system of equations in eq (4.3.1). Similarly, the boundary equilibria are $(K, 0, K, 0)$ and $(0, L, 0, L)$. The trivial and boundary equilibria always exist.

Let (x_c, u_c, y_c, v_c) be a coexisting equilibrium of the system. We assume the dispersal rates to be zero ($d_1 = d_2 = 0$) as the equilibrium points depend on neither d_1 nor d_2. The equilibrium points are same when d_1 and d_2 are non-zero. It is difficult to find the form of positive equilibrium analytically in terms of parameters but by doing some mathematical analysis we find the conditions for existence of positive equilibrium. Consider the predator-prey dynamics in patch 1 to see the existence of positive equilibrium (x_c, u_c) in patch 1. Since the system is homogeneous, similar analysis can be applied to patch 2 for (y_c, v_c). To show the existence of positive equilibrium, we find the prey and

predator nullclines from the equations:

$$r\left(1-\frac{x}{K}\right)-\frac{\alpha u}{h+x}=0, \tag{4.3.2a}$$

$$s\left(1-\frac{u}{L}\right)+\frac{\beta x}{h+x}=0. \tag{4.3.2b}$$

From equations (4.3.2a) and (4.3.2b), we get

$$u=\frac{r}{\alpha K}(K-x)(h+x)=:F(x). \tag{4.3.3a}$$

$$u=\frac{L}{s}\left(s+\frac{\beta x}{h+x}\right)=:G(x). \tag{4.3.3b}$$

The intersection of the two nullclines in eq (4.3.3a) and (4.3.3b) in the first quadrant will give the coexisting equilibrium points of the system (4.2.2). To find the intersection of the nullclines, we find the positive root of the polynomial $F(x)-G(x)$,

$$\frac{r}{\alpha K}(K-x)(h+x)-\frac{L}{s}\left(s+\frac{\beta x}{h+x}\right)=0$$

On simplification, a polynomial of degree three is obtained as

$$Ax^3+Bx^2+Cx+D=0,$$

where $A=rs, B=2hrs-Krs, C=2hKrs-h^2rs-KLs\alpha-KL\alpha\beta$, and $D=-h^2Krs+hKLs\alpha$.

This suggests that there are at most three positive equilibria. Here, $\max(F(x))=\frac{r}{K\alpha}(K+h)^2$ at $x=\frac{K-h}{2}$. Clearly, $G(x)$ is a monotonically increasing function as $G'(x)>0$. Moreover, $G(x)\to L+\frac{L\beta}{s}$ as $x\to\infty$. Also, $x\to -h$ is an asymptote of $G(x)$.

The zeroes of $F(x)$ are $-h$ and K whereas $G(x)$ has only one zero at $-\frac{sh}{\beta+h}$ which lies in the interval $(-h,K)$. As $-h<-\frac{sh}{\beta+s}$, $F(0)=\frac{rh}{\alpha}$, and $G(0)=L$. Based on this analysis, we can present sufficient conditions for the existence of no, one, two, and three equilibria as follows:

(i) If $L>\frac{r}{4\alpha}(K+h)^2$, then there exists no positive equilibrium of the system within the patch as the functions $F(x)$ and $G(x)$ will not intersect in the first quadrant (Figure 4.3.1a).

(ii) If $L < \frac{rh}{\alpha}$ and $G(x) < F(x)$ in $\left(0, \frac{K-h}{2}\right)$ then the isolated system has unique positive equilibrium. This follows from the fact that the functions $F(x)$ and $G(x)$ will intersect at exactly one point in the first quadrant as mentioned in Figure 4.3.1b.

(iii) If $\frac{rh}{\alpha} < L < \frac{r}{4\alpha}(K+h)^2$ and $G\left(\frac{K-h}{2}\right) < \frac{r}{4\alpha}(K+h)^2$, then there exist two positive equilibrium of the system because The functions $F(x)$ and $G(x)$ will intersect at two points in the first quadrant as shown in Figure 4.3.1c.

(iv) If $L < \frac{rh}{\alpha}$, $G(x) > F(x)$ for a small interval of $(0, \frac{K-h}{2})$, and $G\left(\frac{K-h}{2}\right) < \frac{r}{4\alpha}(K+h)^2$, then the system has three positive equilibrium. Since, the functions $F(x)$ and $G(x)$ will intersect at three points in the first quadrant (Figure 4.3.1d).

Hence, our system can have no, one, two, or three positive equilibria. In the similar we can get the conditions for existence of (y_c, v_c) for the isolated patch 2. Thus, the coupled system can have at most three positive equilibrium.

4.3.2 Stability of equilibria

It is worth noting that the coexisting equilibrium within the system remains independent of the values of d_1 and d_2. We examine if dispersal rates affect the ecological interactions between prey and predator in our model. In particular, we are interested to explore the impacts of dispersal on the stability of coexisting equilibrium. To determine stability of a coexisting equilibrium, we analyze the eigenvalues of the Jacobian matrix of the linearised version of system (4.2.2). The Jacobian matrix at any equilibrium, say, (x^*, u^*, y^*, v^*) is given by,

$$J(x^*, u^*, y^*, v^*) = \begin{pmatrix} \Gamma_{11} - d_1 & \Gamma_{12} & d_1 & 0 \\ \Gamma_{21} & \Gamma_{22} - d_2 & 0 & d_2 \\ d_1 & 0 & \Gamma_{33} - d_1 & \Gamma_{34} \\ 0 & d_2 & \Gamma_{43} & \Gamma_{44} - d_2 \end{pmatrix} \tag{4.3.4}$$

where

$$\Gamma_{11} = 1 + r\left(1 - \frac{2x^*}{K}\right) - \frac{\alpha u^* h}{(h+x^*)^2}, \quad \Gamma_{12} = -\frac{\alpha x^*}{h+x^*},$$
$$\Gamma_{21} = \frac{\beta h u^*}{(h+x^*)^2}, \quad \Gamma_{22} = 1 + s\left(1 - \frac{2u^*}{L}\right) + \frac{\beta x^*}{h+x^*},$$

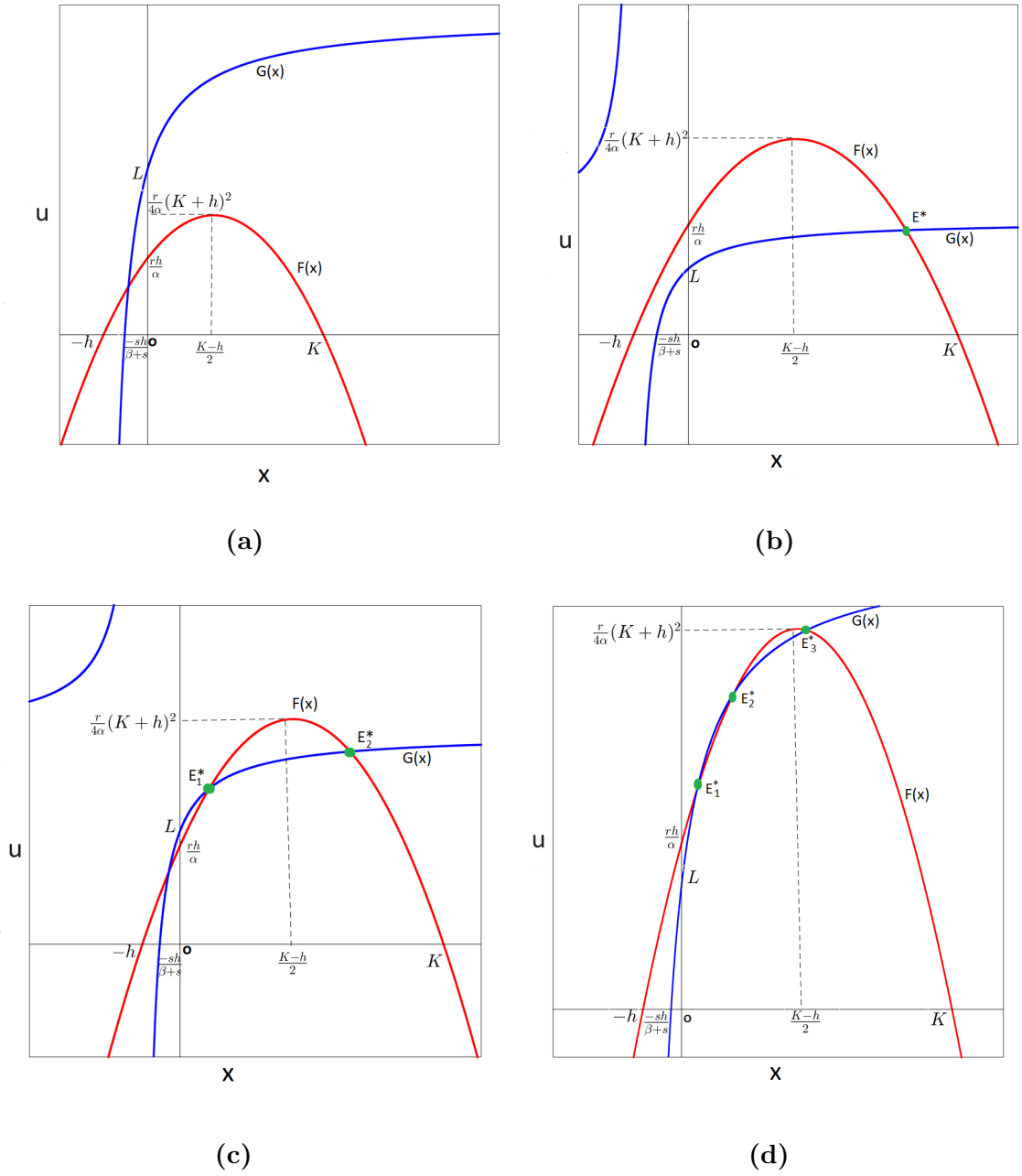

Figure 4.3.1: The intersection of nontrivial prey nullcline (red solid line) and the nontrivial predator nullcline (blue solid line). (a) No positive equilibrium exists. (b) E^* is the positive equilibrium point (green solid dot). (c) E_1^* and E_2^* are the positive equilibria. (d) E_1^*, E_2^*, and E_3^* are the positive equilibria. The dashed black line represents the maximum of $F(x)$.

$$\Gamma_{33} = 1 + r\left(1 - \frac{2y^*}{K}\right) - \frac{\alpha v^* h}{(h+y^*)^2}, \quad \Gamma_{34} = -\frac{\alpha y^*}{h+y^*},$$
$$\Gamma_{43} = \frac{\beta h v^*}{(h+y^*)^2}, \quad \text{and} \quad \Gamma_{44} = 1 + s\left(1 - \frac{2v^*}{L}\right) + \frac{\beta y^*}{h+y^*}.$$

If the absolute values of the eigenvalues of $J(x^*, u^*, y^*, v^*)$ are less than unity then the equilibrium (x^*, u^*, y^*, v^*) is asymptotically stable.

Since $x^* = y^*$ and $u^* = v^*$, we have

$$\Gamma_{11} = \Gamma_{33}, \Gamma_{12} = \Gamma_{34}, \Gamma_{21} = \Gamma_{43}, \text{and}\, \Gamma_{22} = \Gamma_{44}.$$

Hence the matrix (4.3.4) can be expressed as,

$$J = \begin{bmatrix} J_1 & J_2 \\ J_2 & J_1 \end{bmatrix},$$

where

$$J_1 = \begin{bmatrix} \Gamma_{11} - d_1 & \Gamma_{12} \\ \Gamma_{21} & \Gamma_{22} - d_2 \end{bmatrix} \text{ and } J_2 = \begin{bmatrix} d_1 & 0 \\ 0 & d_2 \end{bmatrix}.$$

The characteristic polynomial can be written as,

$$\det(J - \lambda I_4) = \det(J_1 + J_2 - \lambda I_2).\det(J_1 - J_2 - \lambda I_2), \tag{4.3.5}$$

where

$$J_1 + J_2 = \begin{bmatrix} \Gamma_{11} & \Gamma_{12} \\ \Gamma_{21} & \Gamma_{22} \end{bmatrix} \text{ and } J_1 - J_2 = \begin{bmatrix} \Gamma_{11} - 2d_1 & \Gamma_{12} \\ \Gamma_{21} & \Gamma_{22} - 2d_2 \end{bmatrix}.$$

I_4 and I_2 are identity matrix of order 4 and 2, respectively.

For $\det(J_1 + J_2 - \lambda I_2) = 0$, the characteristic polynomial is

$$C_1(\lambda) := \lambda^2 - (\Gamma_{11} + \Gamma_{22})\lambda + \Gamma_{11}\Gamma_{22} - \Gamma_{12}\Gamma_{21}, \tag{4.3.6}$$

and the same for $\det(J_1 - J_2 - \lambda I_2) = 0$ is

$$C_2(\lambda) := \lambda^2 - (\Gamma_{11} + \Gamma_{22} - 2d_1 - 2d_2)\lambda + (\Gamma_{11} - 2d_1)(\Gamma_{22} - 2d_2) - \Gamma_{12}\Gamma_{21}. \tag{4.3.7}$$

In the isolated patch ($d_1 = d_2 = 0$), $C_1(\lambda)$ and $C_2(\lambda)$ are the same. Since, only $C_2(\lambda)$ depends on d_1 and d_2, we focus on introducing dispersal to the system to see its stabilizing or destabilizing effect on the coexisting equilibrium.

Theorem 4.1. *If the coexisting equilibrium of the system (4.2.2) is unstable (or saddle) in the isolated patch then it remains unstable (or saddle) in the non-isolated patch.*

Proof. At least one of the eigenvalues of the matrix J lies outside the unit circle if the coexisting equilibrium of the system (4.2.2) is unstable in the isolated patches. Hence we can say that

$$|\lambda_i| > 1 \text{ for } i = 1, 2, 3, 4.$$

By introducing dispersal, and using identity (4.3.5), we can state that at least two eigenvalues obtained from $C_1(\lambda) = 0$ still remain outside the unit circle. Thus, the system (4.2.2) remains unstable in non-isolated patches as well. Similar argument can be made if the coexisting equilibrium is a saddle in the isolated patch. □

If the coexisting equilibrium is stable in the isolated patches, then all eigenvalues of J are such that,

$$|\lambda_i| < 1 \text{ for } i = 1, 2, 3, 4.$$

We now verify whether dispersal can cause instability into the system.

Theorem 4.2. *In the absence of dispersal rate of prey (or respectively predator) while increasing only the dispersal rate of predator (or respectively prey) destabilizes the coexisting equilibrium of the system (4.2.2).*

Proof. Given the eigenvalue expression

$$\lambda_\pm = \frac{1}{2}\Big(- 2d_1 - 2d_2 + \Gamma_{11} + \Gamma_{22} \pm \sqrt{4\Gamma_{12}\Gamma_{21} + (2d_1 - 2d_2 - \Gamma_{11} + \Gamma_{22})^2}\Big)$$

and setting $d_2 = 0$, the expression simplifies to

$$\lambda_\pm = \frac{1}{2}\left(-2d_1 + \Gamma_{11} + \Gamma_{22} \pm \sqrt{4\Gamma_{12}\Gamma_{21} + (2d_1 - \Gamma_{11} + \Gamma_{22})^2}\right).$$

The equation

$$4\Gamma_{12}\Gamma_{21} + (2d_1 - \Gamma_{11} + \Gamma_{22})^2 = 0$$

has roots $\dfrac{\Gamma_{11} - \Gamma_{22}}{2} \pm \sqrt{|\Gamma_{12}\Gamma_{21}|}$. The function $\omega(d_1) := 4\Gamma_{12}\Gamma_{21} + (2d_1 - \Gamma_{11} + \Gamma_{22})^2$ increases for $d_1 > \dfrac{\Gamma_{11} - \Gamma_{22}}{2} + \sqrt{|\Gamma_{12}\Gamma_{21}|}$. Also,

$$\lambda_- = \frac{1}{2}\left(-2d_1 + \Gamma_{11} + \Gamma_{22} - \sqrt{4\Gamma_{12}\Gamma_{21} + (2d_1 - \Gamma_{11} + \Gamma_{22})^2}\right)$$

$$< \frac{1}{2}(-2d_1 + \Gamma_{11} + \Gamma_{22}).$$

Hence, if $d_1 > \max\left\{\frac{\Gamma_{11}-\Gamma_{22}}{2}+\sqrt{|\Gamma_{12}\Gamma_{21}|}, \frac{2+\Gamma_{11}+\Gamma_{22}}{2}\right\}$ then $|\lambda_-| > 1$ which destabilizes the coupled system. It is noteworthy that this is only a sufficient condition for the eigenvalues to move out of the unit circle.

Similarly we can show that one of the sufficient condition for destabilization of the coexisting equilibrium when $d_1 = 0$ is $d_2 > \max\left\{\frac{\Gamma_{11}-\Gamma_{22}}{2}-\sqrt{|\Gamma_{12}\Gamma_{21}|}, \frac{2+\Gamma_{11}+\Gamma_{22}}{2}\right\}$. □

If the eigenvalue $\lambda_\pm$ passes the unit circle, a bifurcation occurs. Let's now state necessary conditions for occurrence of various bifurcations. Based on the roots of the characteristic polynomial (4.3.6), the following conditions can be stated:

Case I: The roots are real if

$$\gamma := 4\Gamma_{12}\Gamma_{21} + (2d_1 - 2d_2 - \Gamma_{11} + \Gamma_{22})^2 \geq 0. \tag{4.3.8}$$

When the eigenvalues are real then $\lambda_- \leq \lambda_+$. If both eigenvalues lie inside the unit circle without dispersal then with dispersal, λ_- will achieve -1 first. Hence, dispersal moves the eigenvalue λ_- out of the unit circle through negative real axis. Thus stability curve is determined by $\lambda_- = -1$, i.e.,

$$-2d_1 - 2d_2 + \Gamma_{11} + \Gamma_{22} - \sqrt{4\Gamma_{12}\Gamma_{21} + (2d_1 - 2d_2 - \Gamma_{11} + \Gamma_{22})^2} = -2.$$

From the above expression, we define

$$\phi := -\sqrt{4\Gamma_{12}\Gamma_{21} + (2d_1 - 2d_2 - \Gamma_{11} + \Gamma_{22})^2} = -2 + 2d_1 + 2d_2 - \Gamma_{11} - \Gamma_{22}.$$

Case II: The eigenvalues are complex conjugate if

$$\gamma := 4\Gamma_{12}\Gamma_{21} + (2d_1 - 2d_2 - \Gamma_{11} + \Gamma_{22})^2 < 0. \tag{4.3.9}$$

The complex eigenvalues has absolute value one, i.e., $|\lambda_\pm| = 1$, from this condition, we define

$$\xi := 2d_1\Gamma_{22} + 2d_2\Gamma_{11} - 4d_1d_2 = \Gamma_{11}\Gamma_{22} - \Gamma_{12}\Gamma_{21} - 1. \tag{4.3.10}$$

We now examine whether under some parameter set, all the necessary conditions, which are stated above, for existence of bifurcations are possible. Taking the parameter set: $r = 2, K = 1, s = 1, L = 5, \alpha = \frac{8}{10}, \beta = \frac{6}{10}$, and $h = 5$, we plot the stability threshold (bifurcation curves) in d_1d_2-plane in Figure 4.3.2. The red line is the curve $\gamma = 0$. The yellow part represents the region where roots of the characteristic polynomial are complex

while roots are real in the gray regions. When the roots are complex and exactly one in absolute value, we get the black curve in the yellow region which is the Neimark-Sacker bifurcation curve ($\xi = 0$). Similarly when the roots are real and one of roots is exactly -1 then we get the magenta curve ($\phi = 0$) in gray region which is the representation of a flip bifurcation. The coexisting equilibrium is stable in the area bounded by the magenta branches of $\phi = 0$ and $\xi = 0$. Hence, dispersal causes instability of the coexisting equilibrium when the absolute value of $\lambda_{\pm}$ crosses unity to lie outside the unit circle via the magenta and the black curve.

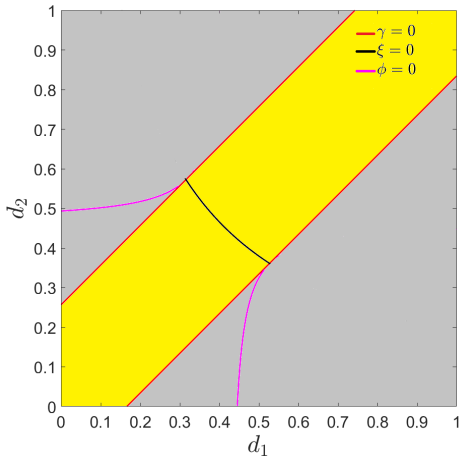

Figure 4.3.2: Bifurcation curves in the d_1d_2-plane: bifurcations occur on the black colored curve in the yellow region and magenta colored curve in the gray region.

4.4 Dynamical behavior

In the previous section, we described the stability region of the coexisting equilibrium and the threshold curve where some possible bifurcation could happen. We explore if the local bifurcation structure is similar on a same bifurcation curve. Further, we investigate the dynamics of the system away from the threshold curve. In this section, we perform numerical simulations to analyze the dynamical behavior of our model in the two parameter space.

4.4.1 Dispersal and bifurcation

We aim to observe various bifurcations, both periodic and non-periodic behavior, the route to chaos, and other complex dynamical changes in the system. We assume the parameters as $r = 2, K = 1, s = 1, L = 5, \alpha = 0.8, \beta = 0.6$, and $h = 5$. Then, the unique

coexisting equilibrium is $(0.620592, 5.331242, 0.620592, 5.331242)$. We individually vary each of the dispersal rates to examine the following three situations:

(i) If the coexisting equilibrium in isolated patches is stable, then we vary either prey or predator dispersal rate to see the changes in the coupled system.

(ii) If the coexisting equilibrium of the coupled system due to either prey or predator dispersal is stable then we note the impact of varying dispersal rate of either species.

(iii) If the coexisting equilibrium is unstable due to coupling of either of the species, then we examine the impact of the dispersal of other species.

In order to investigate the above cases, we fix the values of d_2 and then vary prey dispersal rate along lines L_1 and L_2 (Figure 4.4.1a). Similarly, predator dispersal rate along the lines S_1 and S_2 (Figure 4.4.1b), by fixing the dispersal rate of prey.

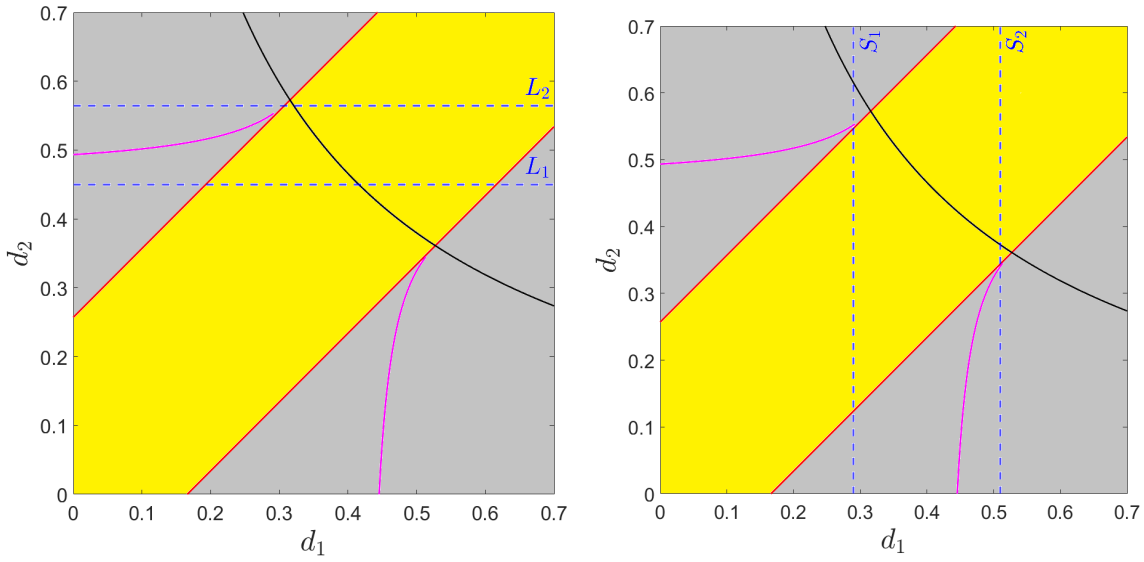

Figure 4.4.1: (a) L_1 and L_2 represent the lines $d_2 = 0.45$ and $d_2 = 0.564$, respectively, in d_1d_2-plane. (b) S_1 and S_2 represent the lines $d_1 = 0.29$ and $d_1 = 0.51$, respectively, in d_1d_2-plane.

4.4.1.1 Flip bifurcation

We vary prey and predator dispersal rate individually to see if similar kind of bifurcation is observed in both scenarios.

Prey dispersal

The unique coexisting equilibrium remains stable when coupled with a fixed predator

dispersal rate in the interval $[0, 0.36)$ with no prey dispersal. To explore the local dynamics around this equilibrium, we iterate the system with an initial condition $(0.5, 4.85, 0.5, 5)$.

First, we focus on varying the prey dispersal rate while keeping the predator dispersal rate at zero. The stability of the coexisting equilibrium persists as long as d_1 remains below the critical value of 0.44532. An intriguing transformation occurs at $d_1 = d_1^* = 0.44532$, leading to a flip-bifurcation. This event smoothly gives rise to a stable period-2 orbit. The period-2 orbit retains its stability for all values of $d_1 < 0.64$. The transition from period-1 to period-2 orbit is a non-catastrophic event (Figure 4.4.2a).

As we further explore the system's dynamics, an additional bifurcation materializes as d_1 surpasses the threshold $d_1 = \widehat{d_1} = 0.64$. The transition that takes place leads to generation of two stable closed invariant curve. Consequently, the system exhibits quasiperiodic behavior. A powerful tool to characterize the periodic, quasiperiodic and chaotic behavior is calculating Lyapunov exponents. For a four-dimensional system, we have four Lyapunov exponents, say, Λ_1, Λ_2, Λ_3, and Λ_4. In a continuous-time system [12], the Lyapunov spectrum for different dynamical behavior is given in **Table 1.9.1**. The Lyapunov exponent spectrum for a four-dimensional discrete-time system [13–16] is provided in **Table 1.9.2**.

The transitions from fixed point $\rightarrow$ periodicity $\rightarrow$ limit cycle which makes the dynamics quasiperiodic can be confirmed by analyzing the Lyapunov exponent in the Figure 4.4.2b using **Table 1.9.2**. We clearly observe that $\Lambda_1 < 0$, $\Lambda_2 < 0$ for $d_1 < \widehat{d_1}$, and Λ_1 settling at zero after the Neimark-Sacker bifurcation in the neighborhood of $d_1 = \widehat{d_1}$. The graphs for Λ_1 and Λ_2 in red and blue color respectively overlap for $d_1 < 0.65$ and separate when system exhibits quasiperiodic behavior. Λ_3 and Λ_4 are always negative. These observations shed light on the intricate and fascinating dynamical changes occurring within the system as we manipulate the parameter d_1.

We observe the similar behavior if d_2 is fixed at any other value in the interval $(0, 0.36)$ while prey dispersal rate is varied as in Figure 4.4.2a.

Predator dispersal

Keeping d_1 fixed in the interval $(0, 0.1)$, the variation in predator dispersal rate leads to the similar scenarios as shown by varying prey dispersal rate. For $d_1 \in (0.1, 0.318)$, we discuss some of the different kind of dynamical behavior obtained by varying d_2. With $d_1 = 0.29$, we plotted the bifurcation diagram in Figure 4.4.2c along the line S_1 (Figure 4.4.1b).

The Lyapunov exponents (Λ_1 and Λ_2) presented to categorize the dynamics (including quasiperiodicity) in Figure 4.4.2d, other Lyapunov exponents are negative. Varying the predator dispersal rate, the coexisting equilibrium initially loses stability through a flip bifurcation where a stable period-2 orbit emerges with a *sudden jump* for $d_2 = 0.552$. Thus, a non-smooth transition of the state, i.e., a catastrophic transition [31] occurs in our system. However, when we varied prey dispersal rate, the transition of period-doubling bifurcation is smooth which we didn't observe in case of predator dispersal variation. The ecological impact of such smooth and non-smooth transition is discussed in a subsequent section. As the dispersal rate further increases, the system transitions back to a quasiperiodic state when the period-2 orbits become unstable, leading to the formation of two stable closed invariant curves. These two curves lose their stability and a stable period-10 orbit emerges which remains stable for $0.622 < d_2 < 0.684$. This period-10 orbit gives birth to ten closed invariant curves as d_2 is increased further (Figure 4.4.2e). Eventually, when $d_2 = 0.69$, a quasiperiodic torus is observed (Figure 4.4.2f) with Lyapunov exponents: $\Lambda_1 = \Lambda_2 = 0$ and Λ_3, $\Lambda_4 < 0$.

4.4.1.2 Neimark-Sacker bifurcation

In the last subsection, we encountered a Neimark-Sacker bifurcation with destabilization of the period-2 orbit. For a fixed $d_2 \in (0.36, 0.494)$, varying d_1 leads to a Neimark-Sacker bifurcation with a smooth transition. Fixing $d_2 = 0.45$, we plotted the bifurcation diagram by varying d_1 in Figure 4.4.3a along the line L_1 (Figure 4.4.1a). The coexisting equilibrium is stable when prey dispersal rate $d_1 < 0.416$. If d_1 approaches 0.416, the eigenvalues of the Jacobian matrix at the positive equilibrium are complex and tend to unity in absolute value. This implies the existence of a Neimark-Sacker bifurcation, and the coexisting equilibrium loses its stability to an invariant closed curve when d_1 crosses 0.416. This behavior of transitioning from stable period-1 orbit (coexisting equilibrium) to quasiperiodicity is also reflected in the Figure 4.4.3b in terms of Lyapunov exponents (Λ_1 and Λ_2). Here, Λ_3 and Λ_4 are negative.

By fixing a value of d_1 in the interval $(0.318, 0.446)$ while varying d_2, a Neimark-Sacker bifurcation occurs causing an instability of the coexisting equilibrium to give birth to a stable invariant closed curve. We examined that the structure of the local bifurcation for predator dispersal is the same as prey dispersal in Figure 4.4.3a.

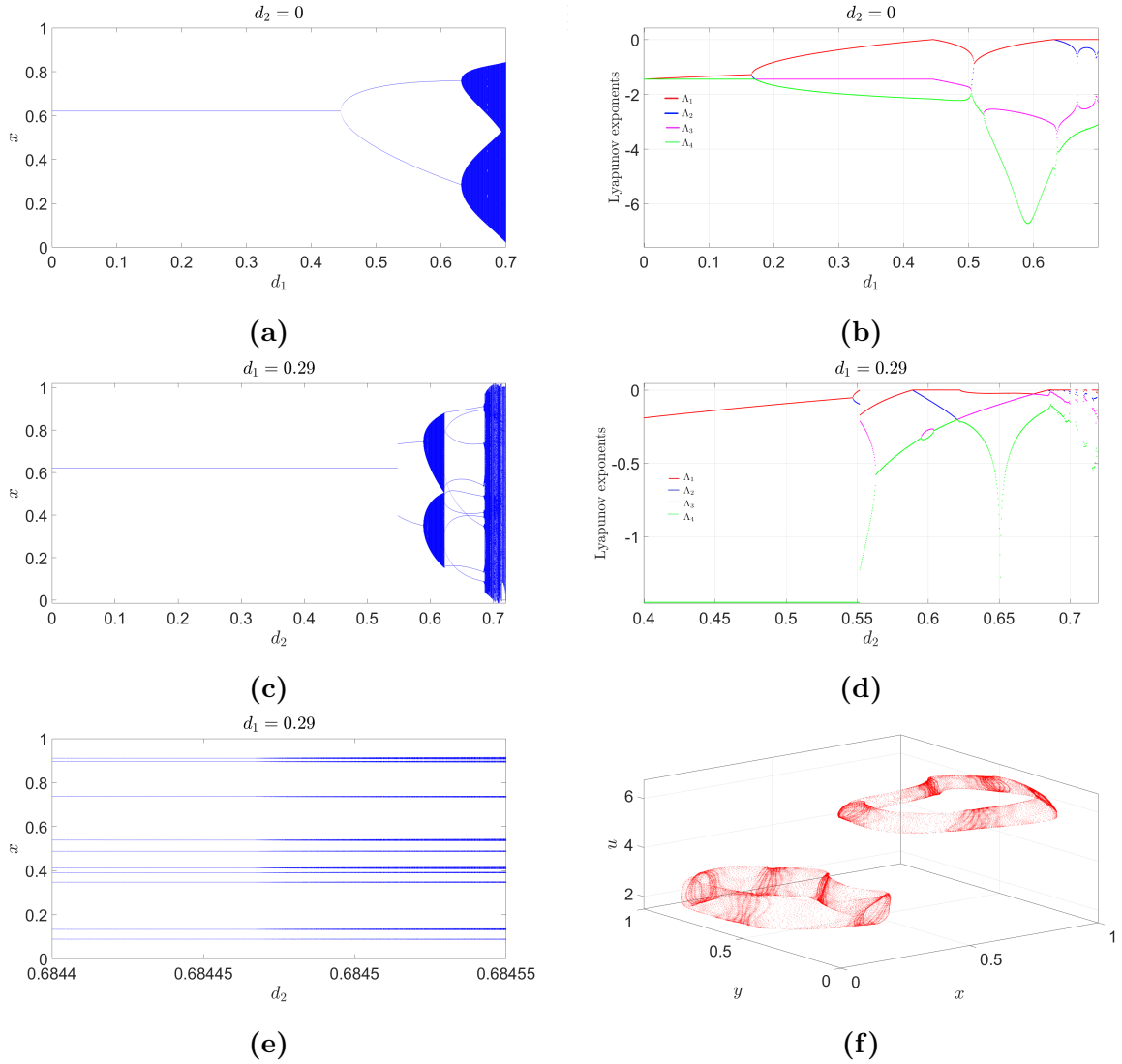

Figure 4.4.2: (a) Flip bifurcation diagram with predator species as prey dispersal rate varies in the absence of predator dispersal. (b) The Lyapunov exponents with respect to bifurcation diagram in (a). (c) Bifurcation diagram with prey species as predator dispersal rate varies when $d_1 = 0.29$. (d) The corresponding Lyapunov exponents to bifurcation diagram in (c). (e) zoomed part of the bifurcation diagram in (c). (f) Phase portrait of the torus structure in xyu-plane for $d_2 = 0.69$.

4.4.1.3 Flip bifurcation followed by Neimark-Sacker bifurcation

Till now, we observed the occurrence of either flip or Neimark-sacker bifurcation at the coexisting equilibrium while varying prey (or predator) dispersal rate when the system was at stable mode. Further, we observed that it destabilizes the equilibrium. Now, we

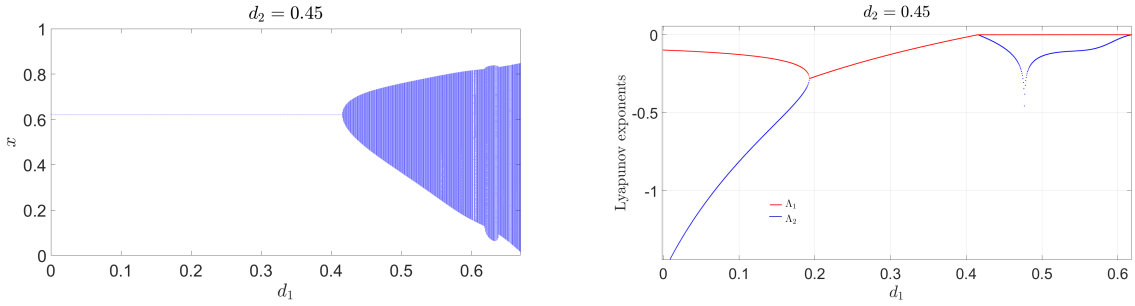

(a) **(b)**

Figure 4.4.3: (a) With fixed $d_2 = 0.45$, Neimark-Sacker bifurcation diagram with prey species as prey dispersal rate varies. (b) The Lyapunov exponents with respect to varying prey dispersal rate.

consider a destabilized system, i.e., fixing d_2 (or d_1) such that the coexisting equilibrium is unstable and vary d_1 (or d_2) to see if it can stabilize the dynamics.

Prey dispersal

For fixed $d_2 \in (0.494, 0.571)$, the coexisting equilibrium in the coupled system is unstable with no prey dispersal. For instance fixing $d_2 = 0.564$ and increasing d_1 along the line L_2 (Figure 4.4.1a), the system shows dynamics as shown in Figure 4.4.4a. The period-2 orbit is stable for $0 < d_1 < 0.3191$, as $d_1 = 0.3191$ the system shows a non-smooth transition to stability of coexisting equilibrium by catastrophic period-halving. Hence, dispersal can stabilize the coexisting equilibrium. At $d_1 = 0.3212$, the coexisting equilibrium loses its stability smoothly to a closed invariant curve which remains stable for $d_1 \in (0.3212, 0.3612)$. When d_1 crosses through 0.3612, the quasiperiodic orbit disappears and a period-2 orbit becomes stable via a catastrophic event, beyond $d_1 = 0.38$ a quasiperiodicity appears in the system smoothly. We also see a periodic window of period-6 in a narrow interval, i.e., $0.4694 < d_1 < 0.4732$. The Lyapunov exponents are shown in Figure 4.4.4b (Λ_3, $\Lambda_4 < 0$). The Λ_1 and Λ_2 graphs merge when the behavior is periodic.

Predator dispersal

When the predator dispersal rate is zero then the system exhibit non-equilibrium states for $0.446 < d_1 < 0.526$. Fixing $d_1 = 0.51$, increase in predator dispersal along the line S_2 (Figure 4.4.1b), leads to stabilization of coexisting equilibrium via a period-halving with a smooth transition at $d_2 = 0.342$. The positive equilibrium is stable before losing its

stability to a closed invariant curve at $d_2 = 0.374$ as shown in figure Figure 4.4.4c and corresponding Lyapunov exponents in Figure 4.4.4d.

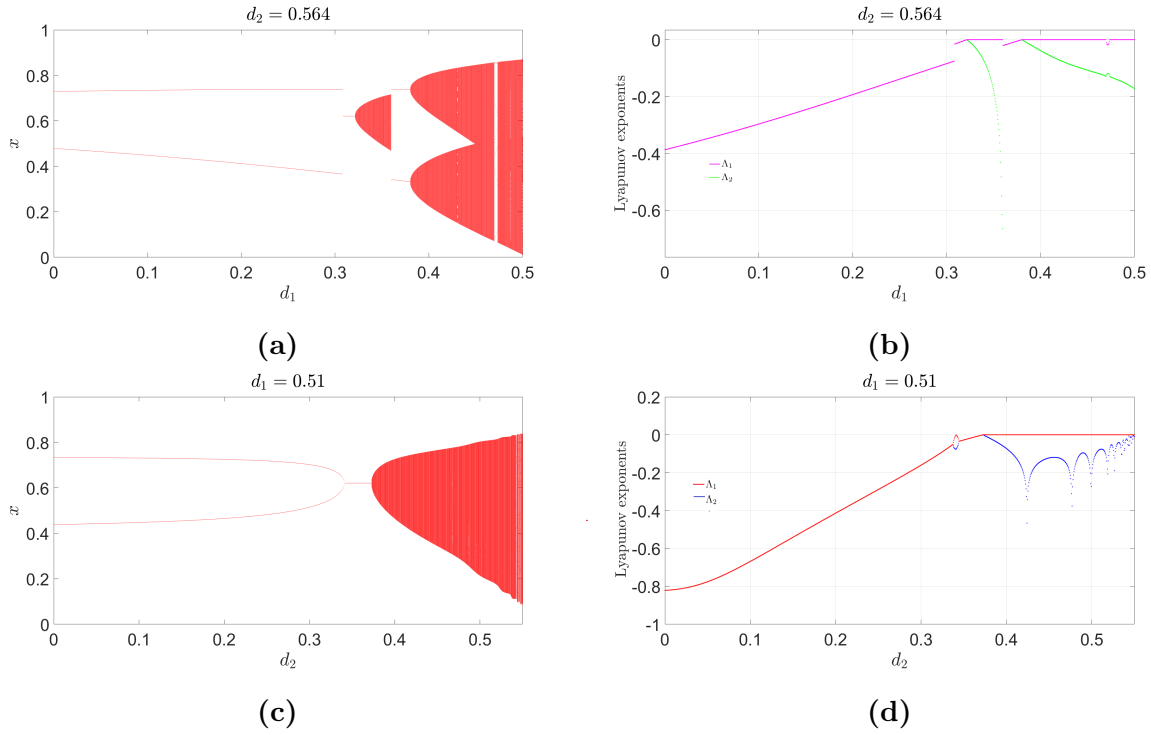

Figure 4.4.4: (a) Bifurcation diagram with prey species as prey dispersal rate varies when $d_2 = 0.564$. (b) The corresponding maximum Lyapunov exponents to bifurcation diagram in (a). (c)Bifurcation diagram with prey species as predator dispersal rate varies when $d_1 = 0.51$. (d) The corresponding maximum Lyapunov exponents to bifurcation diagram in (c).

4.4.1.4 Existence of chaos

Thus far, our exploration has revealed that when predator or prey dispersal is varied separately, it induces quasiperiodicity into the system. Chaotic behavior has not yet emerged in the system.

The bifurcation diagram and Lyapunov exponents for $d_2 = 0.47$ are represented in Figure 4.4.5a and Figure 4.4.5b - 4.4.5c, respectively. The stable equilibrium undergoes a Neimark-Sacker bifurcation as d_1 increases, leading to quasiperiodicity. Upon closer examination, it becomes apparent that elevating the prey dispersal rate induces chaotic behavior in the system. The maximum Lyapunov exponent (Λ_1) for the given fixed values of $d_1 = 0.611$ and $d_2 = 0.47$ registers a value of 0.043145 and $\Lambda_4 < \Lambda_3 < \Lambda_2 < 0$, providing

confirmation of the chaotic dynamics observed in the system. The phase portrait is depicted in Figure 4.4.5d.

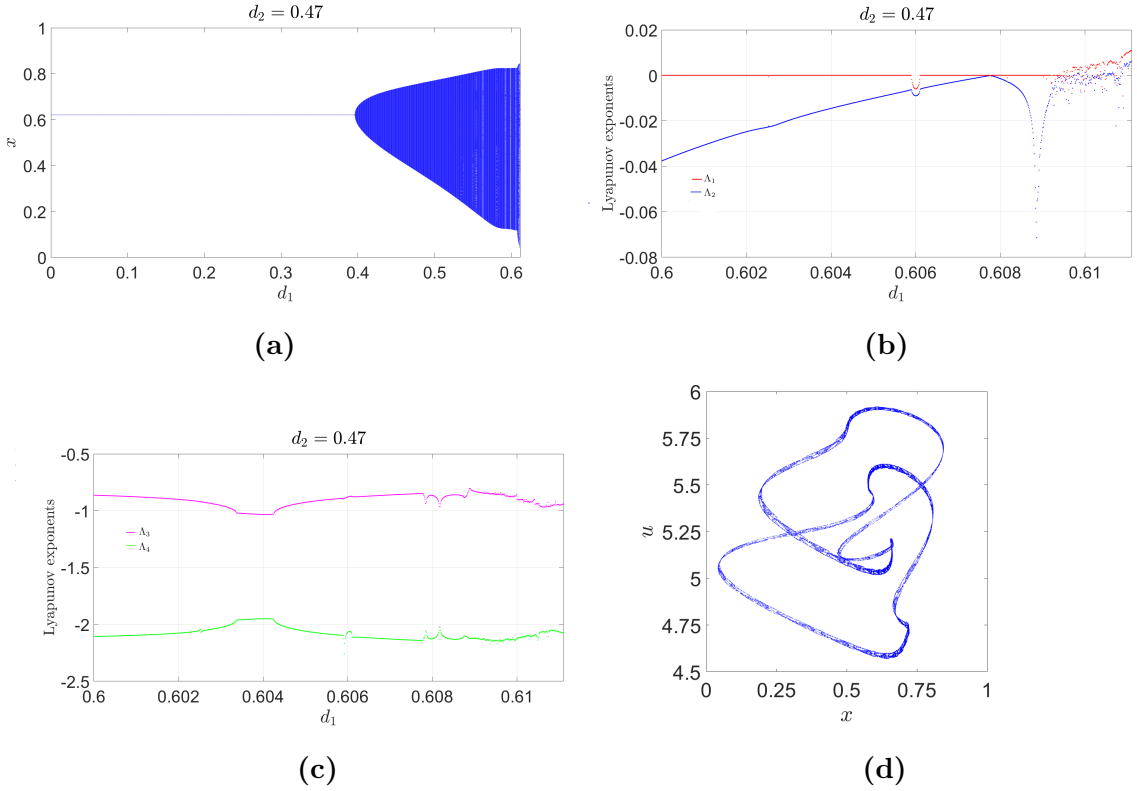

Figure 4.4.5: (a) Bifurcation diagram with predator species as prey dispersal rate varies when $d_2 = 0.47$. (b) The corresponding maximum Lyapunov exponents with respect to varying prey dispersal rate. (c) The chaotic attractor plotted in the (x, u)-plane.

4.4.2 Dispersal and Bistability

In this subsection, we explore the multistable states, aiming to unravel the diverse dynamics that may emerge from the same ecological set up. Upon altering the initial condition, different attractors coexist for the same set of parameter values. We will explore two cases when $d_2 = 0.47$ and $d_2 = 0.564$ while varying prey dispersal rates. We observe following types of multistabilities:

(i) ***Stable coexisting equilibrium and period-2 orbit:***

For $d_2 = 0.564$, we observed the complicated dynamical behavior while varying d_1. For the initial condition $(0.5, 4.85, 0.52, 5)$, the bifurcation diagram is shown in Figure 4.4.4a. If we change the initial condition to $(0.7, 6.3, 0.4, 3.6)$, different dynamical behavior is exhibited by the system. In Figure 4.4.6a, we have plotted

bifurcation diagram for $0.31 < d_1 < 0.36$, for these two different initial conditions. The non-overlapping nature of the two bifurcation diagrams, particularly within a significant range of prey dispersal rates, indicates the presence of more than one attractor. Consequently, the system demonstrates bistability. When $0.3192 < d_1 < 0.3212$, the coexisting equilibrium is stable (small blue colored) for the first initial condition while period-2 orbit (red colored) is stable for the second initial condition. Existence of fixed point and period-2 multistability is rare in ecological models. In this sense, it is a new contribution. This bistability occurs due to the spatial coupling.

(ii) ***Stable period-2 orbit and an invariant closed curve:***
We also observe that a period-2 orbit and a quasiperiodic orbit coexist for the initial conditions $(0.7, 6.3, 0.4, 3.6)$ and $(0.5, 4.85, 0.5, 5)$, respectively, for $d_1 \in (0.3212, 0.36)$. The Lyapunov exponents for these two initial conditions are plotted in Figure 4.4.6b. The difference in the dynamical behavior is clear from the Lyapunov curves: $(0.7, 6.3, 0.4, 3.6)$ in blue (Λ_1) and magenta (Λ_2) color while $(0.5, 4.85, 0.5, 5)$ in red (Λ_1) and green (Λ_2) color.

(iii) ***Stable period-27 and chaotic attractor:***
In the last subsection 4.4.1, we plotted the bifurcation diagram varying prey dispersal with $d_2 = 0.47$, using the initial condition $(0.5, 4.85, 0.52, 5)$ and observed that the system undergoes a Neimark-Sacker bifurcation where the transition to chaotic behavior is reached through quasiperiodicity. Now, we plotted another bifurcation diagrams using the initial conditions $(0.5, 5, 0.52, 5)$ and $(0.5, 4.85, 0.52, 5)$ in blue and red color, respectively in Figure 4.4.6c. Also the Lyapunov exponents for these two initial conditions don't coincide (Figure 4.4.6d). We chose $d_1 = 0.611$ to plot a phase portrait in the (x, u)-plane where the initial conditions $(0.5, 5, 0.52, 5)$ leads to a chaotic behavior (blue color) and $(0.5, 4.85, 0.52, 5)$ lands on a stable period-27 orbit (red color) in Figure 4.4.6e.

The basin of attraction for a two dimensional system is relatively easier to plot [68]. However, it is a bit challenging to draw for a system of three dimension but the basin is still much visible. The basin of attraction for a four dimensional system is plotted by keeping initial conditions for two state variables fixed and varying initial conditions for the other two state variables as demonstrated in Brugnago *et al.* [127]. However, we

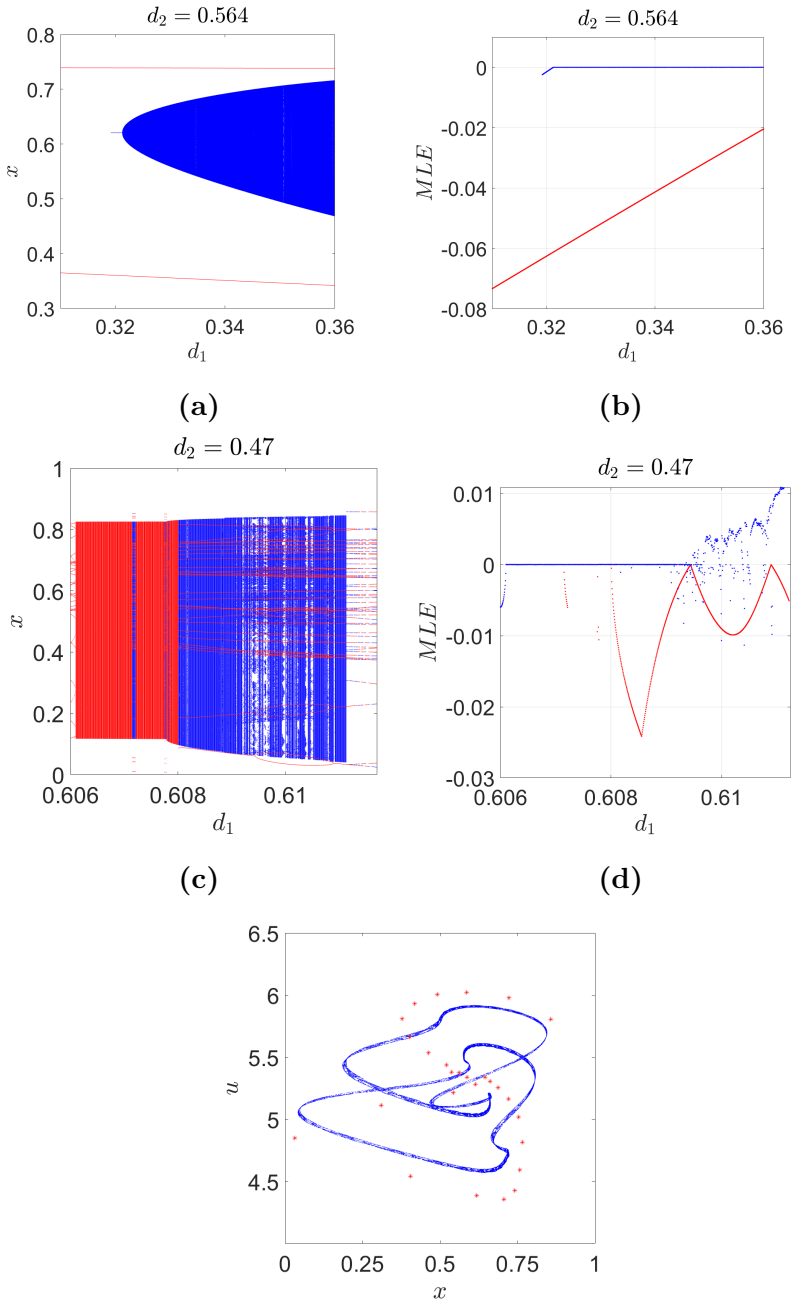

Figure 4.4.6: (a) Bifurcation diagram with varying d_1 and $d2 = 0.564$ using initial conditions $(0.5, 4.85, 0.52, 5)$ in blue color and $(0.7, 6.3, 0.4, 3.6)$ in red color. (b) The maximum Lyapunov exponents for two different initial conditions for $d_2 = 0.564$. (c) Bifurcation diagram with two different initial conditions for $d_2 = 0.47$. (d) The Lyapunov exponents for two initial conditions. (e) Two different attractors for different initial conditions: chaotic attractor (blue) and period-27 (red).

employ the technique used by Gabrick *et al.* [128], where we fix only initial condition for one state variable and vary initial condition the other three. For plotting the basins of attraction of the three bistabilities mentioned above, we vary x_0, y_0 between 0.1 to 0.3, u_0 is varied from 0.4 to 0.6, and fix $v_0 = 0.5$. These basins of attraction are shown in Figure 4.4.7.

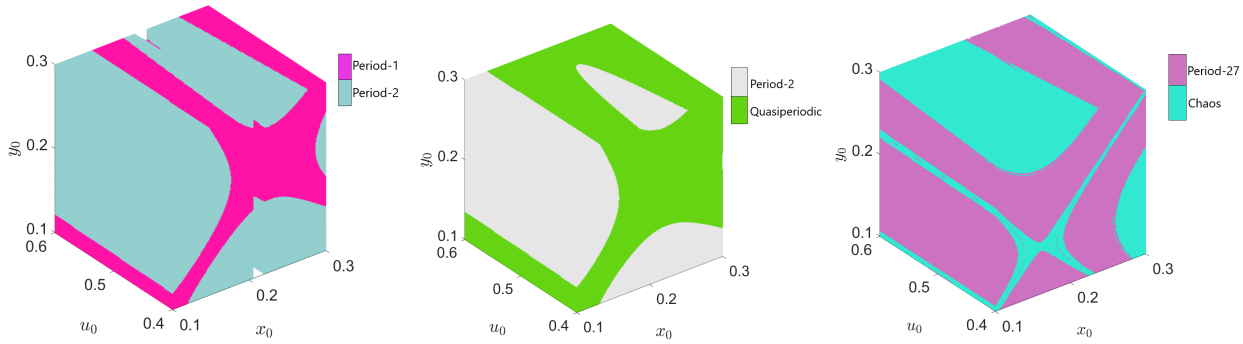

Figure 4.4.7: Basin of attraction for bistability of (a) period-1 and period-2 attractor, (b) an invariant closed curve and period-2 attractor, and (c) period-27 and chaotic attractor.

4.5 Bi-parameter space analysis

In previous section, we observed various bifurcations while varying either prey or predator dispersal rate individually. We examined that increase in dispersal rate can lead to both stabilization and destabilization of the coexisting equilibrium. We obtained period-2 and period-10 orbits till now but there is a need to examine the occurrence of other periodic orbits and intrigue complex dynamics in the two-parameter (d_1d_2-plane) space. Therefore, we shall explore the impact of varying both prey and predator rates simultaneously.

4.5.1 Existence of positive solution

To gain insights into the dynamics of the system in the $d_1d_2 - plane$, we conduct an extensive two-parameter analysis, ranging from 0 to 0.8 for both d_1 and d_2, keeping the other parameters fixed. Such coupled maps could produce negative solutions too [92,129]. For each combination of these dispersal rates (d_1, d_2), we examine whether our system exhibited a positive or negative solution. In Figure 4.5.1a, the yellow region indicate parameter combinations where the predator and prey can coexist in both patches. The green region signifies parameter combinations where the trajectories are divergent.

4.5.2 Maximum Lyapunov exponent and isoperiodic diagrams

Continuing our ecological exploration, we delve deeper into the positive solution region of our predator-prey model within the parameter space. To investigate the dynamics within this region, we turn our attention to the maximum Lyapunov exponents diagram. This diagram offers a distinction between periodic, chaotic, and quasiperiodic behavior. The transition from periodic to quasiperiodic behavior outlines the Neimark-Sacker bifurcation curve. The color map in the Figure 4.5.1b serves as a visual guide, representing the spectrum of maximum Lyapunov exponent values we've obtained. In this map, parameter values shaded in a gradient from light to dark yellow correspond to periodic behavior. Parameter values colored black indicate quasiperiodic dynamics. Meanwhile, the green and blue regions on the map signify chaotic motion. The white region is for the prey extinction in both patches.

Furthermore, we construct an isoperiodic diagram within the same positive solution region. In Figure 4.5.1c, red region indicates the stability of coexisting equilibrium. The cyan region represented periodic-2 orbits, implying that the transition from period-1 to period-2 region represent the flip-bifurcation curve. Black areas denoted various other periodic orbits. The gray region in the isoperiodic diagram marked non-periodic behavior, which could be further divided into quasiperiodic and chaotic regions, aligning with the observations in the maximum Lyapunov exponent diagram Figure 4.5.1b.

4.5.3 Organized periodic structures

In our in-depth analysis of the maximum Lyapunov exponents and isoperiodic diagrams, a compelling pattern emerges, revealing a fundamental and intrinsic route to chaos through quasiperiodicity in our model. The maximum Lyapunov exponents and isoperiodic diagram show the presence of organized periodic structures. These periodic structures collide, corresponding to the occurrence of phase-locking (or frequency locking) phenomena in the quasiperiodic regime. When two frequencies interact non-linearly (or commensurate) and the ratio of the two is a rational number, we say that the frequencies are phase-locked [14]. This occurrence of phase-locking leads to the formation of organized periodic structures called Arnold tongues. The head of the Arnold tongues lies in the chaotic region, while the V-shaped tail is immersed in the quasiperiodic regime. The periodic regime with periods $10, 16, 22, 26, 54, 62$ and so on are clearly marked using different colors in the isoperiodic

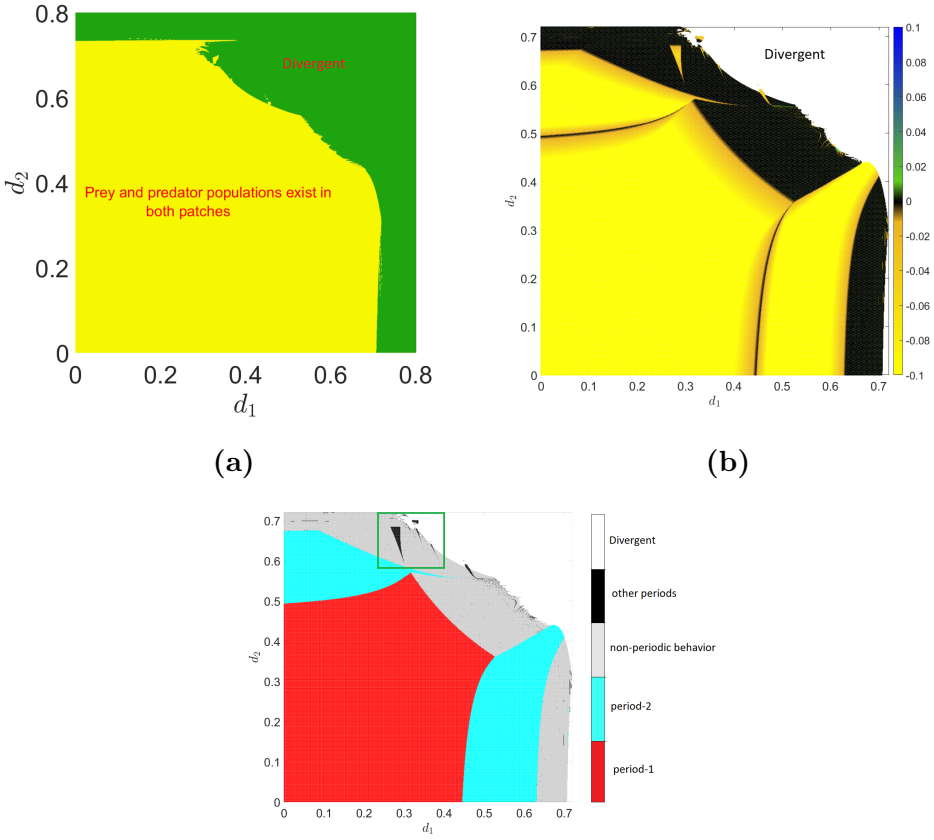

Figure 4.5.1: (a)Existence of positive solution in the d_1d_2-plane: yellow region where both population exist and green region is where the solution is divergent. (b) Maximum Lyapunov exponent diagram in d_1d_2-plane for $0 \leq d_1, d_2 \leq 0.8$. The values of maximum Lyapunov exponent for associated color represented in the colorbar. (c) Isoperiodic diagram for d_1d_2-plane. The different colors represent the periodic and non-periodic regions as mentioned in the colorbar.

diagram. These Arnold tongues are similar to structures observed in circle maps and are associated with rotation numbers $1/10, 1/16, 1/22, 1/26, 1/54, 1/62$ and so on. To further explore and highlight these intricate structures, we zoom in on the maximum Lyapunov exponents and isoperiodic diagrams (on the green square in Figure 4.5.2). We observe colored regions representing various periodic behavior of different periods, with the period-2 regions in cyan color. Prominently, we identified the period-10 Arnold tongues in the system indicated by magenta color. We also notice the Arnold tongues with period-$16, 22, 26, 54$ and 62 in various colors denoted in the color in the figure.

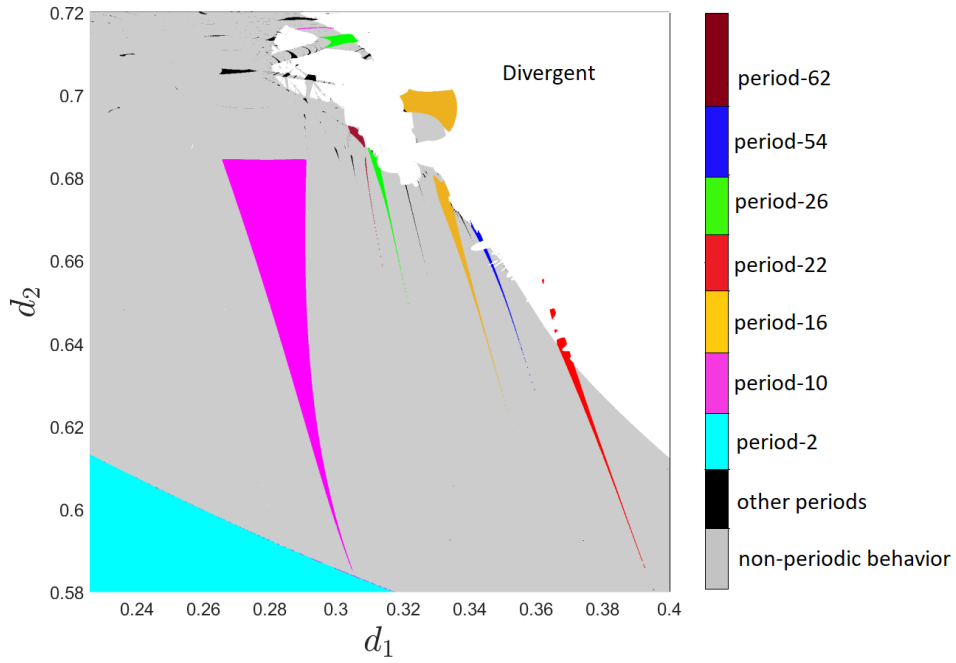

Figure 4.5.2: Magnification of Figure 4.5.1c: isoperiodic diagram for $0.226 \leq d_1 \leq 0.4$ and $0.58 \leq d_2 \leq 0.72$.

4.5.4 Arnold tongues and shrimp structures

So far, we were unable to detect the presence of shrimp structures but we were curious to see if those exist in our model. In order to achieve our goal, we take another parameter set: $r = 2.16, s = 0.5, K = 35, L = 20, \alpha = 0.62, \beta = 0.43$, and $h = 5$. We obtain similar kind of smooth and non-smooth transition when bifurcations occur as observed in the previous parameter set. The bifurcation curves for flip and Neimark-Sacker bifurcation are alike to Figure 4.4.1a-4.4.1b.

We plot the maximum Lyapunov exponents and isoperiodic diagram in the d_1d_2-plane. Figure 4.5.3a shows the values of maximum Lyapunov exponent for different values of d_1 and d_2, revealing three topologically nonequivalent dynamical behaviors with different color maps: plane colored cyan leads to stable periodic behavior, the region black indicates quasiperiodic dynamics, and the magenta zone demonstrates chaotic motion.

We further classify the periodic behavior by finding the period of the trajectories for different values of d_1 and d_2. Figure 4.5.3b depicts the isoperiodic diagram with varying both dispersal rates simultaneously. The white region represents divergent behavior, while the colored region is for periodic and non-periodic regions. The maroon region in the

lower left corner shows the stable region, which is separated from the unstable region of coexisting equilibrium (or period-1) by Neimark-Sacker and flip bifurcation curves in the d_1d_2-plane. The dark green colored region represents the stable period-2 orbits. The light pink color indicates non-periodic behavior which, in the maximum Lyapunov exponents diagram, can be distinguished as the quasiperiodic and chaotic regions. The other periodic region is represented in black.

Next, we magnify the maximum Lyapunov exponents and isoperiodic diagram for $0.86 \leq d_1 \leq 0.915$ and $0 \leq d_2 \leq 0.45$. The periodic regions are cyan colored in Figure 4.5.3c. We distinguish between the periods in Figure 4.5.3d. The periodic regime with periods $10, 11, 12, 13, 14, 15, 16$, and so on are clearly marked using different colors in the isoperiodic diagram. There is a collection of infinite periodic structures arranged in a period-adding sequence. Self-similarity is observed in these organized periodic structures. Although the bifurcation structures are similar for both parameter sets but the orientation of Arnold tongues for the previous set is along d_2 (Figure 4.5.2) while in case of new parameter set its along d_1 (Figure 4.5.3d).

The red rectangle in the isoperiodic diagram (Figure 4.5.4a) shows the presence of another important periodic structure submerged in the chaotic regime, known as a shrimp-like structure with a head and four tails. The Figure 4.5.4b shows the maximum Lyapunov exponents diagram and Figure 4.5.4c depicts the isoperiodic diagram for $0.911 \leq d_1 \leq 0.913$ and $0.245 \leq d_2 \leq 0.262$. The head of the shrimp structure, colored green, corresponds to values of (d_1, d_2) which exhibit period-94 orbits. As we move towards the tail of the structure, period-94 x 2 (period-188) oscillations are observed. This is part of the period-bubbling cascade leading to chaos. Similarly, the yellow part is the periodic orbit of period-46 which is doubled to period-92 in blue color, and the doubled again to period-184 in magenta color as a part of the period-doubling cascade. The light pink region is the non-periodic behavior while gray represents the other periodic orbits.

4.6 Ecological implications

We have discussed many complex dynamics and bifurcations where both smooth and non-smooth transitions occur. One might ask: what is the significance of such type of bifurcations and catastrophic events in the ecological scenario? In cases where trajectories approach equilibrium, determining population size over an extended period is relatively

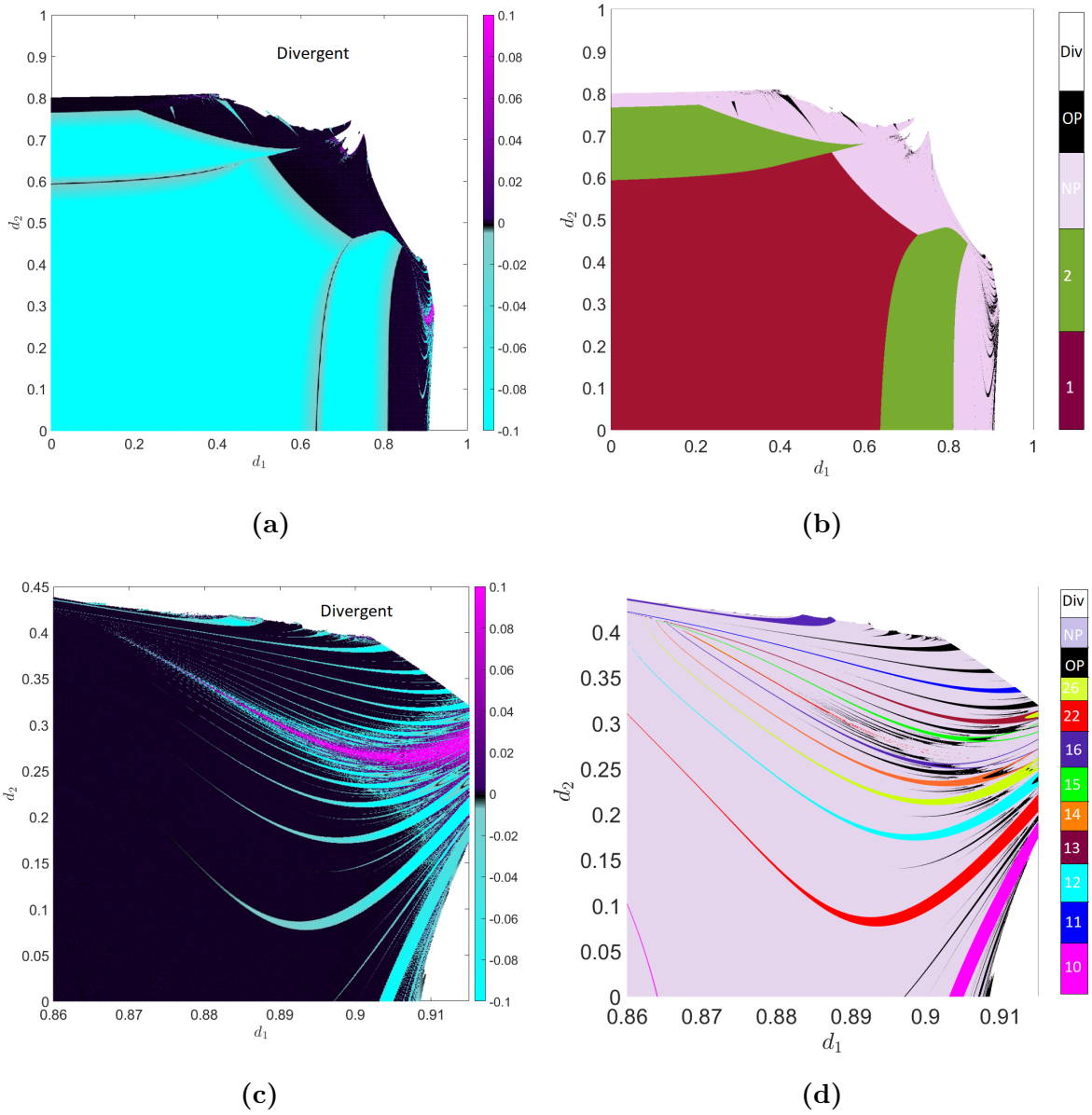

Figure 4.5.3: (a) Maximum Lyapunov exponent diagram in d_1d_2-plane (b) Isoperiodic diagram for $0 \leq d_1 \leq 1$ and $0 \leq d_2 \leq 1$. (c) Magnification of Figure 4.5.3a (d) Magnification of Figure 4.5.3b for $0.86 \leq d_1 \leq 0.915$ and $0 \leq d_2 \leq 0.45$. In the color map, div stands for divergent solutions. OP and NP represent the other periodic orbits and non-periodic behavior, respectively. The initial condition used is $(22.5, 34.08, 22.5, 27.52)$.

straightforward. On the other hand, dealing with unstable equilibria in non-equilibrium dynamics, assessing population levels becomes challenging. One viable approach is to estimate a time-averaged (mean) stock, which is accepted to be a reasonable measure for quantifying population levels. We already know the formulae for mean population in the

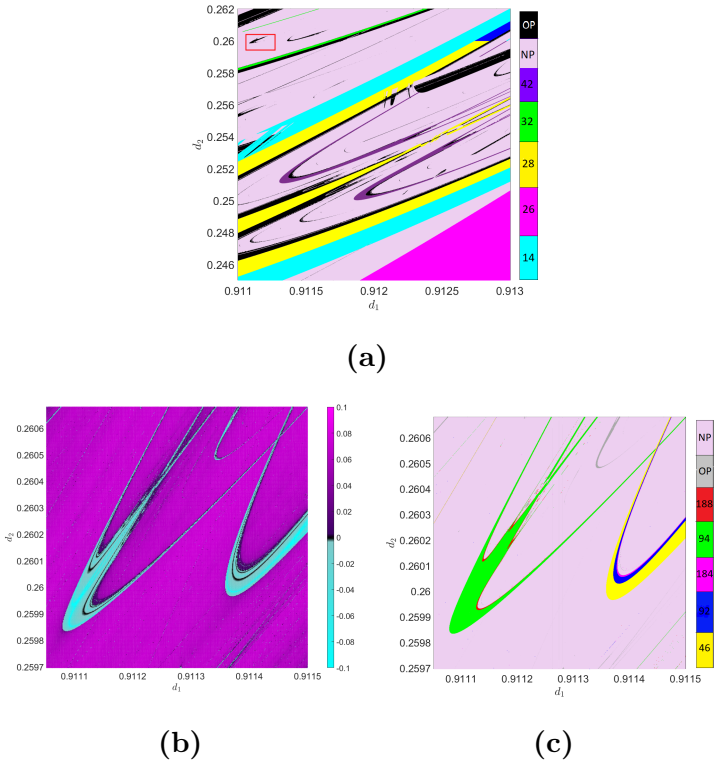

Figure 4.5.4: (a) Isoperiodic diagram for $0.911 \leq d_1 \leq 0.9115$ and $0.245 \leq d_2 \leq 0.262$. (b) MLE diagram and (c) isoperiodic diagram of magnification of red box in Figure 4.5.4a for $0.911052 \leq d_1 \leq 0.9115$ and $0.259696 \leq d_2 \leq 0.26068$. In the color bar, OP and NP represent the other periodic orbits and non-periodic behavior, respectively. The initial condition used is $(22.5, 34.08, 22.5, 27.52)$.

discrete systems (section 2.6). We analyze the change in population stocks when prey or predator dispersal rate is varied. We will use the first parameter values $r = 2, s = 1, K = 1, L = 5, \alpha = 0.8, \beta = 0.6, h = 5$. From now on, prey and predator population indicates prey and predator species in one of the patch, respectively. The change in stock size for either species is in both the patches are the same.

Varying prey dispersal rate:

First, we vary the prey dispersal rate to observe the overall change in the population of both species. We consider three cases: $d_2 = 0$, $d_2 = 0.45$, and $d_2 = 0.564$, which have a complete dynamical analysis provided in the Figure 4.4.2a, Figure 4.4.3a, and Figure 4.4.4a. For fixed $d_2 = 0$, the coexisting equilibrium is stable for $d_1 \in [0, 0.4432)$ as shown in Figure 4.6.1a. A smooth decrease in the mean population is observed after a flip bifurcation occurs at $d_1 = 0.44532$. Subsequently, at $d_1 = B_1$, another bifurcation converts

a period-2 orbit into quasiperiodicity, continuing the population decline. However, a small increase in population size is noted when d_1 exceeds 0.7. Similarly, for fixed $d_2 = 0.45$, the equilibrium state shows a constant stable population, but a smooth decrease in mean stocks is observed after a Neimark-Sacker bifurcation at $d_1 = 0.416$ (Figure 4.6.1b). In this case, no increase in population size is observed.

The case for fixed $d_2 = 0.564$ is more complex, showing a couple of non-smooth transitions. Figure 4.6.1c captures all the changes in the mean population stocks. The coexisting equilibrium is unstable for d_1 in the interval $[0, 0.3191)$. Within this range, the mean prey population decreases while the mean predator population increases. The coexisting equilibrium becomes stable through a flip bifurcation over a very narrow range, but then immediately loses stability to an invariant closed curve, maintaining the same mean population behavior. At $d_1 = B_2$, more dynamic changes occur in the system, yet the mean prey population continues to decrease while the mean predator population continues to increase. However, as the prey dispersal rate increases further, both populations decrease simultaneously beyond $d_1 = 0.38$ onward. After $d_1 = B_3$, there is a decrease in mean predator population while prey population continues to decrease.

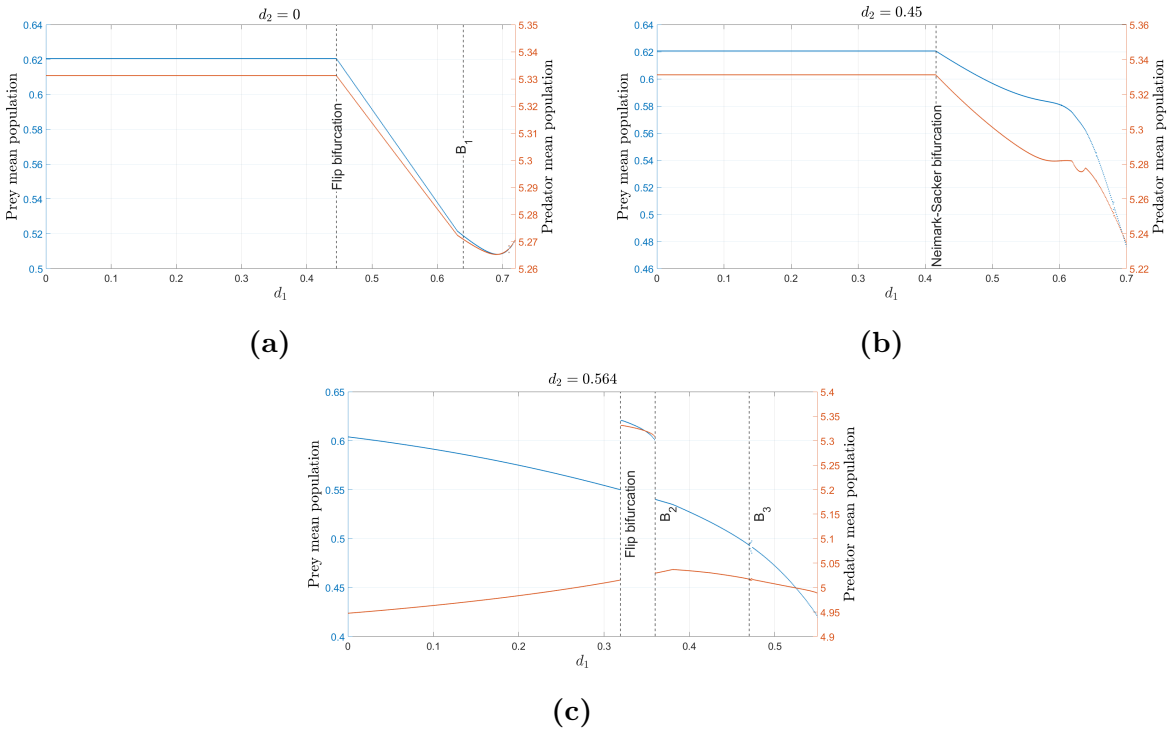

Figure 4.6.1: Mean prey and predator density with varying d_1 with initial condition $(0.5, 4.85, 0.52, 5)$ for (a) $d_2 = 0$, (b) $d_2 = 0.45$, and (c) $d_2 = 0.564$.

Varying predator dispersal rate:

Next, we vary the predator dispersal rate for the three scenarios: $d_1 = 0, d_1 = 0.29$, and $d_1 = 0.51$ as discussed in the Figure 4.4.4c and Figure 4.4.2c (subsection 4.4.1). For $d_1 = 0$, both species are stable at the coexisting equilibrium for d_2 in the interval $[0, 0.493)$. After a flip bifurcation, both mean populations decrease smoothly for $d_2 < 0.675$. Following $d_2 = B_4$, the mean prey population increases while the mean predator population continues to decrease as shown in Figure 4.6.2a. A similar behavior is observed for $d_1 = 0.29$ (Figure 4.6.2b). However, the key difference is that in this case, the transition at the flip bifurcation ($d_1 = 0.552$) is catastrophic, resulting in a sudden decrease rather than a smooth one. After $d_2 = B_5$, there is a significant increase in the mean prey population while the predator population continues to decrease.

For $d_1 = 0.51$, the system exhibits non-equilibrium states for $0 < d_2 < 0.342$, during which both mean populations increase (Figure 4.6.2c). The coexisting equilibrium becomes stable due to a flip bifurcation at $d_2 = 0.342$, transitioning smoothly and causing the mean population to remain constant at the equilibrium value. As the system shows non-equilibrium behavior for $d_2 > 0.374$, due to the occurrence of a Neimark-Sacker bifurcation, both mean populations decrease smoothly.

4.7 Conclusion

In this chapter, we investigated the possible dynamics of a predator-prey model in a patchy environment, considering both prey and predator dispersal rates to assess their impact on stability. We observed that the system could exhibit no, one, two, or three positive equilibrium points. The equilibrium points of the system remained unchanged regardless of dispersal rates due to the homogeneous patch coupling. However, the dynamic behavior of the system significantly affected with dispersal rates. If the equilibrium point is unstable in the isolated patch, then it remains unstable with coupling as well. The stable coexisting equilibrium point loses stability via a flip or Neimark-Sacker bifurcation. The bifurcation curves and stability zone are shown in the d_1d_2-plane (Figure 4.4.1a- 4.4.1b).

We assume that there is a unique coexisting equilibrium and then individually vary the dispersal rate of prey and predators. We examined three scenarios:

(1) **Stable coexisting equilibrium in isolated patches**: When varying the prey dispersal rate (d_1) while keeping the predator dispersal rate (d_2) at zero, we found that

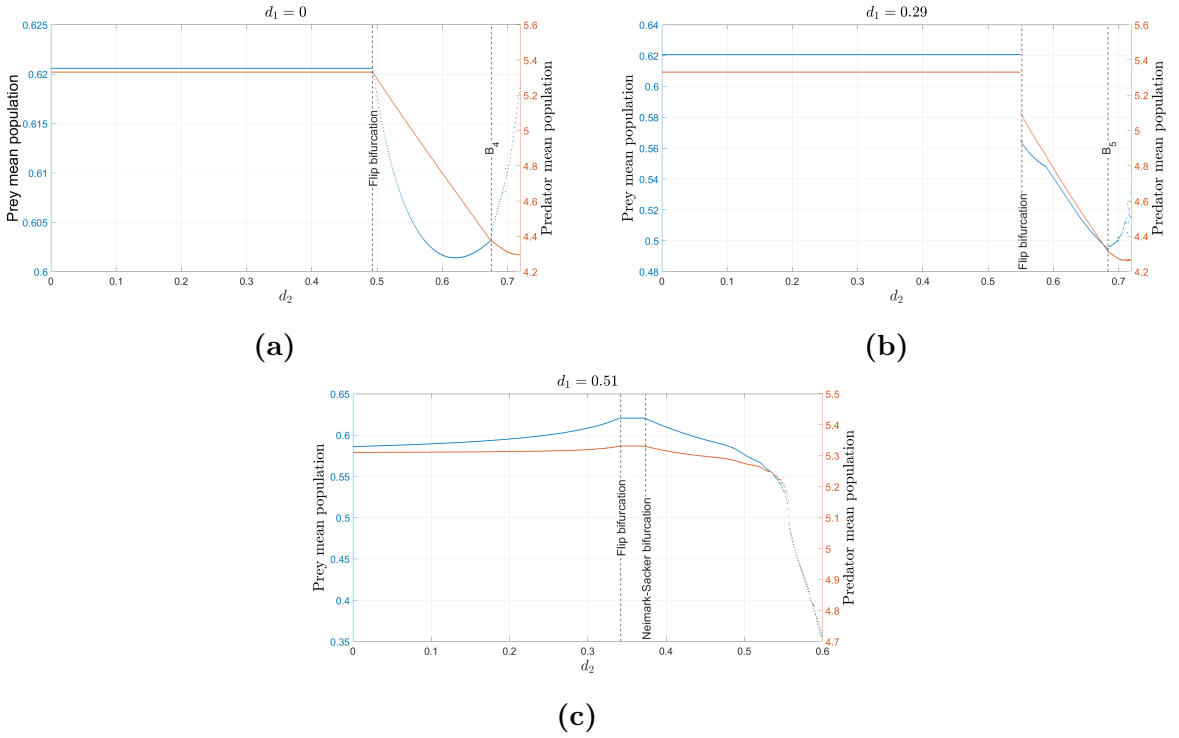

Figure 4.6.2: Mean prey and predator population with varying d_2 with initial condition $(0.5, 4.85, 0.52, 5)$ for (a) $d_1 = 0$, (b) $d_1 = 0.29$, and (c) $d_1 = 0.51$.

the equilibrium remained stable up to a critical value, at which a flip bifurcation occurred via a *smooth* transition, leading to a stable period-2 orbit. Further increase of dispersal rate resulted in quasiperiodic behavior with two stable closed invariant curves. A similar behavior is exhibited when d_2 is varied, keeping d_1 zero.

(2) **Stable equilibrium in the coupled system**: When the prey dispersal rate was fixed at some non-zero value, and the predator dispersal rate varied, we observed that the transition to a period-2 orbit was *non-smooth*, leading to two stable invariant closed curves and then a transition to a stable period-10 orbit, followed by quasiperiodicity with ten closed invariant curves. When predator dispersal is fixed, and prey dispersal is varied, we also observed that the unique equilibrium could lose its stability via a Neimark-Sacker bifurcation, leading to a *smooth* transition from a stable period-1 orbit to quasiperiodicity.

(3) **Unstable equilibrium due to species coupling**: When prey dispersal rate is varied, keeping d_2 fixed, we noted that the system dynamics initially in stable period-2 orbits lead to a stable coexisting equilibrium via a *catastrophic* period-halving phenomenon, and subsequent transitions leading to quasiperiodicity and periodic windows (Figure 4.4.4a). For predator dispersal, with a fixed prey dispersal rate, increasing the

predator dispersal rate led to the stabilization of the coexisting equilibrium via a *smooth* period-halving transitions, with the positive equilibrium losing its stability and iterations settled to a closed invariant curve (Figure 4.4.4c).

We investigated multistable states, uncovering diverse dynamics by altering initial conditions while keeping parameters constant. The different multistable states observed are: (i) stable coexisting equilibrium and period-2 orbits, (ii) stable period-2 orbits with invariant closed curves, and (iii) period-27 orbits and chaotic behavior. The co-stability of coexisting equilibrium and period-2 orbit is a novel result.

To further explore the dynamics in the two-parameter (d_1, d_2) plane, we conducted a comprehensive analysis by varying both dispersal rates simultaneously. We focused on two main perspectives: the maximum Lyapunov exponent and isoperiodic diagram. The maximum Lyapunov exponents diagram characterized periodic, quasiperiodic, and chaotic behaviors while the isoperiodic diagram highlighted stability regions for coexisting equilibria and various periodic orbits. Our analysis revealed significant patterns, such as *Arnold tongues*, which indicate phase-locking phenomena and illustrate transitions from periodic to quasiperiodic and chaotic behaviors. Within these Arnold tongues, we identified periodic regimes with distinct periods like $10, 16, 22, 26, 54,$ and 62(Figure 4.5.2). Further exploration with a different parameter set showed similar bifurcation patterns but with a shifted orientation of Arnold tongues (Figure 4.5.3d). Additionally, we discovered shrimp structures (Figure 4.5.4c) characterized by a head and multiple tails representing period-doubling cascades leading to chaos.

We examined the pattern of mean prey and predator populations in coupled patches by varying their dispersal rates in the non-equilibrium states. The mean population can increase or decrease with the influence of dispersal. Due the catastrophic bifurcation, there can be a sudden jump in the mean population (Figure 4.6.1c and Figure 4.6.2b). This drop in the mean population can be harmful from conversation viewpoint.

CHAPTER 5

Summary and future directions

5.1 Summary

In this thesis, we analyzed discrete-time predator–prey models and explored their dynamical behaviors. The main findings from each chapter are summarized below.

Chapter 2 examined a discrete-time system obtained from the continuous-time Rosenzweig–MacArthur (RM) model through the forward Euler's scheme with a unit integral step size. The main results presented in this chapter were:

(i) The system experienced a Neimark-Sacker bifurcation, resulting in complex behaviors such as quasiperiodicity, periodic doubling, period windows, and chaos.

(ii) Two types of bistability such as periodic–periodic and periodic–chaotic were observed.

(iii) Under sufficient prey (or predator) harvesting, the chaotic behavior eradicates leading to the stabilization of the coexisting equilibrium.

(iv) Species enrichment leads to paradox of enrichment.

(v) The increase in predator mortality rate may enhance the predator stocks.

Chapter 3 investigated a discrete-time system derived from the same continuous-time RM model using the piecewise constant argument. By analyzing the effects of increasing carrying capacity and harvesting efforts, we identified complex phenomena, including periodic orbits, quasiperiodicity, period-bubbling, period-doubling, and chaos. The main results of this chapter were:

(i) An increase in the carrying capacity of the prey species can result in both the stabilization and destabilization of the coexisting equilibrium.

(ii) The model's multistable states were characterized by bistable, tristable, and quadruple attractors.

(iii) In the two-parameter effort plane, Arnold tongues and shrimp-like structures were observed within the quasiperiodic and chaotic regions.

(iv) The phenomena of paradox of enrichment and hydra effect are evident in the model.

Chapter 4 analyzed a discrete-time patchy model with dispersal. The effects of prey and predator dispersal were examined in relation to the stability of the coexisting equilibrium point. This chapter uncovered the following results:

(i) Increases in dispersal rates could both stabilize and destabilize the coexisting equilibrium.

(ii) The stability transitions caused by bifurcations were found to be either smooth or non-smooth.

(iii) A period-10 orbit gave rise to ten closed invariant curves, leading to quasiperiodicity.

(iv) We detected three types of bistability: (a) between coexisting equilibrium and a period-2 orbit, (b) between period-2 orbit with an invariant closed curve, and (c) between a period-27 orbit with a chaotic attractor.

(v) There was prominent existence of Arnold tongues and shrimp structures in the dispersal parameter plane.

This thesis investigated discrete-time predator–prey models derived from the Rosenzweig–MacArthur system, focusing on the effects of prey enrichment, harvesting, and species dispersal. Using bifurcation theory and numerical simulations, we analyze the emergence of complex dynamics, including Neimark-Sacker bifurcations, multistability, quasiperiodicity, and chaos. We explore how varying ecological parameters influence system stability and reveal structured patterns in parameter spaces, such as Arnold tongues and shrimp-like regions. Key ecological phenomena, including the paradox of enrichment and the hydra effect, are examined in both single- and two-patch environment. The findings provide insights into how ecological and spatial factors shape population dynamics in discrete-time systems.

5.2 Future directions

Based on our knowledge, experiences, and challenges faced in this thesis, we further propose some possible future directions as follows:

(i) As discussed in Chapters 2 and 3, alternative discretization techniques such as non-standard finite difference scheme may capture different dynamical properties and lead to new insights into the system's behavior. Investigating how these schemes influence stability, bifurcations, and complex dynamics in the spatial predator-prey model could enhance our understanding of discretization effects in ecological modeling.

(ii) In Chapter 4 , we focused on the dynamics of the coupled system assuming a single coexisting equilibrium in the isolated patch. However, when the isolated patch admits three coexisting equilibria, it would be valuable to investigate how coupling

influences the stability and dynamics of each equilibrium. A comparative study of the stability regions of these equilibria in the coupled system could provide deeper insights into the effects of dispersal and the emergence of complex behaviors in spatially structured populations.

(iii) Another promising avenue for future investigation is the incorporation of heterogeneous dispersal mechanisms into the spatial model. While our current work assumes homogeneous dispersal across patches, real-world ecological systems often exhibit varying dispersal rates due to habitat preferences, environmental gradients, or species-specific traits. Introducing asymmetric dispersal, density-dependent movement, or stochasticity in dispersal patterns could lead to richer dynamical outcomes, including noise-induced transitions, novel bifurcation structures, or altered persistence and extinction thresholds. Exploring these elements would significantly advance our understanding of how realistic dispersal patterns shape spatial population dynamics and ecosystem resilience.

(iv) A further direction worth pursuing is the development and analysis of fractional discrete-time predator-prey model. Investigating how discrete-time fractional-order dynamics interact could reveal new forms of multistability, transient chaos, and complex bifurcation structures. Such models may also offer better agreement with empirical data, providing a more accurate framework for understanding population dynamics in ecosystems.

REFERENCES

[1] Thomas R. Malthus. An essay on the principle of population (1798). *The Works of Thomas Robert Malthus, London, Pickering & Chatto Publishers*, 1:1–139, 1986.

[2] Alfred J. Lotka. Elements of physical biology. *Williams and Wilkins*, 1925.

[3] Vito Volterra. Fluctuations in the abundance of a species considered mathematically. *Nature*, 119(2983):12–13, 1927.

[4] Michael L. Rosenzweig and Robert H. MacArthur. Graphical representation and stability conditions of predator-prey interactions. *The American Naturalist*, 97(895):209–223, 1963.

[5] K.P. Hadeler and I. Gerstmann. The discrete Rosenzweig model. *Mathematical Biosciences*, 98(1):49–72, 1990.

[6] Muhammad Bilal Ajaz, Umer Saeed, Qamar Din, Irfan Ali, and Muhammad Israr Siddiqui. Bifurcation analysis and chaos control in discrete-time modified Leslie–Gower prey harvesting model. *Advances in Difference Equations*, 2020(1):1–24, 2020.

[7] Weiyi Liu and Donghan Cai. Bifurcation, chaos analysis and control in a discrete-time predator–prey system. *Advances in Difference Equations*, 2019:1–22, 2019.

[8] Limin Zhang and Tao Wang. Qualitative properties, bifurcations and chaos of a discrete predator–prey system with weak Allee effect on the predator. *Chaos, Solitons & Fractals*, 175:113995, 2023.

[9] S.M. Shah and Joseph Wiener. Advanced differential equations with piecewise constant argument deviations. *International Journal of Mathematics and Mathematical Sciences*, 6(4):671–703, 1983.

[10] Jason A.C. Gallas. Structure of the parameter space of the Hénon map. *Physical Review Letters*, 70(18):2714, 1993.

[11] Kathleen T. Alligood, Tim D. Sauer, and James A. Yorke. *Chaos.* Springer, 1996.

[12] Guangyi Wang, Xun Zhang, Yan Zheng, and Yuxia Li. A new modified hyperchaotic Lü system. *Physica A: Statistical Mechanics and its Applications*, 371(2):260–272, 2006.

[13] Alexander P. Kuznetsov, Yuliya V. Sedova, and Nataliya V. Stankevich. Dynamics of non–identical coupled Chialvo neuron maps. *Chaos, Solitons & Fractals*, 186:115237, 2024.

[14] Robert C. Hilborn. *Chaos and Nonlinear Dynamics: An Introduction for Scientists and Engineers*. Oxford University Press, 2000.

[15] I. Ya Goldsheid and E. Sorets. Lyapunov exponents of the Schrödinger equation with quasi-periodic potential on a strip. *Helvetica Physica Acta*, 65, 1992.

[16] Suresh Kumarasamy, Irene M Moroz, Sakthi Kumar Sampathkumar, Anitha Karthikeyan, and Karthikeyan Rajagopal. Dynamics and network behavior of a four-dimensional discrete neuron model with magnetic flux coupling. *The European Physical Journal Plus*, 138(8):683, 2023.

[17] R.M. Anderson. *Infectious diseases of humans: dynamics and control*. Oxford University Press, 1991.

[18] Milner B. Schaefer. Some aspects of the dynamics of populations important to the management of the commercial marine fisheries. *Bulletin of Mathematical Biology*, 53(1-2):253–279, 1991.

[19] Pierre-François Verhulst. Notice sur la loi que la population suit dans son accroissement. *Correspondence Mathematique et Physique*, 10:113–129, 1838.

[20] Benjamin Gompertz. On the nature of the function expressive of the law of human mortality and on a new mode of determining the value of life contingencies. *Philosophical Transactions of the Royal Society of London*, 115:513–583, 1825.

[21] P.H. Leslie and J.C. Gower. The properties of a stochastic model for two competing species. *Biometrika*, 45(3/4):316–330, 1958.

[22] John R. Beddington. Mutual interference between parasites or predators and its effect on searching efficiency. *The Journal of Animal Ecology*, 44(1):331–340, 1975.

[23] Robert M. May. *Stability and Complexity in Model Ecosystems*, volume 1. Princeton University Press, 1974.

[24] Robert M. May. Simple mathematical models with very complicated dynamics. *Nature*, 261(5560):459–467, 1976.

[25] W.E. Ricker. Stock and recruitment. *Journal of the Fisheries Research Board of Canada*, 11(5):559–623, 1954.

[26] Raymond J.H. Beverton and Sidney J. Holt. On the dynamics of exploited fish populations. *Springer Science & Business Media*, 11, 2012.

[27] Ronald E. Mickens. Nonstandard finite difference models of differential equations. *World Scientific*, 1993.

[28] A. J. Nicholson and V. A. Bailey. The balance of animal populations.—part I. *Proceedings of the Zoological Society of London*, 105(3):551–598, 1935.

[29] C.B. Hupfaker. Experimental studies on predation: Dispersion factors and predator-prey oscillations. *Hilgardia*, 1:343–383, 1958.

[30] Albert C.J. Luo. *Regularity and Complexity in Dynamical Systems*. Springer, 2012.

[31] Yuri A. Kuznetsov. *Elements of applied bifurcation theory*, volume 112. Springer Science & Business Media, 2013.

[32] Steven H. Strogatz. *Nonlinear dynamics and chaos*. Westview Press, Boulder, CO, second edition, 2015. With Applications to Physics, Biology, Chemistry, and Engineering.

[33] Alan Wolf, Jack B. Swift, Harry L. Swinney, and John A. Vastano. Determining Lyapunov exponents from a time series. *Physica D: Nonlinear Phenomena*, 16(3):285–317, 1985.

[34] S.M. Salman, A.M. Yousef, and A.A. Elsadany. Stability, bifurcation analysis and chaos control of a discrete predator-prey system with square root functional response. *Chaos, Solitons & Fractals*, 93:20–31, 2016.

[35] Lifang Cheng and Hongjun Cao. Bifurcation analysis of a discrete-time ratio-dependent predator–prey model with Allee effect. *Communications in Nonlinear Science and Numerical Simulation*, 38:288–302, 2016.

[36] Dongpo Hu and Hongjun Cao. Bifurcation and chaos in a discrete-time predator–prey system of Holling and Leslie type. *Communications in Nonlinear Science and Numerical Simulation*, 22(1-3):702–715, 2015.

[37] Xiaoli Liu and Dongmei Xiao. Complex dynamic behaviors of a discrete-time predator–prey system. *Chaos, Solitons & Fractals*, 32(1):80–94, 2007.

[38] Sohel Rana and Umme Kulsum. Bifurcation analysis and chaos control in a discrete-time predator-prey system of Leslie type with simplified Holling type IV functional response. *Discrete Dynamics in Nature and Society*, 2017:1–11, 07 2017.

[39] Qamar Din. Complexity and chaos control in a discrete-time prey-predator model. *Communications in Nonlinear Science and Numerical Simulation*, 49:113–134, 2017.

[40] Waqas Ishaque, Qamar Din, Muhammad Taj, and Muhammad Asad Iqbal. Bifurcation and chaos control in a discrete-time predator–prey model with nonlinear saturated incidence rate and parasite interaction. *Advances in Difference Equations*, 2019(1):1–16, 2019.

[41] Muhammad Asif Khan. Chaotic behavior of harvesting Leslie-Gower predator-prey model. *Computational Ecology and Software*, 9(3):67, 2019.

[42] Paulo C. Rech. On two discrete-time counterparts of a continuous-time prey-predator model. *Brazilian Journal of Physics*, 50(2):119–123, 2020.

[43] Michael L. Rosenzweig. Paradox of enrichment: destabilization of exploitation ecosystems in ecological time. *Science*, 171(3969):385–387, 1971.

[44] Peter A. Abrams and James D. Roth. The effects of enrichment of three-species food chains with nonlinear functional responses. *Ecology*, 75(4):1118–1130, 1994.

[45] Sabine Wollrab, Sebastian Diehl, and André M De Roos. Simple rules describe bottom-up and top-down control in food webs with alternative energy pathways. *Ecology Letters*, 15(9):935–946, 2012.

[46] Vinicius Weide, Maria C. Varriale, and Frank M. Hilker. Hydra effect and paradox of enrichment in discrete-time predator-prey models. *Mathematical Biosciences*, 310:120–127, 2019.

[47] Debarghya Pattanayak, Arindam Mishra, Syamal K. Dana, and Nandadulal Bairagi. Bistability in a tri-trophic food chain model: Basin stability perspective. *Chaos: An Interdisciplinary Journal of Nonlinear Science*, 31(7):073124, 2021.

[48] Eduardo Liz and Alfonso Ruiz-Herrera. The hydra effect, bubbles, and chaos in a simple discrete population model with constant effort harvesting. *Journal of Mathematical Biology*, 65(5):997–1016, 2012.

[49] G.P. Neverova, A.I. Abakumov, I.P. Yarovenko, and E. Ya Frisman. Mode change in the dynamics of exploited limited population with age structure. *Nonlinear Dynamics*, 94(2):827–844, 2018.

[50] Jicai Huang, Yijun Gong, and Shigui Ruan. Bifurcation analysis in a predator-prey model with constant-yield predator harvesting. *Discrete Contin. Dyn. Syst., Ser. B*, 18(8):2101–2121, 2013.

[51] Abdul Qadeer Khan. Bifurcations of a two-dimensional discrete-time predator–prey model. *Advances in Difference Equations*, 2019(1):1–23, 2019.

[52] Wenbo Yao and Xianyi Li. Complicate bifurcation behaviors of a discrete predator–prey model with group defense and nonlinear harvesting in prey. *Applicable Analysis*, pages 1–16, 2022.

[53] Michael Sieber and Frank M. Hilker. The hydra effect in predator–prey models. *Journal of Mathematical Biology*, 64:341–360, 2012.

[54] Eduardo Liz. Effects of strength and timing of harvest on seasonal population models: Stability switches and catastrophic shifts. *Theoretical Ecology*, 10(2):235–244, 2017.

[55] Debprasad Pal, Bapan Ghosh, and T. K. Kar. Hydra effects in stable food chain models. *Biosystems*, 185:104018, 2019.

[56] Prabir Das Adhikary, Saikat Mukherjee, and Bapan Ghosh. Bifurcations and hydra effects in Bazykin's predator–prey model. *Theoretical Population Biology*, 140:44–53, 2021.

[57] Saheb Pal. Understanding the hydra effect in predator-dependent functional response models. *Discrete and Continuous Dynamical Systems-B*, 29(1):174–197, 2024.

[58] Tarzan Legović, Jasminka Klanjšček, and Sunčana Geček. Maximum sustainable yield and species extinction in ecosystems. *Ecological Modelling*, 221(12):1569–1574, 2010.

[59] Kyriakos D. Kantarakias, Karim Shawki, and George Papadakis. Uncertainty quantification of sensitivities of time-average quantities in chaotic systems. *Physical Review E*, 101(2):022223, 2020.

[60] Bapan Ghosh, T.K. Kar, and T. Legovic. Relationship between exploitation, oscillation, MSY and extinction. *Mathematical Biosciences*, 256:1–9, 2014.

[61] Eric Tromeur and Nicolas Loeuille. Balancing yield with resilience and conservation objectives in harvested predator–prey communities. *Oikos*, 126(12):1780–1789, 2017.

[62] Arild Wikan and Ørjan Kristensen. Compensatory and overcompensatory dynamics in prey–predator systems exposed to harvest. *Journal of Applied Mathematics and Computing*, 67(1):455–479, 2021.

[63] Víctor Jiménez López and Eduardo Liz. Destabilization and chaos induced by harvesting: Insights from one-dimensional discrete-time models. *Journal of Mathematical Biology*, 82(1):1–28, 2021.

[64] Qibin Fang, Xiaoping Li, and Meiyu Cao. Dynamics of a discrete predator-prey system with Beddington-Deangelis function response. *Applied Mathematics*, 3(4):389–394, 2012.

[65] Qamar Din, Nafeesa Saleem, and Muhammad Sajjad Shabbir. A class of discrete predator–prey interaction with bifurcation analysis and chaos control. *Mathematical Modelling of Natural Phenomena*, 15:60, 2020.

[66] Parvaiz Ahmad Naik, Zohreh Eskandari, Mehmet Yavuz, and Jian Zu. Complex dynamics of a discrete-time Bazykin–Berezovskaya prey-predator model with a strong Allee effect. *Journal of Computational and Applied Mathematics*, 413:114401, 2022.

[67] Vijay Shankar Sharma, Anuraj Singh, Amr Elsonbaty, and A.A. Elsadany. Codimension-one and-two bifurcation analysis of a discrete-time prey-predator model. *International Journal of Dynamics and Control*, pages 1–15, 2023.

[68] Rajni and Bapan Ghosh. Multistability, chaos and mean population density in a discrete-time predator–prey system. *Chaos, Solitons & Fractals*, 162:112497, 2022.

[69] G. C. Layek and N. C. Pati. Organized structures of two bidirectionally coupled logistic maps. *Chaos: An Interdisciplinary Journal of Nonlinear Science*, 29(9), 09 2019.

[70] N. C. Pati, Shilpa Garai, Mainul Hossain, G. C. Layek, and Nikhil Pal. Fear induced multistability in a predator-prey model. *International Journal of Bifurcation and Chaos*, 31(10):2150150, 2021.

[71] Mainul Hossain, Shilpa Garai, Sajad Jafari, and Nikhil Pal. Bifurcation, chaos, multistability, and organized structures in a predator–prey model with vigilance. *Chaos: An Interdisciplinary Journal of Nonlinear Science*, 32(6), 06 2022.

[72] Shilpa Garai, Sarbari Karmakar, Sajad Jafari, and Nikhil Pal. Coexistence of triple, quadruple attractors and wada basin boundaries in a predator–prey model with

additional food for predators. *Communications in Nonlinear Science and Numerical Simulation*, 121:107–208, 2023.

[73] Bo Li, Zohreh Eskandari, and Zakieh Avazzadeh. Strong resonance bifurcations for a discrete-time prey–predator model. *Journal of Applied Mathematics and Computing*, pages 1–18, 2023.

[74] Zohreh Eskandari, Parvaiz Ahmad Naik, and Mehmet Yavuz. Dynamical behaviors of a discrete-time prey-predator model with harvesting effect on the predator. *Journal of Applied Analysis & Computation*, 14(1):283–297, 2024.

[75] Zengyun Hu, Zhidong Teng, Chaojun Jia, Long Zhang, and Xi Chen. Complex dynamical behaviors in a discrete eco-epidemiological model with disease in prey. *Advances in Difference Equations*, 2014:1–19, 2014.

[76] Qianqian Cui, Qiang Zhang, Zhipeng Qiu, and Zengyun Hu. Complex dynamics of a discrete-time predator-prey system with Holling IV functional response. *Chaos, Solitons & Fractals*, 87:158–171, 2016.

[77] Ritwick Banerjee, Pritha Das, and Debasis Mukherjee. Stability and permanence of a discrete-time two-prey one-predator system with Holling type-III functional response. *Chaos, Solitons & Fractals*, 117:240–248, 2018.

[78] Shilpa Garai, N.C. Pati, Nikhil Pal, and G.C. Layek. Organized periodic structures and coexistence of triple attractors in a predator–prey model with fear and refuge. *Chaos, Solitons & Fractals*, 165:112833, 2022.

[79] Xiaoling Han and Ceyu Lei. Stability, bifurcation analysis and pattern formation for a nonlinear discrete predator–prey system. *Chaos, Solitons & Fractals*, 173:113710, 2023.

[80] John Guckenheimer and Philip Holmes. *Nonlinear oscillations, dynamical systems, and bifurcations of vector fields*, volume 42. Springer Science & Business Media, 2013.

[81] Efim Frisman and Matvey Kulakov. Transition from bi-to quadro-stability in models of population dynamics and evolution. *Mathematics*, 11(19):4134, 2023.

[82] Leon Glass and Rafael Perez. Fine structure of phase locking. *Physical Review Letters*, 48(26):1772, 1982.

[83] Tarzan Legović, Jasminka Klanjšček, and Sunčana Geček. Maximum sustainable yield and species extinction in ecosystems. *Ecological Modelling*, 221(12):1569–1574, 2010.

[84] H. Kook, F.H. Ling, and George Schmidt. Universal behavior of coupled nonlinear systems. *Physical Review A*, 43(6):2700, 1991.

[85] Karl E. Kürten and Grégoire Nicolis. Bifurcation scenarios and quasiperiodicity in coupled maps. *Physica A: Statistical Mechanics and its Applications*, 245(3-4):446–452, 1997.

[86] Yu L. Maistrenko, V.L. Maistrenko, A. Popovich, and Erik Mosekilde. Transverse instability and riddled basins in a system of two coupled logistic maps. *Physical Review E*, 57(3):2713, 1998.

[87] Rui Carvalho, Bastien Fernandez, and R. Vilela Mendes. From synchronization to multistability in two coupled quadratic maps. *Physics Letters A*, 285(5-6):327–338, 2001.

[88] Paulo C. Rech, Marcus W. Beims, and Jason A.C. Gallas. Naimark–sacker bifurcations in linearly coupled quadratic maps. *Physica A: Statistical Mechanics and its Applications*, 342(1-2):351–355, 2004.

[89] Sangeeta Rani Ujjwal, Nirmal Punetha, Ram Ramaswamy, Manish Agrawal, and Awadhesh Prasad. Driving-induced multistability in coupled chaotic oscillators: Symmetries and riddled basins. *Chaos: An Interdisciplinary Journal of Nonlinear Science*, 26(6), 2016.

[90] Diogo Ricardo da Costa, Julia G.S. Rocha, Luam S. de Paiva, and Rene O. Medrano-T. Logistic-like and gauss coupled maps: The born of period-adding cascades. *Chaos, Solitons & Fractals*, 144:110688, 2021.

[91] Sachin Bhalekar and Prashant M. Gade. Stability analysis of fixed point of fractional-order coupled map lattices. *Communications in Nonlinear Science and Numerical Simulation*, 113:106587, 2022.

[92] Irina Bashkirtseva and Alexander Pisarchik. Variability and effect of noise on the corporate dynamics of coupled oscillators. *AIP Conference Proceedings*, 2172(1):070004, 2019.

[93] Paulo C. Rech. A coupling of three quadratic maps. *Chaos, Solitons & Fractals*, 41(4):1949–1952, 2009.

[94] Irina Bashkirtseva and Lev Ryashko. Chaotic transients, riddled basins, and stochastic transitions in coupled periodic logistic maps. *Chaos: An Interdisciplinary Journal of Nonlinear Science*, 31(5), 2021.

[95] G.C. Layek and N.C. Pati. Organized structures of two bidirectionally coupled logistic maps. *Chaos: An Interdisciplinary Journal of Nonlinear Science*, 29(9), 2019.

[96] Ryusuke Kon and Dinesh Kumar. Stability of Rosenzweig–MacArthur models with non-diffusive dispersal on non-regular networks. *Theoretical Population Biology*, 150:14–22, 2023.

[97] Paulo C. Rech. Complex dynamics of a linear coupling of two chaotic Lorenz systems. *Brazilian Journal of Physics*, 54(1):15, 2024.

[98] Ross Cressman and Vlastimil Křivan. Two-patch population models with adaptive dispersal: The effects of varying dispersal speeds. *Journal of Mathematical Biology*, 67:329–358, 2013.

[99] Yun Kang, Sourav Kumar Sasmal, and Komi Messan. A two-patch prey-predator model with predator dispersal driven by the predation strength. *Mathematical Biosciences & Engineering*, 14(4):843–880, 2017.

[100] Ali Mai, Guowei Sun, and Lin Wang. Impacts of the dispersal delay on the stability of the coexistence equilibrium of a two-patch predator–prey model with random predator dispersal. *Bulletin of Mathematical Biology*, 81:1337–1351, 2019.

[101] Deeptajyoti Sen and Lenka Přibylová. Complex dynamics in prey-predator systems with cross-coupling: Exploring nonlinear interactions and population oscillations. *Communications in Nonlinear Science and Numerical Simulation*, page 108154, 2024.

[102] Carolin Grumbach, Femke N. Reurik, Juan Segura, Daniel Franco, and Frank M. Hilker. The effect of dispersal on asymptotic total population size in discrete-and continuous-time two-patch models. *Journal of Mathematical Biology*, 87(4):60, 2023.

[103] Vinod P. Saxena. Mathematical modelling of biological populations with and without dispersion. *Research in Statistics*, 1(1):2215638, 2023.

[104] Mohammed O. Al-Kaff, Hamdy A. El-Metwally, Abd-Elalim A. Elsadany, and Elmetwally M. Elabbasy. Exploring chaos and bifurcation in a discrete prey–predator based on coupled logistic map. *Scientific Reports*, 14(1):16118, 2024.

[105] Nicolas Bajeux and Bapan Ghosh. Stability switching and hydra effect in a predator–prey metapopulation model. *Biosystems*, 198:104255, 2020.

[106] Binandita Barman and Bapan Ghosh. Dynamics of a spatially coupled model with delayed prey dispersal. *International Journal of Modelling and Simulation*, 42(3):400–414, 2022.

[107] Richita Ghosh, Umesh Kumar Verma, Sarika Jalan, and Manish Dev Shrimali. Chimeric states induced by higher-order interactions in coupled prey–predator systems. *Chaos: An Interdisciplinary Journal of Nonlinear Science*, 34(6), 2024.

[108] Paulo C. Rech, Marcus W. Beims, and Jason A.C. Gallas. Generation of quasiperiodic oscillations in pairs of coupled maps. *Chaos, Solitons & Fractals*, 33(4):1394–1410, 2007.

[109] Enrique C. Gabrick, Eduardo L. Brugnago, Ana L.R. de Moraes, Paulo R. Protachevicz, Sidney T. da Silva, Fernando S. Borges, Iberê L Caldas, Antonio M. Batista, and Jürgen Kurths. Control, bi-stability, and preference for chaos in time-dependent vaccination campaign. *Chaos: An Interdisciplinary Journal of Nonlinear Science*, 34(9), 2024.

[110] Nao Takashina and Akihiko Mougi. Effects of marine protected areas on overfished fishing stocks with multiple stable states. *Journal of Theoretical Biology*, 341:64–70, 2014.

[111] Bapan Ghosh, Debprasad Pal, T.K. Kar, and Jose C. Valverde. Biological conservation through marine protected areas in the presence of alternative stable states. *Mathematical Biosciences*, 286:49–57, 2017.

[112] Irina Vortkamp, Christian Kost, Marita Hermann, and Frank M. Hilker. Dispersal between interconnected patches can reduce the total population size. *bioRxiv*, pages 2022–04, 2022.

[113] Nguyen Ngoc Doanh, Tri Nguyen-Huu, and Pierre Auger. Connectivity between two fishing sites can lead to an emergence phenomenon related to maximum sustainable yield. *Journal of Theoretical Biology*, page 111913, 2024.

[114] Nao Takashina, Akihiko Mougi, and Yoh Iwasa. Paradox of marine protected areas: Suppression of fishing may cause species loss. *Population Ecology*, 54:475–485, 2012.

[115] Bapan Ghosh, Frédéric Grognard, and Ludovic Mailleret. Natural enemies deployment in patchy environments for augmentative biological control. *Applied Mathematics and Computation*, 266:982–999, 2015.

[116] Sourav Kumar Sasmal and Dibakar Ghosh. Effect of dispersal in two-patch prey–predator system with positive density dependence growth of preys. *Biosystems*, 151:8–20, 2017.

[117] Sangeeta Saha and G.P. Samanta. Influence of dispersal and strong Allee effect on a two-patch predator–prey model. *International Journal of Dynamics and Control*, 7:1321–1349, 2019.

[118] Shaban Aly and M. Farkas. Bifurcations in a predator–prey model in patchy environment with diffusion. *Nonlinear Analysis: Real World Applications*, 5(3):519–526, 2004.

[119] Rachid Mchich, Pierre Auger, and Jean-Christophe Poggiale. Effect of predator density dependent dispersal of prey on stability of a predator–prey system. *Mathematical Biosciences*, 206(2):343–356, 2007.

[120] Yang Kuang and Yasuhiro Takeuchi. Predator-prey dynamics in models of prey dispersal in two-patch environments. *Mathematical Biosciences*, 120(1):77–98, 1994.

[121] J.C. Poggiale. Predator-prey models in heterogeneous environment: Emergence of functional response. *Mathematical and Computer Modelling*, 27(4):63–71, 1998.

[122] Yun Kang and Carlos Castillo-Chavez. Multiscale analysis of compartment models with dispersal. *Journal of Biological Dynamics*, 6(sup2):50–79, 2012.

[123] Guowei Sun and Ali Mai. Stability analysis of a two-patch predator–prey model with two dispersal delays. *Advances in Difference Equations*, 2018(1):1–9, 2018.

[124] Wonhyung Choi, Kwangjoong Kim, and Inkyung Ahn. Predator-prey models with prey-dependent diffusion on predators in spatially heterogeneous habitat. *Journal of Mathematical Analysis and Applications*, 525(1):127130, 2023.

[125] Pierre Auger, Bob Kooi, and Ali Moussaoui. Increase of maximum sustainable yield for fishery in two patches with fast migration. *Ecological Modelling*, 467:109898, 2022.

[126] Philip Erm, Andrew Balmford, Nils C. Krueck, Nao Takashina, and Matthew H. Holden. Marine protected areas can benefit biodiversity even when bycatch species only partially overlap fisheries. *Journal of Applied Ecology*, 61(4):621–632, 2024.

[127] Eduardo L. Brugnago, Enrique C. Gabrick, Kelly C. Iarosz, José D. Szezech, Ricardo L. Viana, Antonio M. Batista, and Iberê L. Caldas. Multistability and chaos in seirs epidemic model with a periodic time-dependent transmission rate. *Chaos: An Interdisciplinary Journal of Nonlinear Science*, 33(12), 2023.

[128] Enrique C. Gabrick, Elaheh Sayari, Paulo R. Protachevicz, José D. Szezech Jr., Kelly C. Iarosz, Silvio L.T. de Souza, Alexandre C.L. Almeida, Ricardo L. Viana, Iberê L. Caldas, and Antonio M. Batista. Unpredictability in seasonal infectious diseases spread. *Chaos, Solitons & Fractals*, 166:113001, 2023.

[129] N.C. Pati. Spiral organization of quasi-periodic shrimp-shaped domains in a discrete predator–prey system. *Chaos: An Interdisciplinary Journal of Nonlinear Science*, 34(8), 2024.